FOLDING AND ASSEMBLY OF CYTOSKELETAL PROTEINS UNDER FORCE - FROM SINGLE MOLECULE STUDIES OF DYSTROPHIN TO STUDIES OF INTACT CELLS

Christine Carag Krieger

A DISSERTATION

in

Chemical and Biomolecular Engineering

Presented to the Faculties of the University of Pennsylvania in Partial

Fulfillment of the Requirements for the Degree of Doctor of Philosophy

2011

_____

Dennis E. Discher, Ph. D.
Supervisor of Dissertation

_____

Raymond J. Gorte, Ph. D.
Graduate Group Chairman

DISSERTATION COMMITTEE

H. Lee Sweeney, Ph. D.
Chairman of Physiology

John C. Crocker, Ph. D.
Associate Professor

Matthew J. Lazzara, Ph. D.
Assistant Professor

To Taylor

Without his patience and support this thesis would not have been accomplished.

Acknowledgements

First and foremost I would like to thank my advisor Dennis Discher. Through his indulgence I had the opportunity to work on many projects and learn several techniques. I will always be grateful for the exposure I had to different fields and their diverse ways of thinking. I would also like to thank Dan Safer, Nishant Bhasin, and Colin Johnson for giving me a good start at the beginning of my graduate career, former lab members Florian Rehfeldt and Rich Tsai for making lab a fun place to work, Allison Zajac and Beca Tenney for teaching me what it means to be a cell biologist, and finally Alexis Wallen for her continuous support.

ABSTRACT

FOLDING AND ASSEMBLY OF CYTOSKELETAL PROTEINS UNDER FORCE - FROM SINGLE MOLECULE STUDIES OF DYSTROPHIN TO STUDIES OF IN INTACT CELLS

Christine Carag Krieger

Dennis E. Discher

Changes in tertiary and quaternary structure of proteins within the actin cytoskeletal network are a likely way cells read mechanical signals from their environment. However, showing that these conformational changes occur as a result of mechanical stress and that such changes are important to the function of the cell is a major challenge. This thesis seeks to address these questions using a cohort of molecular biophysical and cell biological methods applied in increasingly complex contexts. First, the importance of force-driven unfolding to function and how changes in unfolding pathway correlate with diseased states was determined with single molecule Atomic Force Microscopy on nano-constructs of wild-type and mutant forms of dystrophin. Biophysical studies showed that the ability to fold into mechanically stable, spectrin-type helical bundle domains and the preservation of cooperative unfolding were common characteristics of functional truncated dystrophins. Second, a newly developed in-cell cysteine labeling technique demonstrated stress-enhanced repeat unfolding within spectrin in wild-type red blood cells under shear stress versus static conditions, thus demonstrating that forced unfolding is not just an *in vitro* phenomena. The importance of the cytoskeletal network

to spectrin function was also demonstrated in mutant, 4.1R-null red blood cells, where the intrinsic properties of spectrin remain intact but the network integrity is compromised by absence of 4.1R. Loss of network integrity was evident in a decrease in spectrin unfolding under stress. Repeat unfolding was accompanied by changes in associations of spectrin with its binding partners in a time- and stress- dependent manner, indicating that the erythrocyte cytoskeleton exhibits a graded response to stress. Lastly, with cardiomyocytes derived from embryonic stem cells, the importance of stress to quaternary structure of actinin within the sarcomeric cytoskeleton and its effects on cell-wide function was tested in cells adhered to elastic substrates. Substrate stiffness sets the load on these spontaneously contracting cells, and differences in load lead to cytoskeletal reorganization with significant effects on cardiogenic development. Taken together, these findings present evidence of various cytoskeletal proteins – especially in the spectrin superfamily – as mediators of mechanical signaling within cell.

TABLE OF CONTENTS

LIST OF TABLES

LIST OF FIGURES

Preface

How a cell senses physical aspects of its surroundings is currently an open question in cell and developmental biology. The fact that cells do feel their mechanical environment and that such signals are important is complementary to well-established and widely accepted changes in a tissue's mechanical properties in disease. In its essence, the process of cellular mechanotransduction can be described in two or three steps: 1) an active cell imposes a force on its surroundings (which does not apply, for example, to an inactive red blood cell); 2) a force or mechanical signal is resisted and 'read' by the cytoskeleton; and 3) the cell collectively processes that mechanical signal and remodels itself accordingly. While each step in this process poses many unanswered questions, the work in this thesis largely focuses on molecular details of the second step. Central to many proposed hypotheses is the idea that the cell takes advantage of force-induced structural deformations which occur dynamically in strategically located proteins. The pattern of structural changes depends on the nature of the signal, and decoding such information provides a means for mechanotransduction. Therefore the ability to measure and predict how cytoskeletal proteins deform under stress would seem instrumental to understanding cellular responses to a mechanical signal. One challenge, however, is accurately assessing the structural perturbations of a protein in its native environment. Many cytoskeletal components such as actin, myosin, integrin, etc. have been extensively characterized *in vitro*, but whether the various results are relevant to these proteins in a cellular network is unknown. Forced unfolding and conformational events, for example, are likely reversible and fast. Additional quaternary structure changes might also occur, resulting in a cascade of processes that culminate in a cell "feeling" its microenvironment.

This thesis is the culmination of an effort to understand the deformations within proteins of the actin-based cytoskeletal network in response to physical force. Particular focus is given initially to ubiquitous spectrin superfamily proteins and the mechanosensitivity of the helical spectrin repeat domains. Chapter 1 will first review the physiological roles of spectrin, dystrophin, and alpha-actinin – where these proteins are found and why they are believed to be involved in mechanical function. Previous *in vitro* studies of the thermodynamic properties of the spectrin repeat domain are described and followed by introduction of a newly developed cysteine labeling technique used to detect the unfolding of spectrin repeat domains within the spectrin network of human red cells (Johnson, Tang, Carag et. al., *Science* 2007). The results establish that forced unfolding of repeat domains occurs *in vivo* while leaving open the question of whether forced dissociation of proteins competes with unfolding. Mechanotransduction in adherent cells will also be introduced with spontaneously contracting embryonic heart muscle cells which – based on recent studies (Engler, Carag-Krieger et. al., *JCS* 2008) – seem a reasonable cell model to help in the elucidation of the physical forces experienced by the cytoskeleton. While Chapter 1 aims to highlight some of the main questions of this thesis, a further goal of the first chapter is to describe specific contributions of this thesis' author to the cited publications.

Chapter 2 presents mass spectrometry mapping of dystrophin together with single-molecule experiments on truncated dystrophin polypeptides based on naturally occurring deletional mutations found in Becker Muscular Dystrophy (BMD). The studies provide insight into the mechanical function of the spectrin-type three-helixrepeat domain and multiple variants, establishing guidelines for the design of truncated

dystrophins of possible use in treatments of Duchenne Muscular Dystrophy (DMD) (Krieger, *Cytoskeleton* 2010.).

Chapter 3 focuses on forced unfolding in competition with forced dissociation in cysteine labeling studies of mouse red blood cell membranes, both wild-type (wt) and 4.1R-null derived cells. In 4.1R-null red blood cells, the intrinsic properties of spectrin remain intact, but the stability of the cytoskeletal network is severely compromised by the loss of 4.1R: loss of mechanical integrity of the network was evident in a decrease of shear-enhanced spectrin labeling. In addition, the associations of spectrin with its binding partners proves time and stress dependent, indicating that the red cell cytoskeleton exhibits a graded response to stress.

In the final research chapter, Chapter 4 describes the effects of substrate stiffness on chick embryo-derived cardiomyocytes and the development of stem cell derived cardiomyocytes (SCD-CM). With such systems, cysteine labeling can be applied to nucleated, adherent cells. Equally important is the understanding that emerges for the role of cell-generated forces on cytoskeletal structure.

A final chapter provides broader conclusions and perspectives for future work.

CHAPTER ONE

Spectrin proteins, the mechanical mediators of the cell

Sustaining structure under force – a fundamental role of the cytoskeleton

Cytoskeletal proteins control cell morphology as the cell moves, grows, or is pulled upon. Given the number of processes a cell will undergo throughout its lifetime, the cell must maintain its structure or suitably remodel itself under a wide range of force. Whether forces are produced internally or originate from external sources, the cytoskeleton must resist collapse and simultaneously protect the membrane, organelles, and other cytosolic components from injury. This implies that built within the cytoskeletal network is a mechanism to relieve excess energy. What has recently come to light is that controlled unfolding of domains within these proteins may be an integral part of that function. Protein structure is held together by covalent, hydrophobic, electrostatic, and hydrogen bonds, all of which require energy to release. Covalent bonds are too strong to be affected by common biological forces, while individual hydrogen bonds are too weak to dissipate a significant amount of energy – though collectively hydrogen bonds can be a formidable energy barrier. The strength of hydrophobic bonds can vary depending on the surface area of the contact region. Likewise, the energy within an electrostatic interaction is largely solvent dependent. Different combinations of hydrophobic contacts and electrostatic bonding form a limitless array of possible domain stabilities. Proteins can therefore be tuned to withstand forces below a specified threshold and unfold only

when network strains exceed that threshold. Strategic location of these proteins in areas of high force exposure would effectively shield the entire cell from mechanical trauma with minimal resource investment. If such proteins exist, then it follows that the cell would use them to gain information about their physical surroundings. Clusters of proteins or protein domains of multiple stabilities form a mechanosensory complex, where the configurations of conformational changes create a message that can be read by the cell and hopefully one day decoded by humans.

Spectrin proteins are likely candidates for molecular mechanosensors because they are located in high stress areas. Members of this superfamily (Fig 1.1), comprised of spectrin, alpha actinin, dystrophin, and utrophin, directly bind to actin and play significant roles in the cytoskeleton. Spectrin tetramers form a network that lines the cytosolic side of the plasma membrane and is largely responsible for the cortical stability of virtually all cell types (Prasain 2009). Additionally, erythrocytic spectrin, an isoform found in red cells, has been shown to be the source of red cell extensibility (Mohandas 1994, Discher 2000). Dystrophin, unique to muscle tissue, and utrophin, a ubiquitous form of dystrophin, are also found at the plasma membrane and form a crucial connection between the actin cytoskeleton and the extracellular matrix (ECM) via a membrane-bound signaling complex called the dystroglycan complex (DGC). Dystrophin is known to be involved in force transmission and protection of the membrane during muscle contraction, although the molecular basis of its function is not fully understood (Petrof 1993). Alpha-actinin, another ubiquitous protein, bundles actin fibers and is dispersed throughout the cytoskeleton. Like its relatives, alpha-actinin binds to known signaling complexes such as the z-disk in muscle. Furthermore, all these proteins are directly involved in signaling (Broderick 2005, Djinovic-Carugo 2002) and

some contain binding sites within structure (Rybakova 2006, Bois 2005). This known signaling function in conjunction with localization to highly strained regions of the cell supports the supposition that spectrin proteins function as mediators of mechanical information.

Molecular extensibility of the spectrin repeat domain

Spectrin repeat domains are the source of spectrin family protein flexibility (Broderick 2005). This motif consists of a right-handed triple-helical structure mainly held together by hydrophobic contacts between helices (Fig. 1.2). Contrary to other protein motifs, spectrin repeats do not have a defining amino acid sequence. The sequence homology between repeat domains, even within the same protein, is relatively low, about 80% (Broderick 2005). The size of the individual helices and the length of the linkers between them can also be different, though the size of the repeat as a whole is conserved. Multiple repeats are present in series forming a higher order domain rod domain, which defines the mechanical properties of the protein.

The repeat domains have been the subject of many *in vitro* studies generating much conflicting data. One interesting feature of the rod domain is that spectrin repeats are connected by a continuous helix, i.e. the last helix of the first domain is continuous with the first helix of the second domain (Kusunoki 2004). Protein constructs of 3-5 repeats melt in a two-step process at 55-60°C, suggesting that all the repeats unfold simultaneously. On the other hand, individual repeats have been shown to have a wide range of melting temperatures as low as 25°C (An 2006). The helical linker is a likely source of cooperativity in the rod domain; a marginally stable repeat flanked by two very stable repeats may in turn melt at a higher temperature or vice versa. However, thermal softening at physiological temperatures could preferentially melt the helical linker,

reducing cooperative unfolding between repeats (Law 2003a). In terms of mechanical function, a rod domain containing repeats that unfold in discrete stages would have a greater ability to relieve force for long durations and greater sensitivity to force signals. Previous single molecule experiments have shown that spectrin repeats unfold under forces ranging from 20-30 pN (Rief 1999, Law 2003b) and refold once tension is removed (Rief 1999) Therefore unfolding of more than one domain could alleviate the tension produced by a handful of myosins IF these domains unfold independently. Conversely, if domains unfold cooperatively, then the same 20-30 pN would unfold multiple repeats, greatly increasing the extension of the rod domain in a short amount of time, but decreasing the amount of energy the protein can absorb. Atomic force microscopy (AFM) on sections of the rod domain from spectrin and dystrophin demonstrated that cooperative unfolding between domains does occur (Fig 1.3) (Bhasin 2005). Yet dystrophin has hinge regions inserted within the rod domain, and AFM studies on the dystrophin rod domain have shown that the hinge regions interrupt cooperative unfolding (Fig 1.3) (Bhasin 2005). Preventing complete unfolding of the rod domain at low forces may be the physiological role of the hinge regions. Perhaps the phenomena of cooperative repeat unfolding takes place in only a few members of the spectrin family. Alternatively, repeat domains may cooperatively unfold under some scenarios but not others, something not easily detected with biochemical or single molecule techniques. Another possibility is that a spectrin family protein contains a number of repeats that do cooperatively unfold and some that do not, complicating efforts to define the mechanical properties of the whole protein through investigation of a few domains.

In situ force-induced unfolding detected by cysteine labeling

In vitro research has put forward many interesting ideas about the purpose of the spectrin repeat domains and how they are supposed to work, but which of these ideas apply in a physiological setting cannot be determined until new approaches are developed to study these domains in a different context. The nature of biochemical and single molecule techniques restricts investigations to small sections of the protein. Looking at the protein in its entirety is only a slight improvement because protein-protein interactions are essential to its function. First off, all spectrin family proteins are immobilized at their ends, through its actin binding domain (ABD) at the N-terminus and other protein binding domain at its C-terminus. Second, not all family members operate as monomers. Alpha-actinin forms homo-dimers, and spectrin forms hetero-dimers, which go on to associate with themselves into a tetramer. Only dystrophin and utrophin have been shown to be monomeric (Broderick 2005). Third, spectrin family proteins commonly bind to additional proteins through sites within their rod domains. These quaternary associations shape the mechanical environment of the protein and affect the ultimate operation of the repeat domains.

Thiol-attached probes have been extensively used in the past to study structure and assembly of proteins in solution. Non-physiological changes in temperature or pH are common perturbations and can be useful for acquiring thermodynamic information but are not suitable for ascertaining the structural stability of proteins under force as is relevant to cell biology. Techniques that apply to cells have the advantage of studying proteins in a more natural environment. Binding of conformation-sensitive antibodies would seem like one suitable approach, but imaging of bound antibodies generally requires cells to be fixed and fixation would not necessarily capture small structural changes sustained during force exposure. In addition, very few conformation-sensitive

antibodies are available, and it would seem desirable to look at changes in several proteins at a time. Re-engineering cells to express fluorescent 'GFP' type proteins that might exhibit a stress-dependent change in signal, such as FRET, is not only a cumbersome process but requires one to know what proteins are stressed and where in the protein the tags should be placed. Shot-gun cysteine labeling (Johnson 2007) is a technique that combines the precision of biochemical studies with the broader advantages of modern cell biology and proteomic methods. This technique follows the same principles as solution-based thiol labeling, in which cysteines buried within the protein fold will be labeled at slower rates than cysteines exposed to solution. Experimental conditions that alter conformation will change labeling rates. By using membrane-permeable thiol probes, protein structure can be investigated while the protein remains inside an intact cell. Because labeling is irreversible and can occur in seconds, transient conformation changes can be captured. Moreover, by using Mass Spectrometry to identify labeled proteins and their labeled sites, the 'Cys Shotgun' Mass Spectrometry (CS-MS) technique labels all proteins and can therefore uncover structural changes in a number of proteins simultaneously.

In this thesis, the CS-MS technique was used to validate unfolding of spectrin repeat domains while spectrin proteins were in their native cytoskeletal network. To verify that repeats unfold as a result of force exposure, the labeling kinetics of buried cysteines must adhere to the thermodynamic constraints set by the physical parameters of the system (Fig 1.4). Force-enhanced labeling cannot occur until there is sufficient energy to overcome the barriers to unfolding. Similarly, the number of force-enhanced labeling events should increase with increasing amounts of force until a saturating level of energy is obtained. If labeling does not increase in a dose-dependent manner, or occurs below

the minimum energy threshold, exposure of that cysteine was not force induced. For spectrin repeats, the probability of unfolding with a given amount of force is described by a force version of the Linderstrom-Lang (fLL) equation (Fig 1.4), where energy barriers to shear stress were determined from the collective single-molecule experiments.

Motivations

Becker Muscular Dystrophy provides insight into the molecular basis of spectrin repeat function

Duchenne Muscular Dystrophy (DMD) is a debilitating disease caused by exon deletions in the dystrophin gene (Chamberlain 2002). The resulting truncated protein is misfolded and degraded. Continued absence of dystrophin from the sarcolemma ultimately leads to tissue necrosis. Because of the protein's large size, efforts have been devoted to developing truncated 'mini' dystrophins for use in gene therapy (van Deutekom 2001). Most mini-dystrophin designs give priority to reestablishing the connection between the actin cytoskeleton and the DGC. The rod domain is considered expendable; the minimal numbers of repeat domains are included to act as a spacer between the actin binding domain (ABD) at the N-terminus and the DGC binding domain at the C-terminus (Sweeney 2000). Development of mini-dystrophins is largely a trial and error process. Biochemical techniques can be used to ascertain the structural stability of truncated dystrophins in solution. However, stability in static conditions or under thermal and chemical stress is not necessarily an accurate predictor of the dystrophin's stability under physical stress. Single molecule force microscopy can directly measure the structural stability of the repeat domains under shear, but not in the protein's natural setting. Most cell biology techniques indirectly assess mini-dystrophin function in the cell. Immunostaining showing localization of the mini-dystrophin to the muscle cell membrane is often classified as a successful treatment (Wang 2000), yet this

static view does not test the construct's performance during contraction. While animal models can be used to measure muscle performance after treatment (Yuasa 1998), these physiological tests do not offer molecular-scale insight into dystrophin folding, assembly, and function. A deeper understanding of dystrophin function would facilitate design of suitably truncated dystrophins and hasten their use in therapy.

Truncated dystrophins naturally occur in a milder form of muscular dystrophy, Becker muscular dystrophy (BMD) (England 1990). Both BMD and DMD are the result of deletions in the dystrophin gene. One important difference is the preservation of the genetic reading frame in BMD mutations, as opposed to the complete disruption caused by DMD mutations, and is the basis of antisense oligonucleotide (AON) therapy (Chamberlain 2002). In this therapy, the DMD mRNA reading frame is restored through additional, carefully selected, exon deletions. AONs are delivered to dystrophic muscle and bind selected exons in the pre-mRNA, resulting in excision by the spliceosome during processing. Restoration of the reading frame should produce a stably folded, presumably functional protein. Nevertheless, BMD has a wide range of phenotypes from completely asymptomatic to mildly better than DMD, suggesting that regaining the ability to translate the mutant gene is only one step in producing an adequate dystrophin replacement.

Though the genetic reading frame is restored, the preservation of the structural frame is unknown. Even if secondary structure is maintained, it is the tertiary packing of the alpha helices that is vital to dystrophin's ability to dissipate force during contraction. Non-native repeat domains, resulting from the truncation, would not have the same mechanical properties as the missing domains and therefore not compensate for that loss. Further changes in cooperative unfolding may disrupt the functionality of the

entire protein. Loss of cooperative unfolding decreases protein extension, weakening the actin-ECM connection. Conversely, enhanced cooperative unfolding decreases the energy the protein can absorb, resulting in transmission of that energy to the membrane and possible damage. Chapter Two of this thesis examines the diverse BMD phenotypes, which present natural case studies of "successfully designed" and "inadequately designed" truncated dystrophins. Cataloguing the qualities commonly found in asymptomatic or mild BMD dystrophins was done to discern which traits were necessary for function.

Altered network configuration of mutant red cell cytoskeletons demonstrate the importance of quaternary structure to spectrin mechanical function

Spectrin family proteins cannot function in isolation. Force is transferred through physical contacts to the network of cytoskeletal proteins. From the perspective of the individual protein, it is pulled at the ends connected to the network. From the perspective of the cell as a whole, it is sheared, and force must propagate from the site of strain to the proteins. For that reason proteins associated with members of the spectrin family are also important to force transmission, though they themselves may not unfold.

Hereditary elliptocytosis is a disease where red blood cell shape is perturbed due to mutations in cytoskeletal proteins. These mutations weaken the mechanical strength of the membrane, shortening the life-span of the cell. Malfunctions in the spectrin network are commonly the cause of the disease, though the molecular reasons for this are not clear (Gallagher 2004). Erythrocytic spectrin has two isoforms which heterogeneously dimerize, then form tetramers. These tetramers assemble into a mesh-like network, which is the source of red cell elasticity. The molecular basis for spectrin elasticity and how the above mutations lead to disease is controversial. One theory is that spectrin

tetramer association is broken and reformed, allowing the spectrin network to expand under shear (An 2002). Another theory purports that individual spectrin domains are unfolded in a force-dependent manner, which has recently been shown in red blood cell ghosts under shear stress (Johnson 2007). In both cases, these changes in conformation/association occur at short time-scales and only under shear. Because of spectrin's large size, most in vitro solution or force microscopy experiments looked at spectrin peptides and rarely approached the complexity of studying the spectrin tetramer, much less the spectrin network. Structural studies of spectrin within its cytoskeletal network under shear would provide the best information for determining the molecular basis of spectrin elasticity. It is also important to remember that network break down could also be caused by mutations in spectrin's associated proteins. Protein 4.1R is a cytoskeletal protein that links spectrin to the actin cytoskeleton and assembles membrane proteins such as glycophorin C, band 3, and p55. Red blood cells completely lacking protein 4.1R are osmotically fragile and more susceptible to shear stress. Thermal stability of 4.1R deficient red cells, which is directly related to spectrin stability, is normal (Tchernia 1981). Membrane strength and elasticity can be restored by addition of the 4.1R fragment containing the 4.1/actin/spectrin binding site, suggesting that physical linkage between spectrin and actin is more important to mechanical strength than the association integral proteins. Chapter Three describes use of the newly developed CS-MS technique to study unfolding of repeat domains as well as possible changes in spectrin tetramerization and associations in wild-type and 4.1R-null red cells, where the 4.1R-null red cells present a scenario cytoskeletal failure is caused by weakened network associations rather than faults in spectrin.

Embryonic muscle – a system to test spectrin repeat unfolding in nucleated cells.

Unlike red cells, which are sheared while suspended in fluid, most other tissue cells – from mesenchymal stem cells to myocytes and more – require adhesion to survive, and one recently appreciated facet of their force-function relationship is that matrix elasticity regulates and organizes the cytoskeleton. Generally, a stiff matrix leads to more stress fiber formation and a larger intracellular tension. It is generally believed that cells actively probe their surrounding matrix, and cytoskeletal proteins somehow help measure matrix elasticity, but even the qualitative description of this process is unclear. Does a cell apply a specific amount of force to its substrate and measure its internal deformation, or does a cell apply exert force on its substrate until a pre-decided deformation is achieved? The mode of force-sensing used by the cell may be developmental stage or tissue specific. CS-MS can be used to discriminate between modes; however the value of the CS-MS technique to is the ability to compare extent of labeling to known kinetic models such as the fLL equation. In order to apply the fLL equation to labeling studies, it is necessary to know the magnitude of the force applied to the cytoskeleton. For cells in solution, the force applied to the cytoskeleton can be assumed to be directly proportional to the shear stress applied to the bulk fluid. For adherent cells, that picture is much more complicated. Given the known interplay between cell and matrix, it can be argued that, at steady state the force exerted by the cell is proportional to the elasticity of the matrix; therefore the force experienced by the cytoskeleton is directly related to the actomyosin contractility. Unfortunately, this relationship is set after cytoskeletal remodeling and the initial steps of force sensing have past. At the outset of force sensing, a cell likely uses the disparities between the force applied and the force received to recognize the suitability of its matrix stiffness, so using techniques such as traction force microscopy to measure force output would not necessarily capture what is being sensed by the cell during the release. The challenge is

how can dynamic changes in applied force and sensed force be measured or controlled within a cell in an experimental setting.

The embryonic cardiac muscle system contains virtually all the qualities necessary for an experimental system that can probe force-induced conformational changes in a controlled manner. To begin with, the molecular mechanism behind excitation-contraction coupling is very well characterized. The proteins involved, their functions, and their partners are known. Secondly, the mechanical relationship between the generation of force and output of work is mathematically described in the Hill's equations for muscle, from which the forces exerted by the cell can be assessed by easily measurable traits like contraction velocity. Finally the process of cardiogenesis has also been extensively studied, and changes in continued development provide an easily detected readout of the cumulative forces sensed inside the cell. Previous work with embryonic avian cardiomyocytes has already shown that culture on elastic substrates affect the work efficiency during contraction (Fig 1.5), leading to changes in internal strain (Fig 1.6), and finally resulting in differences in beating behavior and myofibril assembly (Engler 2008). Detailed analysis of such data, coupled with the breadth of pre-existing biochemical and biophysical knowledge, will furnish a quantitative description of the forces experienced by the cytoskeleton at the onset, during, and after contraction. Use of younger, stem-cell derived cardiomyocytes (SCD-CM) would improve these studies, as the simplified contractile machinery enables a more straightforward analysis. Development of this experimental system consisting of embryonic and SCD-CM on polyacrylamide gels, as well as preliminary CS-MS studies is portrayed in Chapter Four of this work.

References

An X, Guo X, Zhang X, Baines AJ, Debnath G, Moyo D, Salomao M, Bhasin N, Johnson C, Discher D, Gratzer WB, Mohandas N. (2006) Conformational stabilities of the structural repeats of erythroid spectrin and their functional implications. J Biol Chem. 281(15):10527-32.

An X, Lecomte MC, Chasis JA, Mohandas N, Gratzer W. (2002) Shear-response of the spectrin dimer-tetramer equilibrium in the red blood cell membrane. J Biol Chem. 277(35):31796-800.

Bhasin N, Law R, Liao G, Safer D, Ellmer J, Discher BM, Sweeney HL, Discher DE. (2005) Molecular extensibility of mini-dystrophins and a dystrophin rod construct. J Mol Biol. 352(4):795-806.

Bois PR, Borgon RA, Vonrhein C, Izard T. (2005) Structural dynamics of alpha-actinin-vinculin interactions. Mol Cell Biol. 25(14):6112-22.

Broderick MJ, Winder SJ. (2005) Spectrin, alpha-actinin, and dystrophin. Adv Protein Chem. 70:203-46.

Chamberlain, J. S. (2002). Gene therapy of muscular dystrophy. Hum. Mol. Genet. 11, 2355–2362.

Discher DE. (2000) New insights into erythrocyte membrane organization and microelasticity. Curr Opin Hematol. 7:117–122.

Discher DE. New insights into erythrocyte membrane organization and microelasticity. Curr Opin Hematol. 2000;7:117–122.

Djinovic-Carugo K, Gautel M, Ylänne J, Young P. (2002) The spectrin repeat: a structural platform for cytoskeletal protein assemblies. FEBS Lett. 513(1):119-23.

England SB, Nicholson LV, Johnson MA, Forrest SM, Love DR, Zubrzycka-Gaarn EE, Bulman DE, Harris JB, Davies KE. (1990). Very mild muscular dystrophy associated with the deletion of 46% of dystrophin. Nature, 343, 180–182.

Engler AJ, Carag-Krieger C, Johnson CP, Raab M, Tang HY, Speicher DW, Sanger JW, Sanger JM, Discher DE. (2008) Embryonic cardiomyocytes beat best on a matrix with heart-like elasticity: scar-like rigidity inhibits beating. J Cell Sci. 121(Pt 22):3794-802.

Haenggi T, Fritschy JM. (2006) Role of dystrophin and utrophin for assembly and function of the dystrophin glycoprotein complex in non-muscle tissue. Cell Mol Life Sci. 63(14):1614-31.

Johnson CP, Tang HY, Carag C, Speicher DW, Discher DE. (2007) Forced unfolding of proteins within cells. Science. 317(5838):663-6.

Koenig M, Kunkel LM. (1990) Detailed analysis of the repeat domain of dystrophin reveals four potential hinge segments that may confer flexibility. J Biol Chem. 265(8):4560-6.

Kusunoki H, Minasov G, Macdonald RI, Mondragón A. (2004) Independent movement, dimerization and stability of tandem repeats of chicken brain alpha-spectrin. J Mol Biol. 344(2):495-511.

Law R, Liao G, Harper S, Yang G, Speicher DW, Discher DE. (2003a) Pathway shifts and thermal softening in temperature-coupled forced unfolding of spectrin domains. Biophys J. 85(5):3286-93.

Law R, Carl P, Harper S, Dalhaimer P, Speicher DW, Discher DE. (2003b) Cooperativity in forced unfolding of tandem spectrin repeats. Biophys. J. 84: 533–544.

Le Rumeur E, Winder SJ, Hubert JF. (2010) Dystrophin: more than just the sum of its parts. Biochim Biophys Acta. 1804(9):1713-22.

Mohandas N, Evans E. (1994) Mechanical properties of the red cell membrane in relation to molecular structure and genetic defects. Annu Rev Biophys Biomol Struct. 23:787–818.

Ortiz V, Nielsen SO, Klein ML, Discher DE. (2005) Unfolding a linker between helical repeats. J Mol Biol. 349(3):638-47.

Ozawa E, Yoshida M, Suzuki A, Mizuno Y, Hagiwara Y, Noguchi S. (1995) Dystrophin-associated proteins in muscular dystrophy. Hum Mol Genet. 4 Spec No:1711-6.

Petrof BJ, Shrager JB, Stedman HH, Kelly AM, Sweeney HL. (1993) Dystrophin protects the sarcolemma from stresses developed during muscle contraction. Proc Natl Acad Sci U S A. 90(8):3710-4.

Petrof BJ, Shrager JB, Stedman HH, Kelly AM, Sweeney HL. (1993) Dystrophin protects the sarcolemma from stresses developed during muscle contraction. Proc Natl Acad Sci U S A. 90(8):3710-4.

Prasain N, Stevens T. (2009) The actin cytoskeleton in endothelial cell phenotypes. 77(1):53-63.

Prasain N, Stevens T. (2009) The actin cytoskeleton in endothelial cell phenotypes. 77(1):53-63.

Rief M, Pascual J, Saraste M, Gaub HE. (1999) Single molecule force spectroscopy of spectrin repeats: low unfolding forces in helix bundles. J Mol Biol. 286(2):553-61.

Rybakova IN, Humston JL, Sonnemann KJ, Ervasti JM. (2006) Dystrophin and utrophin bind actin through distinct modes of contact. J Biol Chem. 281(15):9996-10001.

Sjöblom B, Salmazo A, Djinović-Carugo K. (1995) Alpha-actinin structure and regulation. Cell Mol Life Sci. 65(17):2688-701.

Sweeney HL, Barton ER. (2000) The dystrophin-associated glycoprotein complex: what parts can you do without? Proc Natl Acad Sci U S A. 97(25):13464-6.

Tchernia G, Mohandas N, Shohet SB. (1981) Deficiency of skeletal membrane protein band 4.1R in homozygous hereditary elliptocytosis. Implications for erythrocyte membrane stability. J Clin Invest. 68(2):454-60.

Wang B, Li J, Xiao X. (2000) Adeno-associated virus vector carrying human minidystrophin genes effectively ameliorates muscular dystrophy in mdx mouse model. Proc Natl Acad Sci U S A. 97(25):13714-9.

Yuasa K, Miyagoe Y, Yamamoto K, Nabeshima YI, Dickson G, Takeda SI. (1998). Effective restoration of dystrophin-associated proteins in vivo by adenovirus-mediated transfer of truncated dystrophin cDNAs. FEBS Letters, 425, 329–336.

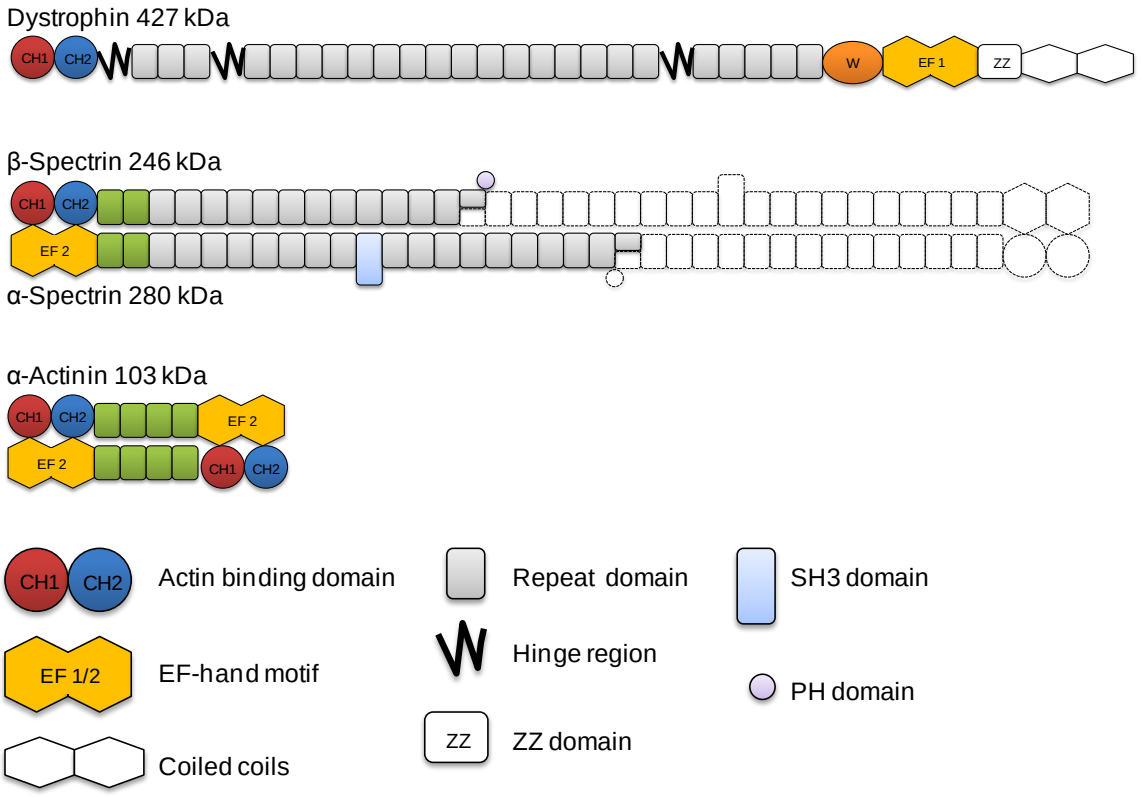

Figure 1.1: Structure of spectrin superfamily proteins.

Spectrin family proteins are comprised of modular domains. The dashed lines indicate how two spectrin heterodimers interact to form a functional spectrin tetramer. Utrophin is very similar structurally to dystrophin except has fewer repeat domains. Numbers in the EF hand regions represent the number of EF hand motifs. Figure was adapted from Broderick et. al.

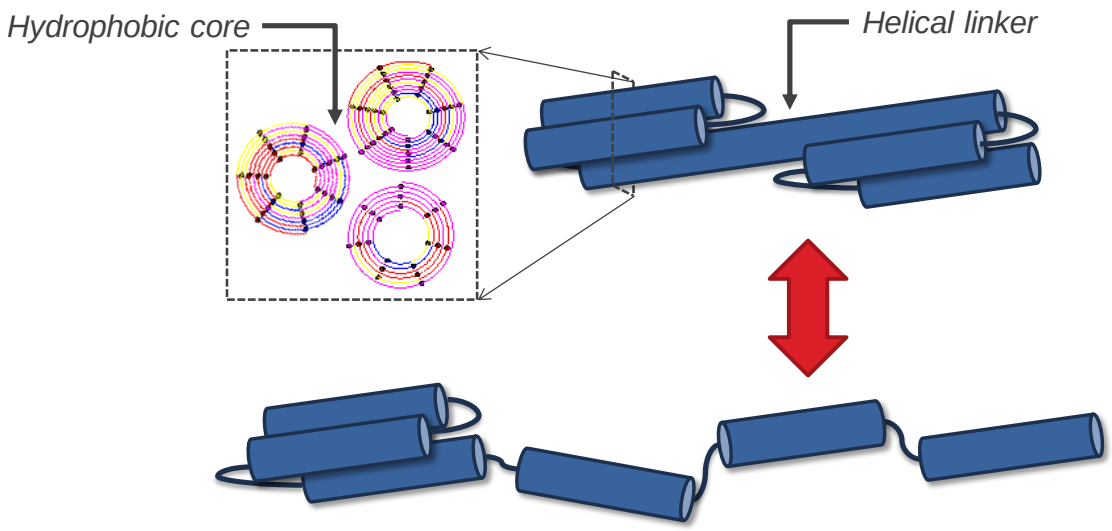

Figure 1.2: Schematic of the spectrin repeat domain

Spectrin repeat domains are defined as three helix bundles held together by hydrophobic interactions. When this domain is stressed, the helices dynamically dissociate and reassociate. The helical linker connecting adjacent domains may confer cooperative unfolding if helicity is maintained. However, the stability of linker structure in physiological conditions is not known.

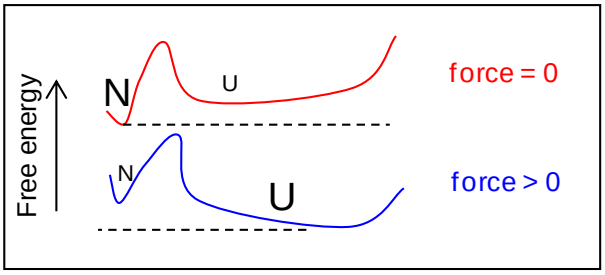

$$N \underset{k_r e^{f\cdot\Delta x'/k_B\cdot T}}{\overset{k_f e^{f\cdot\Delta x/k_B\cdot T}}{\rightleftharpoons}} U \xrightarrow{k_2\cdot c} P$$

$$P(t) = Ck_2k_{1f}e^{f}\left(\frac{e^{-\frac{1}{2}t\left(k_2+k_{1f}e^{f}+k_{1r}e^{f'}-\sqrt{A}\right)}}{\sqrt{A}\left(-\frac{1}{2}k_2-\frac{1}{2}k_{1r}e^{f'}-\frac{1}{2}k_{1f}e^{f}+\frac{1}{2}\sqrt{A}\right)} - \frac{e^{-\frac{1}{2}t\left(k_2+k_{1f}e^{f}+k_{1r}e^{f'}+\sqrt{A}\right)}}{\sqrt{A}\left(-\frac{1}{2}k_2-\frac{1}{2}k_{1r}e^{f'}-\frac{1}{2}k_{1f}e^{f}-\frac{1}{2}\sqrt{A}\right)}\right)+C$$

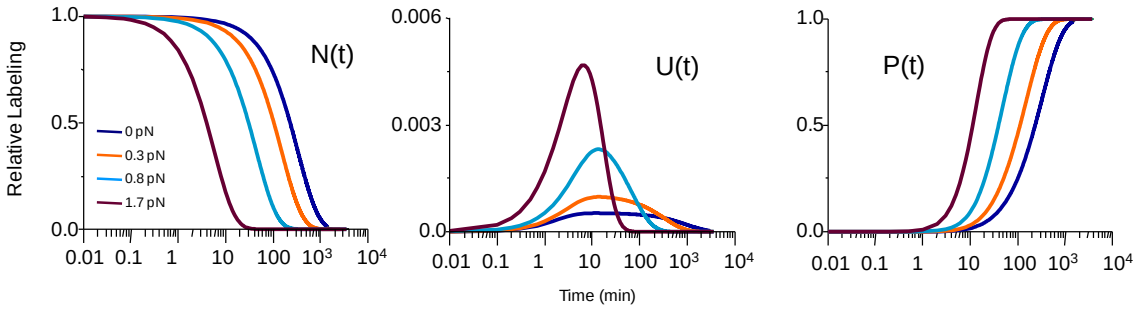

Figure 1.3: Force-dependent Linderstrom-Lang Equation

According to the model, after repeat unfolding, the domain can either refold, burying the cysteine, or remain unfolded long enough for the buried cysteine to be labeled. Under static conditions, the repeat domain will most likely refold. Addition of force shifts the equilibrium from the refolded to unfolded state, increasing the possibility that the buried cysteine will be labeled. Data from biochemical and single molecule unfolding studies were used provide values for the constants in the equation.

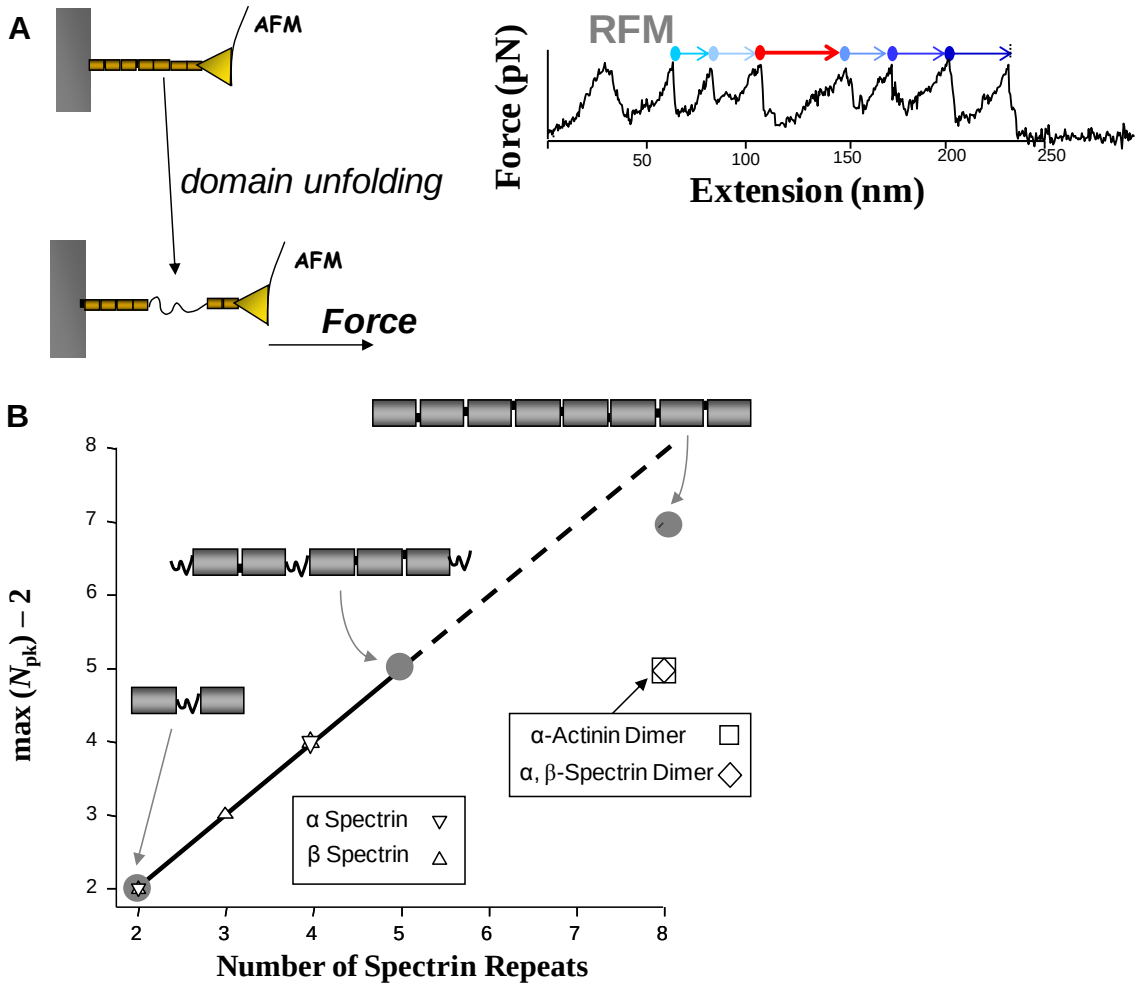

Figure 1.4: Cooperative unfolding in hinged and hinge-free rod domains

(A) Representative multidomain protein extended using AFM. Pulling stochastically unfolds one or more domains. Tandem unfolding is seen in the force-curve as a saw tooth pattern where one peak-to-peak distance is ~2x greater than the others. (B) The *max(N_{pk}) - 2* should match the number of domains in the construct if all domains unfold independently. For rod domains containing hinges, the unit slope indicates that the maximum contribution to the sawtooths is one peak per repeat. Dystrophin RFM, lateral dimers of α, β-spectrin as well as α -actinin, falls just below the trend line clearly indicating tandem repeat unfolding is a common occurrence.

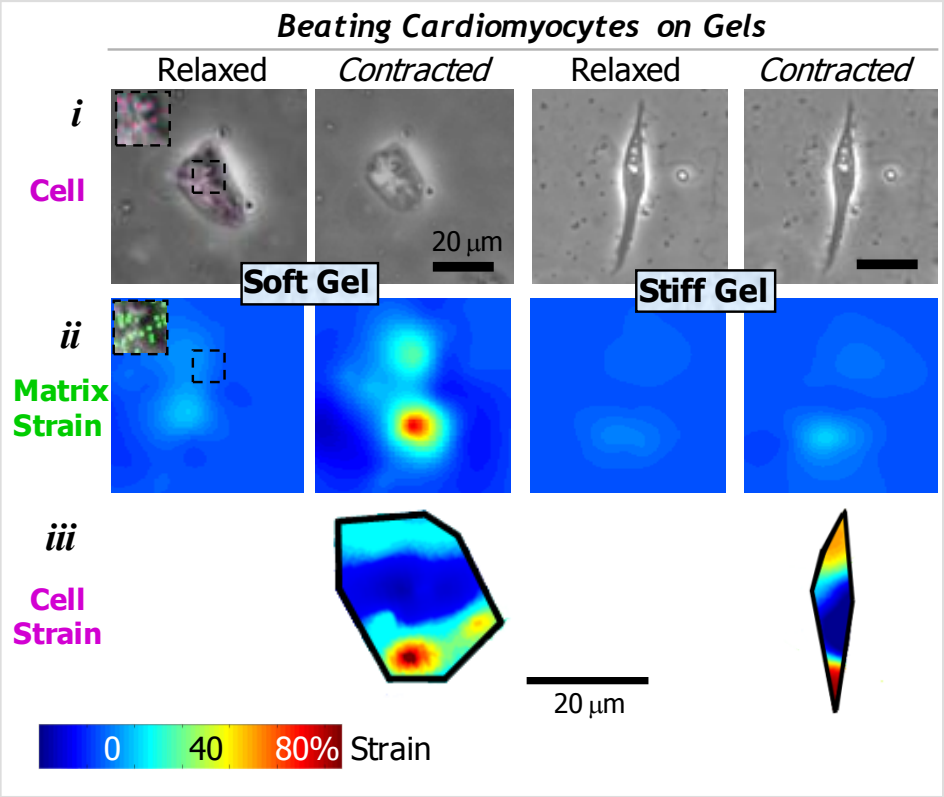

Figure 1.5: Cardiomyocyte and matrix contraction

(A) Cells were imaged in brightfield 3-5 μm above the cell-matrix interface (top panels) and in fluorescence at the cell-matrix interface to observe particle motion during contraction (see inset pseudo-colored beads) in order to determine cellular and matrix deformations, respectively. Note the difference in matrix strain between soft and stiff matrices reflected by decreased deformation (indicated by dashed lines). Figure was adapted from Engler et. al.

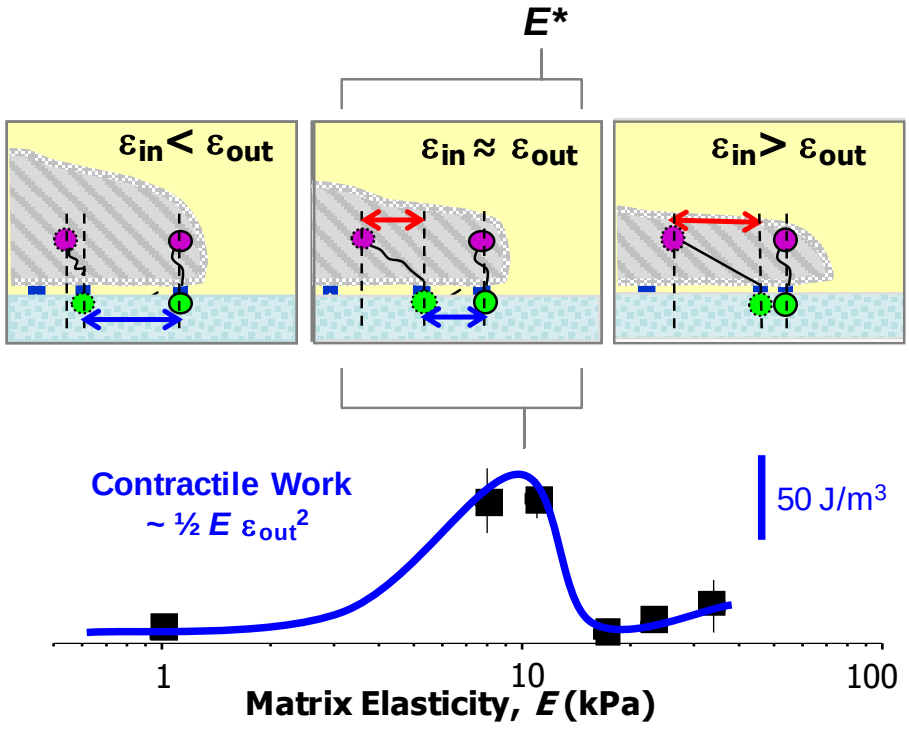

Figure 1.6: Schematic of strained states for soft gels, *E gels, and stiff gels**

While cardiomyocytes on soft gels are greatly deformed during contraction, they have the least intracellular strain. Rather, intracellular strain is greatest on stiff gels where matrix deformation is the least. The contractile 'work' done by cardiomyocytes on the substrate peaks at *E**. Figure was adapted from Engler et al.

CHAPTER TWO

Domain structure of exon-skipped dystrophins designed for treatment of Duchenne muscular dystrophy: cooperativity in forced unfolding as a key design parameter

Cytoskeleton. 2010 67(12):796-807.

Nishant Bhasin helped with experiments. Manu Tewari helped with design on nano-dystrophin constructs. Dan Safer and H. Lee Sweeney supervised protein expression and purification.

Abstract

Force-bearing linkages between the cytoskeleton and extracellular matrix appear important to normal cell viability with a disease such as Duchenne muscular dystrophy (DMD) arising in the absence of the linkage protein dystrophin. Emerging therapeutic efforts for DMD use antisense-mediated skipping of exons to delete nonsense mutations while maintaining reading frame, but the structure and stability of the resulting proteins are not well understood. Here we express and physically characterize dystrophin 'nano'-constructs based on multi-exon deletions that might find use in a large percentage of DMD patients. The primary structure challenge with spliced proteins is addressed first

with Liquid Chromatography Tandem Mass Spectrometry (LC-MS/MS) which is shown capable of detecting tryptic peptides from 53 of dystrophin's 79 exons. Folding predictions for the nano-constructs show novel helical bundle domains can arise out of exon-deleted 'linkers', and secondary structure analyses in solution indeed suggest high helicity with melting temperatures well above physiological (T_m ~ 55-65°C). Extensional forces with an Atomic Force Microscope (AFM) nonetheless unfold the nano-constructs, and the ensemble of unfolding trajectories reveal the number of folded domains per construct, proving consistent with tertiary structure predictions. A mechanical cooperativity parameter for unfolding of tandem repeats is also introduced as the best predictor here of a multi-exon deletion that is asymptomatic. The results thus provide initial insight and confidence in designs with multi-exon deletions.

Introduction

Dystrophin constitutes a critical link between the force-generating cytoskeleton in muscle and the extracellular matrix (Fig. 2.1A). Mutations that block expression of dystrophin lead to DMD, while mutations – including exon deletions – that shorten dystrophin's central rod domain can lead to more mild forms of Becker muscular dystrophy (BMD) or else prove asymptomatic. Dystrophin's rod domain normally consists of two-dozen three-helix bundle domains that are the repeated domains in ubiquitously expressed spectrin superfamily proteins. In red blood cells, these spectrin repeats have been shown to unfold when cells are mechanically sheared at physiological fluid shear stresses (Johnson 2007), and single molecule extension by Atomic Force Microscopy (AFM) has also shown that spectrin and dystrophin repeats unfold under similar forces (Bhasin 2005). However, the structure and stability of dystrophin

deletants have been studied only to a limited extent, mostly in solution (Kahana 1997; Ruszczak 2009), even though emerging therapeutic efforts for DMD involve antisense-mediated deletion of multiple exons within the DMD gene's 79 exons in order to skip nonsense mutations and maintain reading frame.

Combinations of antisense oligonucleotides (AONs) that target multiple exons (e.g. Δ44-54, Fig. 2.1B) can be problematic in application due in part to inefficient skipping (Aartsma-Rus 2006; Aartsma-Rus 2007), but one such AON cocktail has been theorized to rescue up to 63% of DMD patients by transforming the DMD phenotype into an asymptomatic or mild BMD phenotype (Béroud 2007). Human clinical trials with a single AON designed to skip exon 51 (van Deutekom 2007) lead to modest levels of protein (<35% of normal controls) using standard antibody approaches that remain state of the art in expression analysis (Freund 2007), but the limited availability of antibodies can be constraining if one needs to assess expression from every exon. Multi-exon deletion studies would benefit from such assessments, and initial efforts at proteomic profiling of dystrophin in muscle suggest detectability (Lewis 2009). Here we address this primary structure issue by Liquid Chromatography Tandem Mass Spectrometry (LC-MS/MS), and we then assess the secondary and tertiary structure of dystrophin deletants.

Exon deletions of potential interest for treating patients (Table 2.1) generally disrupt the spectrin-like repeats since exons and repeats possess distinct phasing (Fig. 2.2). Truncated dystrophins might nonetheless fold to form novel repeat domains that contribute protective properties of the full-length protein, but proper insight into what constitutes functional dystrophin structures could help guide AON-achievable designs. Proline-rich 'hinge' regions (H2, H3) appear unique to dystrophin when compared to

spectrins and have been assumed to be unfolded, but there is evidence that H3 can mechanically couple repeats (Bhasin 2005). Structure and stability have traditionally been studied in solution with chemical denaturants and temperature changes, but single molecule AFM studies allow one to apply more relevant mechanical forces. Most AFM studies in the past have focused on obtaining deeper insight into known folded structures, whereas the goal here was to obtain insight into unknown structures. Here, homology modeling based on spectrin type repeats was used to predict the folding of domains that result from key exon deletions, and then domain structures and stability were assessed by thermal denaturation and AFM, with the latter providing insight into the number of folded domains and linker or hinge regions. We examined truncated dystrophins that naturally occur in BMD plus a truncated dystrophin not yet found in any patients but predicted to yield stably folded domains.

Materials and Methods

Mass Spectrometry

C2C12 myoblasts were cultured by established methods (e.g. Engler 2004) and differentiated for 14 days. C2C12 lysates were prepared for standard 1D-SDS-PAGE followed by in-gel trypsinization on the 460 kDa band that was then submitted for MS/MS following standard methods (Engler 2008).

Structural predictions

The helical content of nano-constructs was predicted using Psi Pred as described previously (Bhasin 2005). The hydrophobic packing of the helices was determined manually with helical wheel predictions that often indicated a hydrophobic core upon

packing of the helices into a spectrin-like helical bundle domain. Homology prediction in conjunction with secondary structure predictions suggest that linking regions are purely helical and may fold into respective modular "molten" globules.

Plasmid Construction and Protein Preparation

Becker-based mini-dystrophin constructs were made by PCR, using the native central rod fragment of dystrophin as a guide. A start codon-embedded NdeI site, an additional stop codon, and an EcoRI site were engineered into PCR primers such that the PCR product could be subcloned into expression vector pMW172. Construct R15~L4~R23 only included a His-tag. Non-native splice sites in each construct are indicated by ~.

Resulting plasmids were used to transform *Escherichia coli* strain BL21 (Star)DE3 (Invitrogen). Bacteria were grown at 37°C in Luria-Bertani medium with 200 μg/ml of ampicillin, to an A_{600nm} of 0.8–1.0, and expression was induced by addition of 1 mM isopropyl-β-D-thiogalactoside. After 3–4 h, cells were harvested by centrifugation at 5000g for 10 min and frozen in liquid N_2. The frozen cell pellet (~10 ml, from 2 L of culture) was thawed for 10 min at 25°C and lysed by resuspension in 40 ml of Cellytic B (Sigma-Aldrich) containing 1 mM phenylmethylsulfonyl fluoride, 10 mg/ml of leupeptin, and 10 mg/ml of aprotinin. After 15 min at 25°C, the cell lysate was clarified by centrifugation at 45,000g for 15 min; centrifugation and all subsequent steps were performed at 4°C. For constructs R16~L1~R21, R18~L2~R21, and R15~L3~R23, the supernatant was loaded onto a DEAE-cellulose column (Whatman DE-52, 2.5 cm × 30 cm) pre-equilibrated with 20 mM Hepes (pH 7.0), 1 mM dithiothreitol, 1 mM sodium azide, and eluted at 35 ml/h with a 325 ml × 325 ml gradient of 0–0.5 M sodium chloride in Hepes buffer; fractions were collected at 12 min intervals. The expressed

protein, identified by SDS-PAGE, eluted about halfway through the gradient. Solid ammonium sulfate was added to the pooled peak fractions to a final concentration of 1.6 M, and the material was applied to a 1.5 cm × 30 cm column of Butyl ToyoPearl 650 M (Tosoh Bioscience) in 1.6 M ammonium sulfate, 20 mM Hepes (pH 7.0), 1 mM dithiothreitol, 1 mM sodium azide. The column was eluted at 10 ml/h with a descending gradient of 1.6 M–0 M ammonium sulfate in 150 ml. Fractions were collected at 10 min intervals, and fractions containing the purified protein were identified by SDS-PAGE, pooled, and dialyzed against 100 volumes of phosphate buffered saline, with two changes. For construct R15~L4~R23 a final concentration of 6 M urea was added to crude lysate, and the cell pellet was resuspended in 6 M urea and centrifuged at 45,000g for 15 min 3×. Crude lysate and urea washes were combined and applied to a Ni-NTA Superflow column. Protein was eluted according to manufacturer's instructions. Concentration was determined from the A280 nm using an extinction coefficient of 1.313 at 1 mg/ml, calculated from the amino acid composition.

Following similar methods (Bhasin 2005), stable monomer was ultimately purified by gel permeation chromatography in phosphate-buffered saline (PBS) and kept on ice for AFM studies. Immediately before use, any protein aggregates were removed by centrifugation 2°C for 1 hour; and monodispersity was verified by dynamic light scattering.

Circular Dichroism Measurements

Circular dichroism spectra were measured and analyzed as before (Bhasin 2005) at a number of temperatures using a 1 mm path length cell on a Jasco J715 spectropolarimeter in the same buffer (PBS, pH 7.4) as that used in the AFM experiments. The instrument was calibrated with d-10-camphorsulfonic acid. Samples

were equilibrated at each temperature for 20 min before taking measurements. Each spectrum was the average of three measurements. Circular dichroism spectra for each nano-construct were also measured at 25 °C with 40% v/v TFE.

Fluorescence Spectroscopy

All tryptophan fluorescence experiments were carried out as described elsewhere (Johnson 2007b) using a UV fluorometer from Photon Technology Instruments with a set excitation wavelength of 275 nm. The emission spectrum was monitored between 310-370 nm for each scan. Samples consisted of 480 µL of PBS buffer (pH=7.5) and 20 µL of 1 mg/mL protein utilizing a 1 mL cuvette with 1cm path length. Temperature scans from 21-80 °C were collected at 2°C increments with appropriate time to thermoequilibriate at each temperature. A blank buffer sample spectrum was also collected for background subtraction. Emission intensities at 350 nm were analyzed using the previously reported methods.

Atomic Force Spectroscopy

50 µl of 0.1 mg/ml protein solution was adsorbed on freshly cleaved mica for 30 min at room temperature per (Bhasin 2005). All measurements were carried out in PBS using a Nanoscope-E Multimode AFM (Digital Instruments, Santa Barbara, CA) equipped with a liquid cell. Sharpened silicon nitride (Si_3N_4) cantilevers (Park Scientific, Sunnyvale, CA) of nominal spring constant k_C = 10 pN/nm were typically used, with equivalent results obtained using 30 pN/nm cantilevers. k_C was measured for each cantilever using the manufacturer's directions at each temperature, and additional calibrations were performed as described previously. Experiments were done at imposed displacement rates of 1 nm/msec = 1 µm/sec. Thousands of surface to tip contacts were collected and

analyzed with the aid of a semi-automated, visual analysis program custom written in C++. Since protein unfolding events are stochastic and the experiment intrinsically random in many ways, collecting and analyzing thousands of peaks is necessary to provide an accurate statistical survey of extensible unfolding. Initial results at the beginning of a many hour experiment were similar to those obtained at the end of the experiment. Force spectrograms, or sawtooth patterns for each construct were analyzed by categorizing each according to the number of peaks (N_{pk}) as well as peak-to-peak lengths ($l_{pk\text{-}pk}$).

Results

Mass Spectrometry Mapping of Dystrophin Primary Structure

As AON (and RNAi) therapies emerge, there is an increasing need to detect and even quantify proteins with complex splicing patterns. Evidence of changes in RNA from RT-PCR or other methods is simply not sufficient and antibody-based methods do not always yield the same results; in the cited human trials, for example, the efficiencies of exon skipping ranged from 49 to 90% for four patients while the amount of dystrophin in total protein extracts (with one antibody in Westerns) ranged from 3 to 12% of that found in a control specimen and from 17 to 35% for the immunofluorescent intensity ratio of dystrophin to laminin α2 relative to control (van Deutekom 2007). LC-MS/MS has emerged over the last decade as a powerful new method to conduct protein mapping of tryptic peptides, and it is used here to map dystrophin primary structure and perhaps provide some realism to detailed protein analyses of multi-exon deletions that are likely to be needed for patients.

Multiple dystrophin peptides were detected in 4 of 5 LC-MS/MS studies of lysates from myotube cultures (see methods). Primary structure coverage of dystrophin in each run ranged from 3-20%, with a combined sequence coverage of 27%, and the 57 detectable peptides appear cumulatively scattered throughout the entire length of protein (Fig. 2.2). Indeed, when mapped back into the 79 exons that transcribe full-length dystrophin, 53 exons (or 67%) yield detectable tryptic peptides. These cumulated MS results could certainly supplement immunodetection of exon-deleted forms of dystrophin; for example, in the four deletion constructs considered next, all yield peptides from exons that are immediately upstream and downstream of the deletion or else just one exon removed, and all but two of the deleted exons also yield detectable peptides. Because multiple AON's need to act on the same pre-mRNA in order to achieve the desired multi-exon skipping, the ability to detect peptides from supposedly deleted exons is necessary to troubleshoot the fidelity of splicing and to know the primary structure or protein or, very possibly, protein spliceoforms actually expressed in patients treated with multiple AONs.

Dystrophin nano-constructs and Structural predictions

DMD-causing mutations in a representative database (Fokkema 2005) are summarized in Table 2.1 together with exons that would be targeted if these specific patients were to undergo AON-therapy. Percentages of DMD patients that have mutations in the deleted exons and would therefore have the same truncated dystrophin are also shown together with an indication of predicted phenotype (e.g. mild BMD), assuming that exon skipping works perfectly. There are many combinations of mutations and therapeutic deletions but only a handful of truncated dystrophins are functionally in-frame as illustrated with Δ45-51 which is the truncated dystrophin for four different DMD mutations. We

designed nano-constructs of dystrophin (Fig. 2.3) based on four representative deletions: Δ49 has a typical BMD phenotype, Δ44-54 has a milder BMD phenotype, Δ45-51 is completely asymptomatic, and Δ42-55 has not been found in any patients so far but is predicted to be in-frame.

In most types of structural studies of large proteins such as dystrophin, signals from the bulk of the protein dominate the signal from any key region of interest, and so nano-constructs were designed here to maintain phasing with at least one repeat on either side of the deletion-created 'linker' region of unknown structure (Table 2.2). This linker region is the site where two dystrophin domains are spliced together as a result of exon deletion; for example, L1 in the nano-construct R16~L1~R21 results from deletion of exons 45-51 (Fig. 2.3A). We distinguish normal from abnormal sequence, respectively, with '-' versus '~'. Secondary structure and tertiary structure predictions were done on each linker region to assess whether: (i) the linker region can fold into a stable repeat domain, or (ii) folding of the linker domain might disrupt folding of native neighboring domains. In the former case, the number of amino acids seems important: the linker region in construct R16~L1~R21 (Fig. 2.3B) has a contour length well within the range of a single repeat domain, whereas L2 in construct R18~L2~R21 appears long enough to fold into two domains. Interestingly, L2 does not result from splicing together of two repeat domains but instead results from splicing of a single repeat to the hinge H3 (Fig. 2.1A), which has been shown to be helical (Bhasin 2005) but not necessarily folded into a stable tertiary structure. In contrast, linker L3 in construct R15~L3~R23 is too long for two repeat domains but falls short of forming three repeat domains, and L4 in R15~L4~R23 is much too short for even one repeat domain (Fig. 2.3C, D). This alone is not alarming because long helical linker regions between repeat domains are

characteristic for this protein. In general, the helical content in the linker regions appears preserved, and tertiary folding through bundling of helices is driven by the need to shield hydrophobic patches. This occurs in L1, where one helix from repeat 17 easily substitutes for the missing helix in repeat 20.

L2 proved an interesting case where the tertiary structure prediction shows warping or twisting in one of the novel repeat domains, most likely due to the flexibility of the hinge region. Despite, or perhaps because of, the flexibility in the hinge region, L2 was able to fold into two repeat domains. L3 was also able to fold into two repeat domains as well as a smaller, helical domain. The smaller domain formed between the two non-native repeat domains and is the residual of repeat 21. Its tertiary structure shields the hydrophobic patches that were exposed after removal of the majority of repeat 21. L4 had a similar problem where it was not long enough to form a full repeat domain. Only two of the three helices from repeat 22 remained. According to the "in-frame" model, repeats 15 and 23 in R15~L4~R23 were still in phase and should remain stable. One of the drawbacks of the structure predictions is that, due to the pre-existing helical nature of the peptide, the predictions will be biased towards giving the linker region a helical structure. However, doing so exposes hydrophobic patches on the helices, and whether that perturbation is strong enough to create a novel domain, as shown in L3, and whether that domain is stable under force must be determined experimentally.

Solution studies by Circular Dichroism

CD was used to measure thermal stability of the nano-constructs and to then estimate their helical content (e.g. Fig. 2.7). Melting temperature (Tm) provides a simple metric of thermal stability even though physiological temperatures rarely differ from 37°C, and

we find that the melting temperatures of R16~L1~R21 and R18~L2~R21 (Table 2.3) are both very close to the Tm reported for the full-length rod domain (Kahana 1997). R15~L3~R23 and R15~L4~R23 had slightly lower Tm, but all constructs should be highly stable at physiological 37°C.

For helicity determinations at 37°C, CD was done in PBS with or without trifluoroethanol (TFE), which tends to stabilize helical structure to a maximum value less than 100% helicity. One hypothesis was that linker structures might not be especially stable in PBS at physiological temperature, and TFE might therefore increase %-helicity. Three of the four nano-constructs showed %-helicity well above 50%, consistent with a mostly helical bundle structure. With TFE, the asymptomatic nano-construct R16~L1~R21 showed the greatest helicity and the biggest change relative to PBS, but the fact that this deletant is asymptomatic in humans suggests this physically measurable difference in secondary structure is not critically important to structure-function. The R15~L4~R23 showed the lowest %-helicity overall, but %-helicity in TFE could not be determined because of TFE-induced aggregation; whether the low helicity was due to L4 being a random coil thus could not be determined.

Tryptophan fluorescence can be used to assess changes in solvated structure prior to or during complete unfolding. With R15~L4~R23, aggregation was again a problem. Two of the other three constructs showed Tm similar to those found by CD, but for R15~L3~R23 the Tm appeared near physiological temperature, indicating that for a significant fraction of this construct's ten Trp's solvent exposure changes at physiological temperature. Two Trp's at the ends of repeats are predicted in modeling to be solvent exposed (thus constant signal). Four Trp's located in L3 (Fig. 2.3C) likely account for 50% of changes in signal intensity, and we speculate that these Trp's become exposed to

solvent at lower temperature than the hydrophobic tryptophans sequestered in wild type dystrophin repeats 15 and 23 because the latter repeats have been recently expressed and reported to unfold with Tm ~ 65°C (Mirza 2010). CD and Trp fluorescence measurements therefore suggest that wild-type repeat domains induce helicity in L3 but these adjacent bundles have little influence on bundling into a physiologically stable tertiary structure.

Domain counts and lengths by Forced extension

AFM was used to determine the number of unfoldable domains as well as the mechanical forces required to unfold stably folded domains. In such single molecule forced extension studies of spectrin family helical bundle proteins (Rief 1999; Law 2003; Bhasin 2005), domains unfold in a stochastic fashion with force spectrograms appearing as sawtooth patterns (Fig. 2.4, top). Such sawtooth patterns from tip retractions are unique to protein unfolding since other materials such as carbohydrates (Marszalek 2003) and synthetic polymers (Sun 2005) all reportedly show simpler, monotonic, stretching patterns. Thousands of pulling events here provide statistical fingerprints of mechanical unfolding for each nano-construct. If all of the predicted domains are stable, then the maximum number of peaks, max(Npk), seen in a large ensemble of force spectra would match the number of predicted domains plus two (Law 2003); the 'two' accounts for tip desorption events at the beginning and end of a force pull and is based on systematic studies of multiple 2, 3, and 4 spectrin repeat constructs. For the deletion constructs of dystrophin tested here (Fig. 2.4, bottom), the AFM data thus indicates three domains in R16~L1~R21, four domains in R18~L2~R21, and five domains in R15~L3~R23 – which are all in remarkable agreement with the tertiary structure predictions.

The force to a unfold a protein domain depends in general on the log of the extension rate, and rates of muscle sarcomere contraction of order ~μm/sec suggest an extension rate of this magnitude is physiologically reasonable to apply. Past studies of forces to unfold spectrin repeats have revealed unfolding forces in the range of ~20-40 pN (Rief 1999; Law 2003; Bhasin 2005), and the results here (Fig. 2.4, top) appear very similar in magnitude.

The peak-to-peak length (lpk-pk) represents the extension of an unfolded domain before the next domain is stressed to unfold and it therefore defines a domain unfolding length. Furthermore, adjacent domains might be sufficiently coupled to sometimes unfold in tandem – as documented with doubled lengths for various constructs of spectrins (Law 2003) as well as an R8-R15 dystrophin (Bhasin 2005). R16~L1~R21 was the one nano-construct here in which tandem unfolding pathways appear distinct as well as frequent: the cumulated histogram of lpk-pk (Fig. 2.5A) shows a significant number of events for this deletion construct in which unfolding lengths appear at twice the unfolding length of ~20 nm that is typical of a single repeat domain (Law 2003; Bhasin 2005). The widths of all distributions here are noticeably broader than those cited for single repeats. The increased widths highlight the greater diversity of pathways for extending these constructs with possibilities for unfolding 'linker' domains separately or in tandem with canonical repeats.

The greater the number of peaks observed in a sawtooth pattern, the longer the total extension (Fig. 2.4A, top; Fig. 2.5B), even though sawtooths with very large Npk are rare. The length limits calculated as contour lengths from the number of residues (gray regions in Fig. 2.5B; sums in Table 2.2) are approached as expected only for extension curves at the max(N_{pk}). The difference, Δu, between the maximum unfolded length and

the contour length is just 15-25 nm and is much smaller than the $\Delta u \approx 50$ nm reported previously for extension of constructs with dystrophin's native hinge regions (Bhasin 2005). In the latter case, we concluded hinges extended before sawtooth-type unfolding of the repeats, whereas here Δu is so small that it likely reflects fraying or unwinding at the ends of domains.

The best-fit slope of the total unfolded length in a sawtooth versus the number of domains (Fig. 2.5B) shows for both R16~L1~R21 and R18~L2~R21 that the unfolding length per peak is significantly lower than the average domain contour lengths listed in Table 2.2. These slopes reflect an averaging of single and multi-domain unfolding events and understandably exceed the ~20 nm length for the main peak seen in the $l_{pk\text{-}pk}$ distributions. R15~L3~R23 was the only construct for which unfolding length per peak (31.5 nm/peak) and average domain contour length (Table 2.2) were within one standard deviation (35.2 ± 14.3 nm domain).

The synthetic construct, R15~L4~R23, was shown above in solution studies to be structurally less stable than the asymptomatic and BMD-inspired constructs. While AFM extension results are not shown in additional detail here, the maximum peak number for R15~L4~R23 was found to be 3, indicating that not even the two flanking wild-type repeats were stable. Additionally, the unfolding length per domain was only 17 nm, which shows that very few amino acids were in stable helical structures. This seemingly 'negative' construct highlights the potential complexity that can result from deletion of multiple exons in dystrophin.

Discussion

Multi-exon deletions in both asymptomatic and BMD patients (Table 2.1, Fig. 2.1B) lead to novel domain structures (Fig. 2.3, Table 2.2) with physical features both similar to and distinct from normal dystrophin. With DMD patients, similar structures might one day be generated by antisense-mediated skipping of exons – perhaps assessed at the primary structure level with Mass Spectrometry based mapping of exon expression (Fig. 2.2), but all such efforts seem likely to benefit from studies of secondary structure in solution combined with single molecule forced extension that reveals aspects of tertiary structure.

Helicity in solution together with melting temperatures are averaged properties that vary significantly here between nano-constructs (Table 2.3) just as they do for isolated single repeats and tandem repeats (Rusczak 2010). Such measurements might or might not lend insight into the function and mechanics of exon-deleted domains as suggested by the finding here that the one construct that represents an asymptomatic deletion (R16~L1~R21) exhibited the third lowest helicity and also showed the greatest disparity with TFE-induced helicity (Table 2.3). On the other hand, solution studies did quickly demonstrate that R15~L4~R23, with its low helicity, tends to aggregate and might therefore be a poor design for multi-exon skipping therapy.

Forced extension experiments (Figs. 4-5) agree with tertiary structure predictions in terms of the number of unfoldable domains, D, that one can determine from an ensemble of extension curves: $D = \max(N_{pk}) - 2$. The homology modeling here that also predicts D accounts for both helicity (i.e. hydrogen bonding) and packing of helices to sequester hydrophobic residues. We have previously simulated forced extension of tandem repeat spectrins by fully hydrated, atomistic molecular dynamics and found that

helical linkers between domains can either (i) concentrate the strain and stochastically decouple domains or else (ii) remain intact and facilitate unwinding and unfolding of the tandem (Ortiz 2005). The pulling experiments test the strength of the hydrophobic and hydrogen bonds within a domain, and ensemble-level analyses of such processes reveal the number of domains together with the range of forces holding the structures together. Unfolding forces of 20-40 pN are detected here (Fig. 2.4-top) independent of native domain or linker-derived domain and also independent of single or tandem unfolding, and such forces are typical of unfolding 3-helix bundle types of spectrin repeats (Rief 1999; Law 2003; Bhasin 2005). Myosin molecules individually generate peak forces on F-actin of about 6 pN at similar transition kinetics as here (Ishijima 1996), which suggests that the collective action of a half-dozen myosin molecules is sufficient to extensibly unfold dystrophin in muscle. Titin has been calculated to unfold in muscle (Li 2002), despite unfolding forces several-fold higher than dystrophin, and spectrin has been shown to unfold in fluid sheared red blood cells by Cys labeling followed by Mass Spectrometry mapping of sites (Johnson 2007).

The predominant unfolding length per peak of ~20 nm for the nano-constructs (Fig. 2.5A) is also the same as that measured for wild-type dystrophin (Bhasin 2005), and the additional distinct peak at twice this length for R16~L1~R21 provides clear evidence of cooperative tandem domain unfolding. With the other two constructs shown, the peak-to-peak length distributions are broad but do encompass all of the other expected domain transitions when scaled from the full contour length. Mixed modes of unfolding are also clear by comparing the ~20 nm histogram values to the significantly higher 'mean unfolding length' determined from the slopes of total unfolded length versus number of domains, D (Fig. 2.5B). One additional metric of cooperative unfolding is

revealed upon fitting the exponential decays of the N_{pk} distributions with Frequency ~ m-N_{pk}. This gives us integer values for m but is of course equivalent to Frequency ~ (1/m)Npk. We have previously shown in systematic studies of short and long spectrin repeat constructs (Law 2003) that m provides a simple measure of the m-fold fewer ways (i.e. degrees of freedom) for achieving one more unfolded domain (single and tandem) in a protein that spans the gap between AFM tip and surface. For example, with D increasing from 2 to 4 in studies of both α- and β-spectrin, m decreases exponentially from ~5 to ~3; theoretically, for D = 2, there are at most three unfolding pathways inasmuch as unfolding can involve one tandem repeat event and two single repeat events, whereas with D = 4, there are four possible single repeat events plus a combination of these with at least three tandem repeat events. For the nano-constructs here, m ~ 2 for the highly cooperative and asymptomatic R16~L1~R21 while m ~ 4 for the minimally cooperative BMD construct R18~L2~R21 and m is in between for the mild phenotype R15~L3~R23. Because of the inverse relationship, we introduce 1/m as a mechanical cooperativity metric in forced unfolding; 1/m ranges from 0 to 1 and the higher the value, the greater the mechanical cooperativity.

Past AFM results with a dystrophin rod domain and a mild BMD construct (H1-R1-2~H3~R22-24-H4) have indicated how both the Mean Unfolding Length per peak (i.e. slope) and the metric 1/m of cooperativity – as recognized here – vary with total domain number D (curves in Fig. 2.6), and the present results show that all of the nano-constructs here come close to previous results. Remarkably, both unfolding length and cooperativity are best preserved in the 'asymptomatic' construct that deviates the least from past results. Cooperativity deviates the most for the 'BMD' nano-construct, whereas unfolding length deviates the most for the 'Mild' nano-construct. Mechanical

cooperativity might be crucial to dystrophin function and might be the reason that the R16~L1~R21 deletion does not lead to BMD. Forced unfolding of multiple repeats all at once produces – in an instant – an extra long linker between contracting muscle and matrix, thereby maintaining cell anchorage.

Conclusions

The single molecule AFM studies here along with the various bio-informatics analyses appear useful in understanding structure and mechanical cooperativity of repeat domains in exon-skipped dystrophins. Solution studies of secondary structure and stability provided basic information, but single molecule studies confirmed tertiary structure predictions of helical domain formation by exon-deleted 'linkers'. AFM extension experiments also suggested that mechanical cooperativity with tandem domain unfolding might be key to dystrophin function.

References

Aartsma-Rus A, Kaman WE, Weij R, den Dunnen JT, van Ommen GJ, van Deutekom JC. 2006. Exploring the frontiers of therapeutic exon skipping for Duchenne muscular dystrophy by double targeting within one or multiple exons. ***Mol Ther*** 14:401-7.

Aartsma-Rus A, Janson AA, van Ommen GJ, van Deutekom JC. 2007. Antisense-induced exon skipping for duplications in Duchenne muscular dystrophy. ***BMC Med Genet*** 8:43-51.

Béroud C, Tuffery-Giraud S, Matsuo M, Hamroun D, Humbertclaude V, Monnier N, Moizard MP, Voelckel MA, Calemard LM, Boisseau P, Blayau M, Philippe C, Cossée M, Pagès M, Rivier F, Danos O, Garcia L, Claustres M. 2007. Multiexon skipping leading to an artificial DMD protein lacking amino acids from exons 45 through 55 could rescue up to 63% of patients with Duchenne muscular dystrophy. ***Hum Mutat*** 28:196-202.

Bhasin N, Law R, Liao G, Safer D, Ellmer J, Discher BM, Sweeney HL, Discher DE. 2005. Molecular extensibility of mini-dystrophins and a dystrophin rod construct. ***J Mol Biol*** 352:795-806.

Engler A, Sheehan A, Sen S, Bonnemann C, Sweeney HL, and Discher DE. 2004. Myotubes differentiate optimally on substrates with tissue-like stiffness: Pathological implications of stiff or soft microenvironments. ***Journal of Cell Biology*** 166(6): 877-887.

Engler A, Carag C, Johnson C, Raab M, Tang H-Y, Speicher D, Sanger J, Sanger J, and Discher DE. 2008. Embryonic cardiomyocytes beat best on a matrix with heart-like elasticity: scar-like rigidity inhibits beating. ***Journal of Cell Science*** 121: 3794-3802.

Fokkema IF, den Dunnen JT, Taschner PE. 2005. LOVD: easy creation of a locus-specific sequence variation database using an "LSDB-in-a-box" approach. ***Hum Mutat.*** Aug;26(2):63-8.

Freund AA, Scola RH, Arndt RC, Lorenzoni PJ, Kay CK, Werneck LC. 2007. Duchenne and Becker muscular dystrophy: a molecular and immunohistochemical approach. ***Arq Neuropsiquiatr*** 65:73-76.

Ishijima A, Kojima H, Higuchi H, Harada Y, Funatsu T, Yanagida T. 1996. Multiple- and single-molecule analysis of the actomyosin motor by nanometer-piconewton manipulation with a microneedle: unitary steps and forces. ***Biophys. J*** 70:383–400.

Johnson CP, Tang HY, Carag C, Speicher DW, Discher DE. 2007. Forced unfolding of proteins within cells. ***Science*** 317:663-666.

Johnson C, Massimiliano G, Ortiz V, Bhasin N, Harper S, Speicher D, Gallagher P, and Discher DE. 2007b. A pathogenic proline mutation in the linker between spectrin repeats: Disease due to spectrin unfolding. ***Blood*** 109(8):3538-43.

Kahana E, Flood G, Gratzer WB. 1997. Physical properties of dystrophin rod domain. ***Cell Motil Cytoskeleton*** 36:246-252.

Law R, Carl P, Harper S, Dalhaimer P, Speicher DW, Discher DE. 2003. Cooperativity in forced unfolding of tandem spectrin repeats. ***Biophys J*** 84:533–544.

Lewis C, Carberry S, Ohlendieck K. 2009. Proteomic profiling of x-linked muscular dystrophy. ***J Muscle Res Cell Motil*** 30:267-269.

Li H, Linke WA, Oberhauser AF, Carrion-Vazquez M, Kerkvliet JG, Lu H. 2002. Reverse engineering of the giant muscle protein titin. ***Nature*** 418:998–1002.

Marszalek PE, Oberhauser AF, Li H, Fernandez JM. 2003. The force-driven conformations of heparin studied with single molecule force microscopy. ***Biophys J*** 85:2696-2704.

Mirza A, Sagathevan M, Sahni N, Choi L, Menhart N. 2010. A biophysical map of the dystrophin rod. ***Biochim Biophys Acta***. 1804:1796-809.

Ortiz V, Nielsen SO, Klein ML, Discher DE. 2005. Unfolding a linker between helical repeats. ***J Mol Biol*** 349:638-647.

Rief M, Pascual J, Saraste M, Gaub HE. 1999. Single molecule force spectroscopy of spectrin repeats: low unfolding forces in helix bundles. ***J Mol Biol*** 286:553–561.

Ruszczak C, Mirza A, Menhart N. 2009. Differential stabilities of alternative exon-skipped rod motifs of dystrophin. ***Biochim Biophys Acta***. 1794:921-928.

Sun Y, Walker GC. 2005. Viscoelastic response of poly(dimethylsiloxane) in the adhesive interaction with AFM tips. ***Langmuir***. 21:8694-8702.

van Deutekom JC, Janson AA, Ginjaar IB, Frankhuizen WS, Aartsma-Rus A, Bremmer-Bout M, den Dunnen JT, Koop K, van der Kooi AJ, Goemans NM, de Kimpe SJ, Ekhart PF, Venneker EH, Platenburg GJ, Verschuuren JJ, van Ommen GJ. 2007. Local dystrophin restoration with antisense oligonucleotide PRO051. ***N Engl J Med*** 357:2677-86.

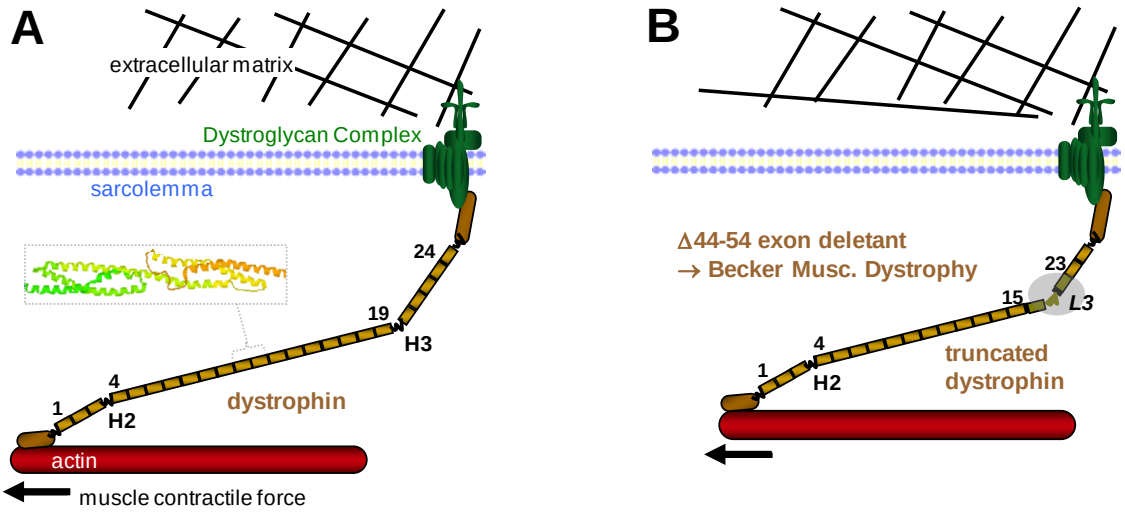

Figure 2.1: Full-length and representative truncated, Becker MD dystrophin in the dystrophin-glycoprotein complex.

Schematic of dystrophin and the dystroglycan complex (DGC). In normal skeletal muscle, the muscle cytoskeleton (actin) is linked by dystrophin to extracellular matrix via the cell membrane. Boxed inset illustrates crystal structure for tandem repeats 2-3 from actinin with triple helix repeats linked by a continuous and extended helix. (A) Wild-type and (B) truncated dystrophin corresponding to milder BMD phenotype with in-frame exon 17-40 deletion.

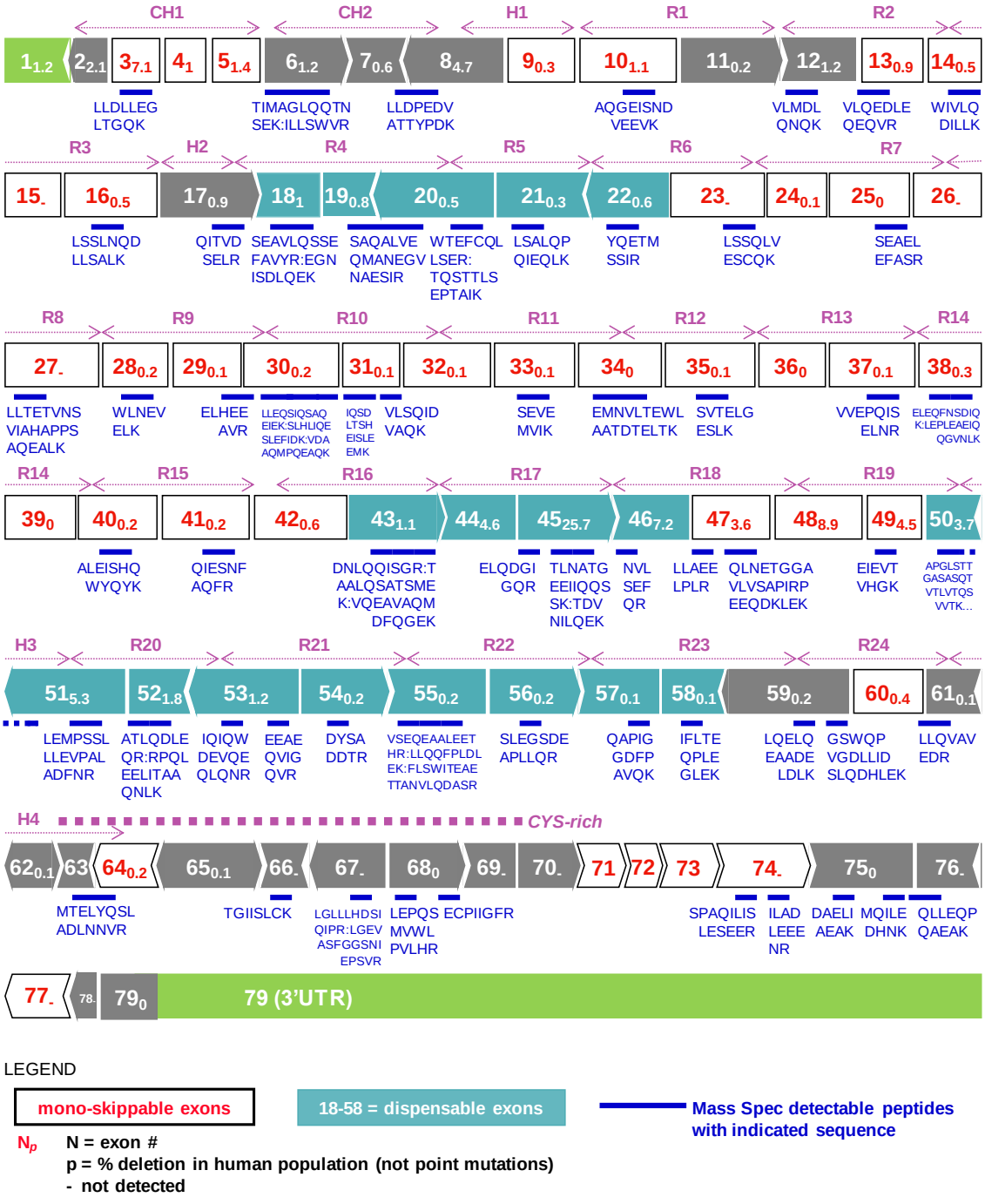

Figure 2.2: Phasing of DMD exons and protein domains with peptides detected by LC-MS/MS.

79 exons contribute to normal, full-length dystrophin, and. phasing of protein domains generally differs from exon boundaries. Each exon or repeat is numbered according to its distance from N-terminus, and the subscript indicates the percentage of DMD patients in the cited database (Fokkema 2005) with that particular exon deletion or duplication. For LC-MS/MS results, mouse and human dystrophin sequences were aligned, and the location of the human analog of the mouse peptide shown in blue, with the indicated sequence of the detected peptide.

Mutations found in Duchenne MD patients	Targeted exons for skipping	Total exon deletions	% DMD patients w/ deletion (s) point mutation in deleted exons	MD phenotype
Deletion exons 45-54	Exon 44	Δ44-54*	66.6 20.4	Mild BMD
Deletion exon 45	Exon 46	Δ45-46	32.9 3.6	Not reported
Deletion exons 45-50	Exon 51	Δ45-51*	58.9 13.2	Asymptomatic
Deletion exons 48-50	Exon 45 + Exon 51	Δ45-51*	58.9 13.2	Asymptomatic
Deletion exons 46-51	Exon 45	Δ45-51*	58.9 13.2	Asymptomatic
Deletion exons 46-50	Exon 45 + Exon 51	Δ45-51*	58.9 13.2	Asymptomatic
Deletion exons 48-50	Exon 51	Δ48-51	22.4 8.3	Asymptomatic
Point Mutation exon 49	Exon 49	Δ49*	4.5 1.0	BMD
Deletion exon 50	Exon 51	Δ50-51	9.0 4.9	BMD
Deletion exons 51-55	Exon 50	Δ50-55	12.4 8.8	Not reported
Deletion exon 52	Exon 51	Δ51-52	7.1 3.5	BMD
Deletion exon 52	Exon 51 + Exon 53	Δ51-53	8.3 4.3	BMD
Deletion exon 52	Exon 53	Δ52-53	3.0 1.7	BMD
		*Basis of constructs studied further here.		
		Δ42-55*	**68.8 20.4**	**Not found in any patient**

Table 2.1: Potential dystrophin deletants created by exon skipping

Domain	**Δ45-51 (asymptomatic)**		**Δ49 (BMD)**		**Δ44-54 (mild)**		**Δ42-55 (n/a)**	
	R16~*L1*~R21		**R18~*L2*~R21**		**R15~*L3*~R23**		**R15~*L4*~R23**	
	name	**l_c (nm)**	**name**	**l_c (nm)**	**name**	**l_c (nm)**	**Name**	**l_c (nm)**
D1	R16	40.6	R18	40.6	R15	36.5	R15	36.5
D2	*L1*	39.9	$L2_a$	42.0	$L3_a$	42.4	L4	22.9
D3	R21	40.2	$L2_b$	41.0	$L3_b$	10.7	R23	47.6
D4	--	--	R21	40.2	$L3_c$	39.0	--	--
D5	--	--	--	--	R23	47.6	--	--
Avg ±S.D.		40.2 ± 0.4		41.0 ± 0.8		35.2 ± 14.3		35.7 ± 12.4

Table 2.2: Predicted unfolding lengths of domains in dystrophin nano-constructs

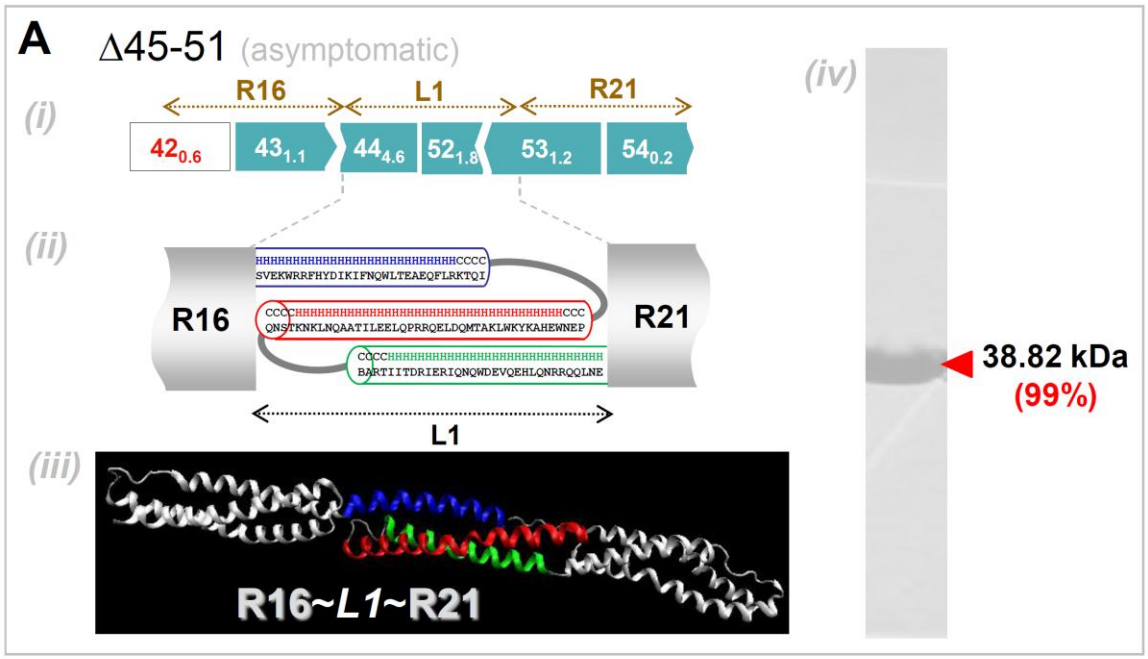
A
Δ45-51 (asymptomatic)
(i)
R16
L1
R21
42 0.6
43 1.1
44 4.6
52 1.8
53 1.2
54 0.2
(ii)
R16
R21
L1
(iii)
R16~L1~R21
(iv)
38.82 kDa
(99%)

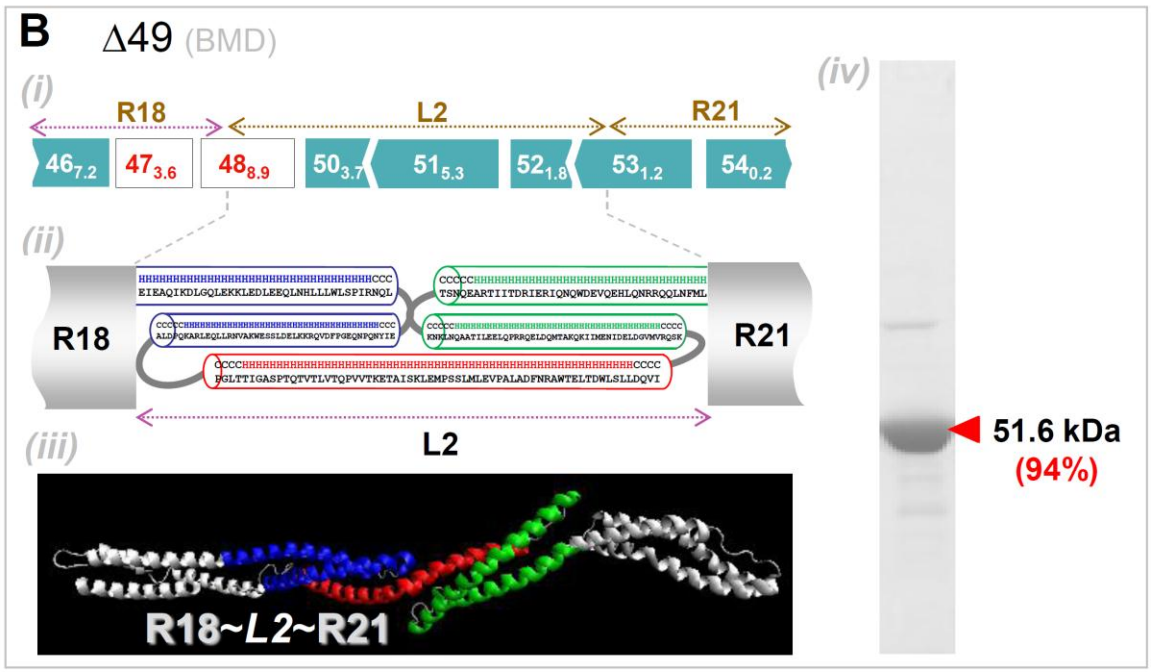
B
Δ49 (BMD)
(i)
R18
L2
R21
46 7.2
47 3.6
48 8.9
50 3.7
51 5.3
52 1.8
53 1.2
54 0.2
(ii)
R18
R21
L2
(iii)
R18~L2~R21
(iv)
51.6 kDa
(94%)

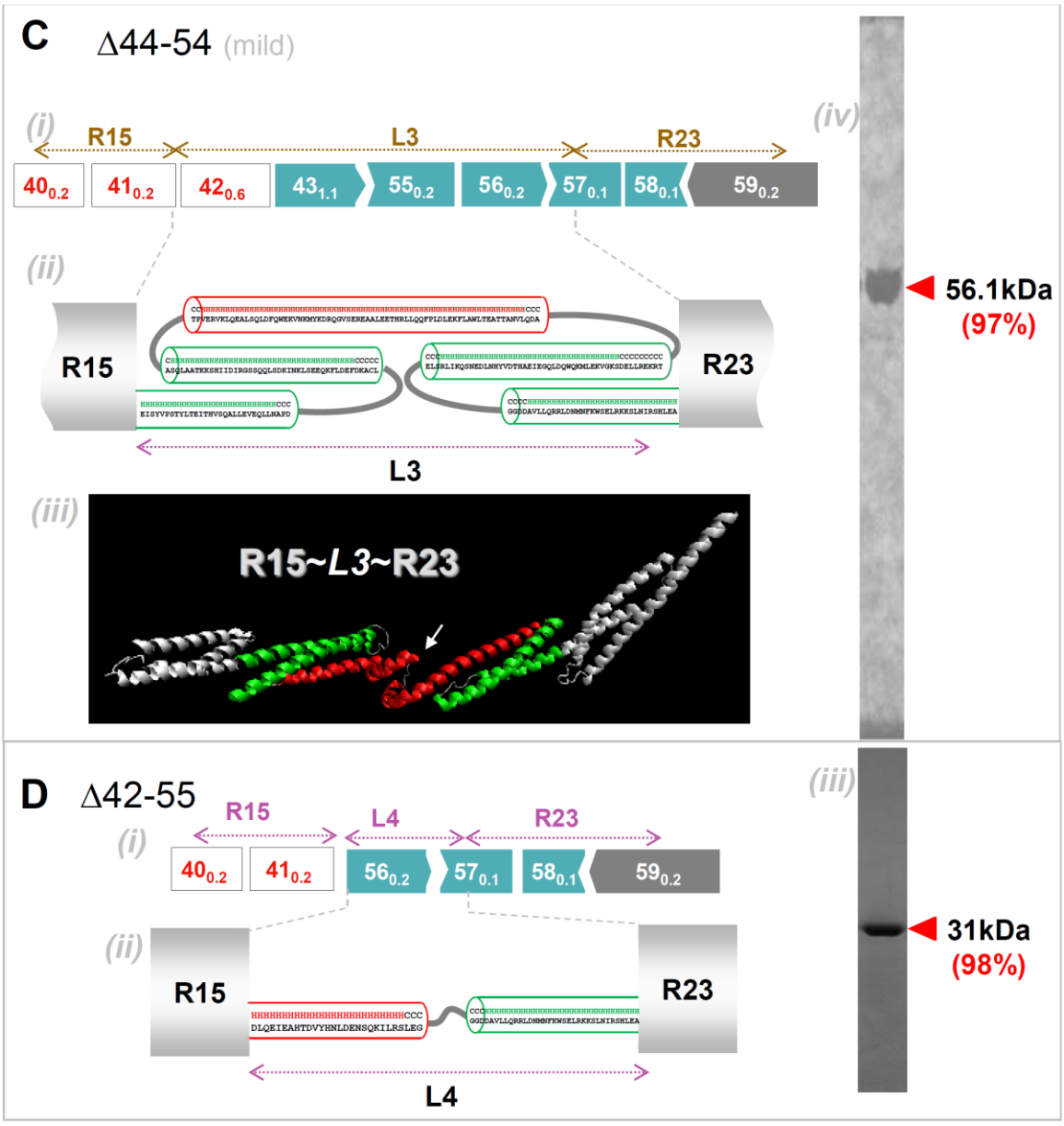

Figure 2.3: Secondary and tertiary structure prediction of BMD-inspired nano-dystrophin constructs.

(A) R16~L1~R21: (i) Exon map (ii) Secondary structure predictions for abnormal 'linker', L1, show this is mostly helical. Helical wheel predictions (not shown) indicate the presence of a hydrophobic core, necessitating packing of the helices into a spectrin-like

domain. (iii) Homology model prediction for L1 with adjacent normal repeats shown in white. Color coding matches that of the structure prediction. (iv) Coomassie blue staining of purified nano-construct in SDS/PAGE, with purity in densitometry of 99%. (B) R18~L1~R21: (i) Exon map. (ii) Linker region L2 is again predicted to be mostly helical and to form two spectrin-like domains. (iii) Homology model for L3 also predicts folding into two repeat domains. (iv) Purified protein. (C) R15~L3~R23: (i) Exon map. (ii) Secondary structure predictions predict L3 to be mostly helical with two spectrin-like domains. (iii) Homology model prediction shows linker L3 might also contain another kink or hinge-like domain as indicated by a white arrow. (iv) Purified protein. (D) R15~L4~R23. (i) Exon map. (ii) The linker region was predicted to be helical, with an unstructured coil region in the middle. (iii) Purified protein.

Nano-Construct (phenotype)	CD T_m (°C)	%-Helicity, 37°C		Tryptophan fluorescence
		in PBS	w/ TFE	T_m (°C)
R16~L1~R21 (Δ45-51) (Asymptomatic)	60	54	85	55
R18~L2~R21 (Δ49) (BMD)	65	60	70	62
R15~L3~R23 (Δ44-54) (Mild)	55	58	75	35
R15~*L4*~R23 (Δ42-55) (N/A)	55	37	n/a	n/a

Table 2.3: Thermal denaturation of dystrophin nano-constructs

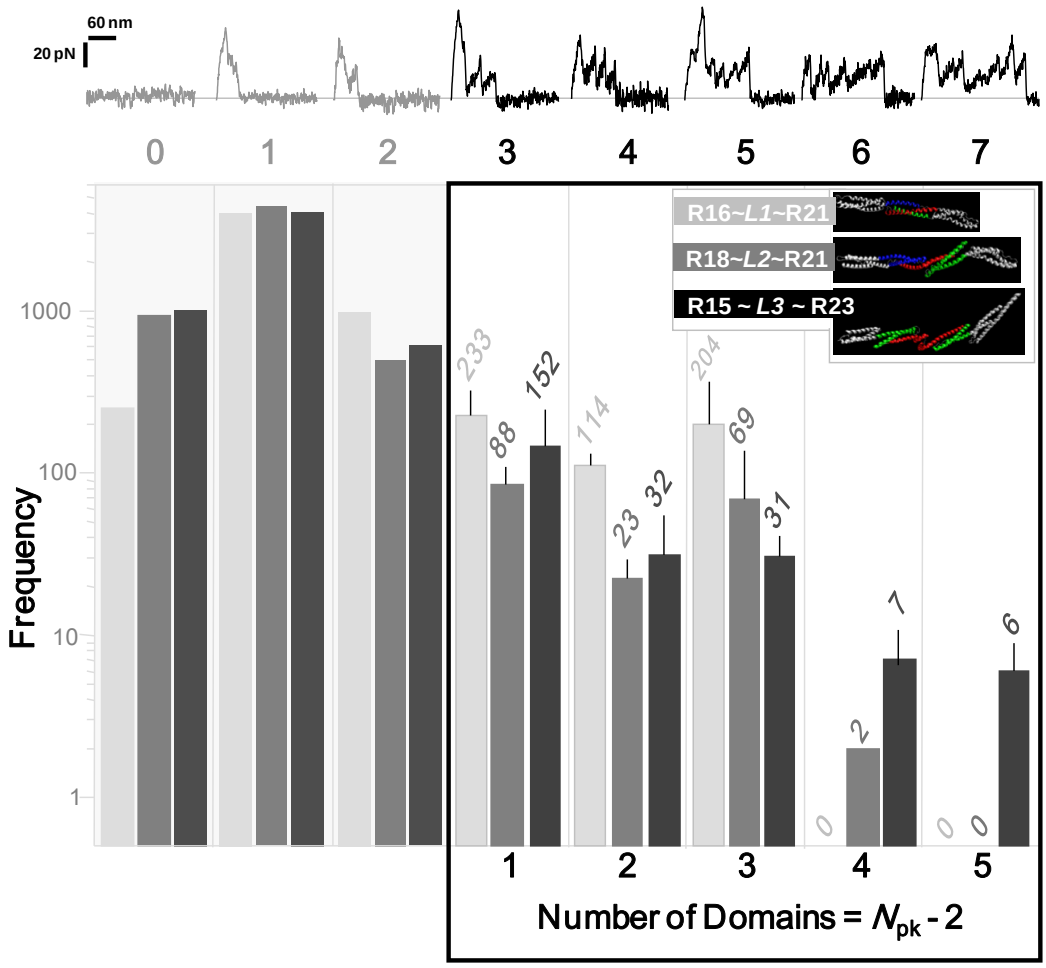

Figure 2.4: Single molecule extension by AFM reveals the unfolding forces and number of protein domains.

(top) Representative sawtooth patterns for domain-by-domain unfolding when extended at 1 nm/msec. (bottom) Number of peaks, N_{pk}, per extension with pre-adsorbed nano-dystrophin constructs R18~L1~R21, R16~L2~R21 and R15~L3~R23. Each experiment involved at least 6000 contacts between AFM tip and protein substrate. For PBS alone, there were only 0-1 peaks ever seen. The first peak and the last peak are ignored as desorption events, so that the number of mechanically detectable domains in is obtained by subtracting these 2 peaks from N_{pk}.

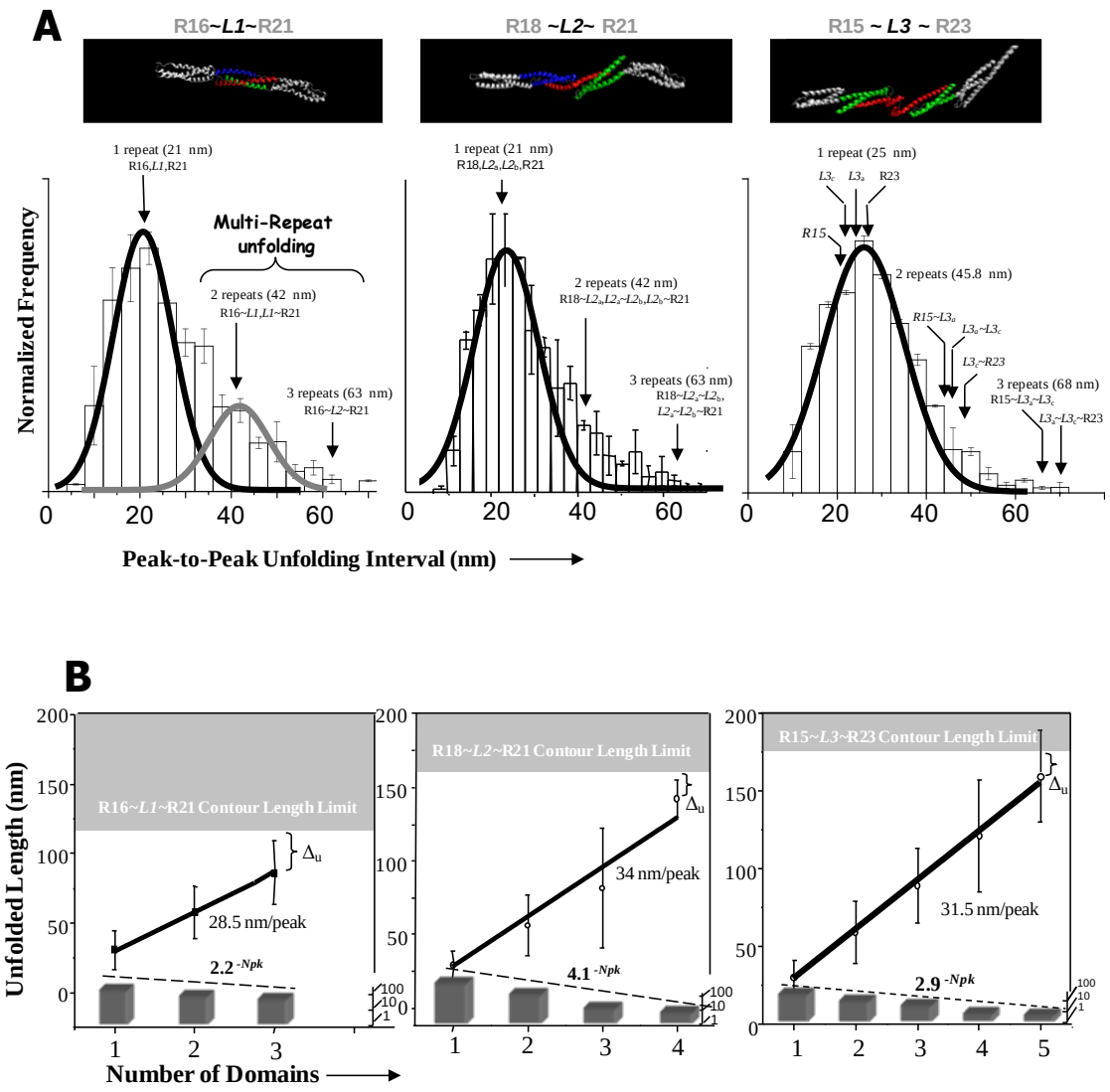

Figure 2.5: Dystrophin nano-constructs' unfolding length statistics.

(A) Histograms for peak-to-peak unfolding lengths for R18~L1~R21, R16~L2~R21 and R15~L3~R23 all show a major peak that was fit with a Gaussian for single domain unfolding centered near ~20 nm. Peaks at ~2× and ~3× the major peak value reflect simultaneous unfolding of multiple repeats. (B) After the 6000-8000 contacts of tip to surface, the total unfolding length (avg. ± S.D.) beyond the second peak is obtained for each sawtooth, which is categorized by N_{pk}. The upper gray regions indicate the

extension limits calculated from Table 2.2, and the slope of the best-fit line through all of the data (including zero total unfolding length at $N_{pk} = 2$) is the average distance between peaks, which accounts for both single and multi-domain unfolding.. The lower bargraph shows frequency distributions of N_{pk} fitted to exponential decays of the form m^{-Npk} with $3 < N_{pk} < \max(N_{pk})$ and the indicated values for m.

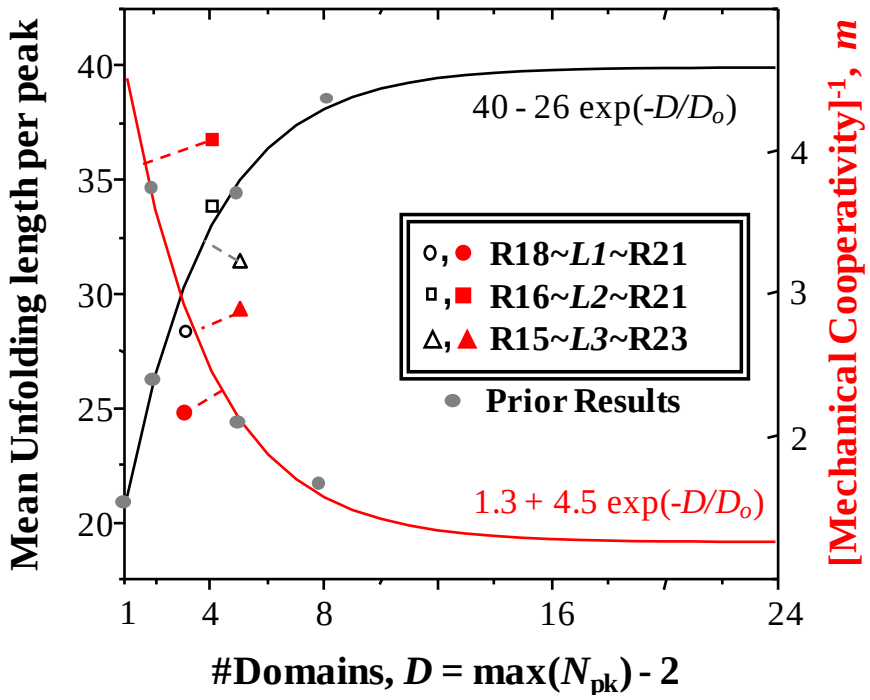

Figure 2.6: Comparison of AFM measures of unfolding lengths and mechanical cooperativity for BMD dystrophin nano-constructs to prior results for native dystrophin constructs.

Calculated *m* and unfolding length per peak for all nano-dystrophin constructs are compared to previous dystrophin constructs. The exponential fits are for the prior results, and the dashed lines indicate deviation of results here from the prior results. BMD nano-dystrophin constructs differ from wild-type in their cooperative behavior.

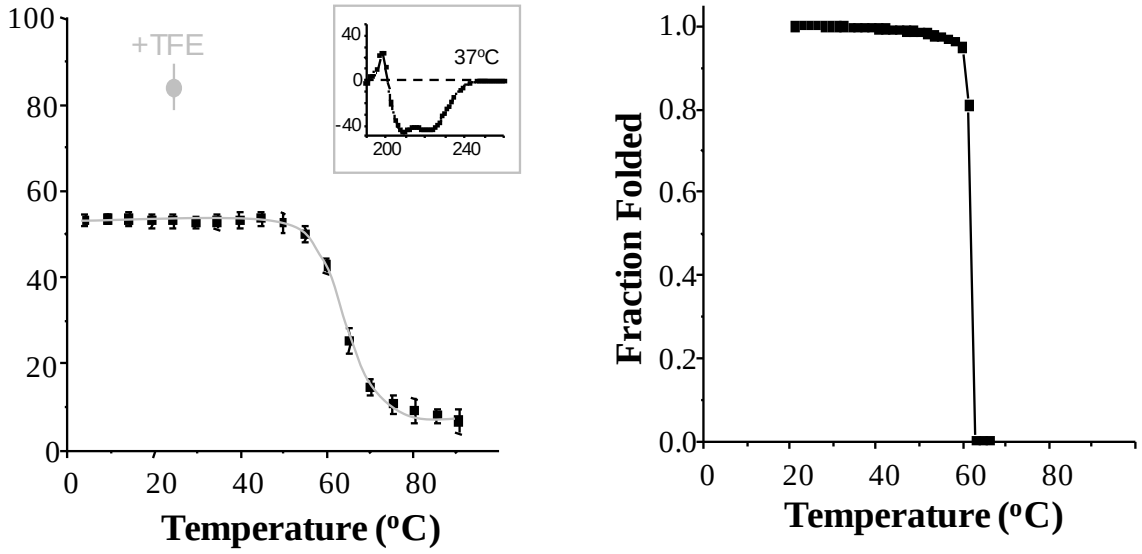

Figure 2.7: Representative thermal denaturation curves

The construct represented is R18~L2~R21. Left: CD curve inset and calculated helicity (see Methods) as a function of temperature; TFE is expected to induce helicity and indeed does. Right: Tryptophan fluorescence results as a function of temperature. For all four constructs, such results are summarized in Table 3 in the text.

Sequence	Run 1	Run 2	Run 3	Run 4
K.ALEISHQWYQYK.R	1			
K.ATLQDLEQR.R	1		1	
K.DNLQQISGR.I	1			
K.EC#PIIGFR.Y				1
K.EEAEQVIGQVR.G	1		1	1
K.EGNISDLQEK.V			1	1
K.EIEVTVHGK.Q	1			
K.ELEQFNSDIQK.L	1			
K.ELQDGIGQR.Q	1			
K.EMNVLTEWLAATDTELTK.R				1
K.FLSWITEAETTANVLQDASR.K	1		1	2
K.GSWQPVGDLLIDSLQDHLEK.V	1			
K.ILLSWVR.Q	1	1	1	1
K.IQSDLTSHEISLEEMK.K	1			
K.LEM*PSSLLLEVPALADFNR.A				1
K.LLAEELPLR.Q	1			
K.LLDPEDVATTYPDK.K	1			
K.LLEPLEAEIQQGVNLK.E	1			1
K.LLEQSIQSAQEIEK.S		1	1	1
K.LLTETVNSVIAHAPPSAQEALK.K	1			
K.LSSLNQDLLSALK.N	1			1
K.LSSQLVESCQK.L	1			
K.MTELYQSLADLNNVR.F	1			1
K.NVLSEFQR.D	1			
K.QLNETGGAVLVSAPIRPEEQDKLEK.K			1	
K.SEAELEFASR.L	1			
K.SEVEMVIK.T	1			1
K.SLHLIQESLEFIDK.Q	1		1	
K.SVTELGESLK.M	1	1		
K.TAALQSATSMEK.V	2		1	1
K.TDVNILQEK.L	1			1
K.TGIISLC#K.A			1	
K.TIMAGLQQTNSEK.I	1		1	
K.TQSTTLSEPTAIK.S	1			
K.VDAAQMPQEAQK.I	2		1	1
K.VLMDLQNQK.L	1		1	
K.VLQEDLEQEQVR.V	1			
K.VQEAVAQMDFQGEK.L	1		1	
K.VVEPQISELNR.R	1	1	1	
K.WLNEVELK.L			1	
R.APGLSTTGASASQTVTLVTQSVVTK.E	1			
R.AQGEISNDVEEVK.E	1			1
R.DAELIAEAK.L			1	
R.DYSADDTR.K	1			
R.ELHEEAVR.K	1			
R.IFLTEQPLEGLEK.L	1	1		1

R.ILADLEEENR.N	1		1	1
R.IQIQWDEVQEQLQNR.R	1			
R.LEPQSMVWLPVLHR.V			1	
R.LGLLLHDSIQIPR.Q			1	
R.LLDLLEGLTGQK.L	1		1	1
R.LLQQFPLDLEK.F	1	1	1	1
R.LLQVAVEDR.V	1		1	1
R.LQELQEAADELDLK.L	1		1	1
R.LSALQPQIEQLK.I	1	1	1	1
R.MQILEDHNK.Q	2	1	1	
R.QAPIGGDFPAVQK.Q	1	1	1	1
R.QIESNFAQFR.R	1			
R.QITVDSELR.K	1			
R.QLGEVASFGGSNIEPSVR.S	1			1
R.QLLEQPQAEAK.V	1		1	1
R.RPQLEELITAAQNLK.N	1			
R.SAQALVEQMANEGVNAESIR.Q				1
R.SEAVLQSSEFAVYR.K	1			
R.SLEGSDEAPLLQR.R	1		1	
R.SPAQILISLESEER.G	1			
R.TLNATGEEIIQQSSK.T	1		1	1
R.VLSQIDVAQK.K	1		1	1
R.VSEQEAALEETHR.L	2		1	
R.WIVLQDILLK.W	1	1	1	1
R.WTEFC#QLLSER.V		1	1	1
R.YQETMSSIR.T			1	1

Table 2.4: Tryptic Peptides of Dystrophin detected by Mass Spectrometry

Spectral counts in the 2nd MS of LC-MS/MS from 4 runs were cumulated. All listed peptides are shown in Figure 2.2.

CHAPTER THREE

Cysteine Shotgun Mass Spectrometry (CS-MS) of stressed Cells reveals cytoskeletal pathways of forced unfolding and dissociation

Blood was provided by Dr. Xiuli An from the New York Blood Center. Mass spectrometry was done by Dr. Hsin-Yao Tang and Dr. David Speicher.

Abstract

Stresses on cells are sustained by the cytoskeleton, but structural responses at the molecular scale in intact cells have been largely a matter of speculation. Cysteine shotgun labeling is used here to directly assess the unfolding and dissociation sequences of the spectrin-actin membrane skeleton within sheared red blood cell ghosts from normal and diseased mice. Sheared samples are compared to static samples at 37°C in terms of cell membrane intensity in fluorescence microscopy, whole protein fluorescence after electrophoretic separation, and tryptic peptide modification in liquid chromatography-tandem mass spectrometry (LC-MS/MS). Spectrin labeling proves the most sensitive to shear while spectrin-binding partners ankyrin and actin exhibit shear-thresholds in labeling and both the ankyrin-binding membrane protein Band 3 and the spectrin-actin stabilizer 4.1R show minimal differentials in labeling. Cells from 4.1R-null mice differ significantly from normal in the shear-dependent labeling of spectrin, ankyrinin and Band 3, with decreased labeling of 4.1R-nulls' spectrin indicating less stress on the

network as spectrin dissociates from actin. Mapping the stress-dependent labeling kinetics of α- and β-spectrin by LC-MS/MS identifies Cys in these anti-parallel chains that are either force-enhanced or force-independent in labeling, with structural analyses indicating the force-enhanced sites are sequestered either in spectrin's triple-helical domains or in interactions with actin or ankyrin. Some domain-buried sites were previously found in human spectrins (Johnson et al, Science 2007), but new shear-sensitive sites identified in both spectrin and ankyrin appear consistent with stress relief through forced unfolding followed by cytoskeletal disruption.

Introduction

A cell's cytoskeleton has multiple roles – including key roles in the physical life of the cell, but how the cytoskeleton responds to physiological stress has been difficult to assess. The simplest mammalian cell, the red blood cell (RBC), possesses a well-elaborated membrane skeletal protein assembly of α- and β-spectrin plus F-actin (Mohandas and Gallagher 2008) with proteins such as band 4.1R (Takakuwa 1986) helping to stabilize the network and ankyrin (Bennett 2009) helping to attach the network to the plasma membrane (Fig. 3.1A). However, it is unclear whether these proteins dissociate and/or unfold as the cytoskeleton is stressed in blood flow. Deeper insight is needed to explain, for example, the strong effects of point mutations that are sometimes distal to protein interaction sites (Giorgi 2001; Maillet 2008). To begin to address such issues we have developed a method to map dynamically exposed Cysteines in proteins of intact cells that are being stressed mechanically, thermally, or by drugs (Johnson 2007a). Cys is relatively hydrophobic, which means that it is frequently buried – wholly or partially – in protein folds as well as protein-protein interfaces, but the thiol

in Cysteine is also highly reactive. Fluorescent dyes allow 'shotgun' labeled cells to be imaged and the labeled proteins to be quantified after separation by gel electrophoresis and, lastly, identified and quantified site-by-site using Cys Shotgun - Mass Spectrometry (CS-MS). Controlled stressing of human RBC membranes with fluid shear stresses at levels similar to in vivo blood flow stresses (< 10 Pa) has thus revealed stress-enhanced Cys labeling at 37 °C. The results suggest that spectrin protects cells from mechanical stresses through forced unfolding of some of the dozens of three-helix repeat domains (Fig. 3.1B) (Johnson 2007a). Whether other membrane skeleton proteins contribute somehow to spectrin unfolding and whether the other proteins show stress-enhanced labeling was not addressed.

Denaturation studies of purified spectrin decades ago showed spectrin repeats unfold collectively and cooperatively only at temperatures well above physiological (Brandts 1977), but in more recent studies in which almost every spectrin repeat was recombinantly expressed, more than a third of the domains unfolded at or below 37 °C (An 2006). Single molecule experiments have shown that spectrin domains – independent of melting temperature – unfold at relatively low force compared to other proteins such as titin (Rief 1999), and the forced unfolding can cooperatively propagate through multiple domains via helical linkers (Law 2003, Ortiz 2005). Loss of cooperativity in spectrin can even lead to disease (Johnson 2007b). A dynamic quaternary structure of the membrane skeleton has also been suggested by studies of RBC ghosts that were resealed after entrapment of spectrin interacting fragments with the finding that competitive incorporation of the fragments is enhanced by shearing the ghosts (An 2002). The latter findings certainly raise the question of how much dissociation occurs relative to spectrin unfolding in the stressed network. One might

hypothesize that if protein-protein interactions have similar energetics as helical folding interactions, then the probability of unfolding one of a dozen or more domains is entropically favored over dissociation.

CS-MS studies of intact human RBC membranes had specifically identified several fluorophore-labeled Cys in α- and β- spectrin that were either known from crystal structures or predicted from homology models to be buried, and these Cys were found to exhibit force-enhanced labeling when compared to other Cys that proved force-independent in labeling. Force-enhanced labeling of other membrane proteins did not appear significant at the stresses and times examined in the previous study (Johnson 2007a). Here, with mouse RBCs, we examine a broader range of time, stress, and membrane proteins using multiple Cys-reactive fluorophores. Normal mouse RBCs are compared here to RBCs from 4.1R null mice, which have been reported to be mechanically fragile (Salomao 2008). Force-enhanced labeling of other proteins documents the potential for quaternary as well as tertiary structure changes. The stress dependence ultimately shows that spectrin repeats exhibit force-enhanced labeling prior to the stress-enhanced labeling of spectrin binding partners. Combined with structural analyses of the labeled sites, the findings thus demonstrate that stress-driven unfolding occurs before network dissociation.

Material and Methods

Reagents

N-(4,4-difluoro-1,3,5,7-tetramethyl-4-bora-3a,4a-diaza-s-indacene-2-yl) iodoacetamide (BODIPY) and monobromobimane FluoroPure grade (mBBr) was purchased from

Invitrogen. N-(Iodoacetaminoethyl)-1-naphthylamine-5-sulfonic acid (IAEDANS) and iodoacetamide (IAM) were purchased from Sigma.

Preparation of ghosts.

Whole blood from 4.1R-null mice was generously supplied from the Mohandas group (New York Blood Center). Wild-type blood was obtained either from the New York Blood Center, together with 4.1R-null blood, or purchased from Covance. Erythrocytes were segregated from whole blood by centrifugation and washed once with isotonic phosphate-buffered saline (PBS; 10 mM sodium phosphate, 150 mM potassium chloride, pH 7.4). Cells were then lysed in approximately 30 volumes hypotonic buffer (5 mM sodium phosphate, 5 mM potassium chloride, 2 mM magnesium chloride pH 7.4). White ghosts were washed with hypotonic buffer until hemoglobin was almost completely removed (approximately 5x) and resealed with isotonic buffer containing 200 μM IAEDANS (Sigma). Pink ghosts were not washed, instead resealed immediately after lysis. Because of the hemoglobin in pink ghosts would compete with spectrin for thiol label, pink ghosts were resealed in isotonic buffer containing 400 μM IAEDANS. The concentration of IAEDANS in pink ghosts was chosen so that the fluorescence intensity of spectrin matched the fluorescent intensity of spectrin in white ghosts loaded with 200 μM IAEDANS after static labeling. Both white and pink ghosts were resealed at room temperature for 30 minutes in the dark.

Labeling of ghosts during shear.

Resealed ghosts were washed once in PBS, then resuspended in labeling solution containing 2 mM Bodipy 504/507 (Invitrogen) or for future mass spec samples, mBBr (Invitrogen) in PBS. Solution was divided into two samples. The static sample was covered in foil and incubated on a heat block at 37°C, and the shear sample was loaded

onto a temperature-controlled cone and plate rheometer set to 37°C. Samples were then sheared at various stresses for up to 1 hour. After shear, ghosts were washed once in ice-cold PBS.

SDS-Page analysis.

Ghosts pre-labeled with IAEDANS, then labeled with BODIPY during shear were lysed with RIPA buffer containing 1% Triton-X 100 at 4°C for 30 minutes, and lysates separated on 3-8% or 7% Tris-Acetate buffered polyacrylamide gels. Fluorescent images were taken immediately after the run was complete, and gels were stained with Coomasie R-250. Fluorescent and Coomassie intensities were measured using ImageJ. For wild type red cells, lysates were run in multiple lanes with different loadings. Proteins were identified based on molecular weight. Fluorescent intensity vs. coomassie intensity plots were made for each band. If $R^2 < 0.9$, lysates were rerun on PAGE gels or experiments repeated. For most samples, $R^2 > 0.95$. Shear-enhanced labeling was calculated by the ratio of slopes of the sheared and static samples, with ratios > 1.1 considered shear-enhanced. All experiments with white ghosts were repeated at least twice and error bars indicate the range of m_{shear} / m_{static} values at that shear stress. Experiments with pink ghosts were done once. Because of the scarcity of 4.1R-null sample, lystates were run in single lanes. Error bars are the estimated range of values based on the variation of 4.1-null m_{static} values from three independent experiments. Fluorescent intensity was normalized by Coomassie intensity, and shear-enhanced labeling was calculated from the ratio of normalized shear:static fluorescent intensities.

LC-MS/MS analysis

For mass spectrometry analysis, ghosts were pre-labeled with IAEDANS and then labeled with mBBr during shear. Lysates were made and separated as described above.

Alpha and beta spectrin bands were excised for in-gel trypsin digest. Tryptic peptides were analyzed by LC-MS/MS on a LTQ-Orbitrap XL mass spectrometer (Thermo Fisher Scientific, Waltham, MA) interfaced with an Eksigent Autosampler/NanoLC-2D system (Eksigent Technologies, Dublin, CA). Peptides were eluted at 300 nL/min using an acetonitrile gradient consisting of 3-28% B over 40 min, 28-50% B over 25.5 min, 50-80% B over 5 min, 80% B for 5 min before returning to 3% B in 1 min. To minimize carryover, a blank cycle was run between each sample. The mass spectrometer was set to perform a full MS scan (m/z 350 – 2000) in the Orbitrap, and the six most intense ions exceeding a minimum threshold of 1,000 were selected for MS/MS in the linear trap with dynamic exclusion enabled. Protein identification was done using the SEQUEST algorithm in BioWorks 3.3.1 (Thermo Fisher Scientific). Data were searched against a mouse database using a partial tryptic constraint with a 1.1 Da precursor mass tolerance, and allowing for methionine sulfoxide, IAM, IAEDANS, or mBBr cysteine modifications. Peptide identifications were filtered using the following criteria: mass tolerance ≤ 5 ppm, $\Delta Cn \geq 0.069$ and $Sf \geq 0.2$. The extent of IAEDANS, mBBr, and IAM labeling at each site was determined from extracted ion chromatograms with identification of each specific Cys achieved through both the m/z of the modified-Cys peptide as well as the MS/MS fragmentation pattern. Ion-flux values of cys-labeled peptides from shear and static samples were normalized by their corresponding cys-IAM ion flux values. Phi values were calculated from the ratios of normalized shear and static ion fluxes, with phi > 1.25 defined as force-enhanced labeling. When multiple peptides were detected for the same cysteine, peptides with the greater ion-flux values were chosen to be represented in Fig. 5.

Sequence alignment and structure predictions

Amino acids of alpha and beta spectrin were numbered according to UnitProt files P08032 and P15508 respectively. All alignments were done with ClustalW 2.0.12 (Thompson 1994). Solvent exposure of cysteines within repeat domains was predicted according to Parry et. al. Heptad position predicted was based on alignment with repeats 16-17 of chick non-erythrocytic spectrin, PDB file 1CUN. For cys-β1159 position was based on alignment with repeats 8-9 in human erythrocytic spectrin, PDB file 1S35. For cys-α129, the CH1 domain was aligned with human α-actinin 3, PDB file 3LUE. Cys-β1883 was aligned with repeats 14-15 of human spectrin, PDB file 3E57. Peptides in ankyrin repeat domains, cys-316 and cys-472, were aligned with crystal structure of ankyrin repeat domains in mouse GA-binding protein β (GABP), PDB file 1AWC. All homology models were generated by MODELLER 9v8 (Sali 1993) based on ClustalW alignments. The coordinates of the mouse spectrin CH1 domain in reference to actin were determined using Chimera, based on the superimposition of the homology model with the CH1 domain in PDB file 3LUE. All images of homology models were produced using Jmol.

Results and Discussion

Stress enhances Cys labeling of spectrin in mouse cell membranes but labeling is less in 4.1R-null mutants

Fluorescence microscopy shows that RBC membranes from normal mice have higher intensity labeling when labeled at higher shear stress (Fig. 3.1C). For all of these studies, RBCs were lysed to remove hemoglobin and its highly reactive cysteines (Chiancone 1970), and then Cys reactive dyes were entrapped. The resealed ghosts were split and either held 'static' at 37°C or else sheared at 37°C at physiological levels of shear stress (<

2 Pascal) in a standard stress-controlled fluid-shearing device for up to 60 min (see Methods). To identify membrane proteins labeled at a specific time and stress and to quantify the labeling per mass, SDS-PAGE gels were run with various loads of solubilized membranes and then imaged in both fluorescence and after Coomassie staining for protein mass (Fig. 3.2A). Cysteines are under-utilized in many cytoskeletal proteins, occurring in spectrin for example at only 1-2 per ~100 amino acids (versus random usage of ~5%), but the proteins are nonetheless labeled robustly by the fluorescent dyes when compared to Coomassie stain. Densitometry of both signals at the various lysate concentrations (Fig. 3.2B) provides a specific labeling level as a slope m for each stress condition, i.e. m_{shear} or m_{static}. A ratio (m_{shear} / m_{static}) > 1 for spectrin was found for all shear stresses tested and indicates force-enhanced labeling, whereas (m_{shear} / m_{static}) = 1 was found for actin at least at low stress (see below). It should be emphasized that labeling under static conditions is non-zero and might be dependent on the particular Cys-reactive dye, but such effects are common to both static and shear samples and are intrinsically incorporated in the (m_{shear} / m_{static}) ratio. We also find that the α-spectrin and β-spectrin are equally labeled (within 5%), which is consistent with Fig.1B's anti-parallel arrangement of molecular 'springs' that are equally stressed.

As a function of shear stress (for 60 min at 37 °C), spectrin's labeling ratio (m_{shear} / m_{static}) increases with increasing stress (Fig. 3.2C). As with white ghosts, pink ghosts with about ~20% of the physiological concentration of hemoglobin show increased labeling with increased shear stress, both for spectrin separated by SDS-PAGE and in fluorescence imaging of the sheared ghosts (after a final hemolysis). Ghost membranes and spectrin bands were labeled about twice as much after being stressed at 2 Pa versus 1

Pa, with relatively tight error bars. Additional labeling of pink ghosts perhaps reflects the enhanced viscosity and stress in such ghosts.

Importantly, loss of 4.1R decreases spectrin labeling overall. The labeling appears non-linear and almost step-like. The maximum labeling at high stress is also only 50% higher than static cell labeling. Band 4.1R therefore has an important effect on network dynamics.

Shear-enhanced labeling of spectrin was fit to a force-dependent Linderstrom-Lang (fLL) equation (Fig. 3.2C, inset) which models a stress-dependent shift in equilibrium from native folded (or associated) domains to unfolded (or dissociated) domains followed by irreversible labeling of exposed Cysteines. Spectrin labeling in normal mouse RBCs, as with normal human RBCs (Johnson 2007a), fits the fLL equation (see Table 3.1 for fit parameters). However, the step-like results for 4.1R-null cells do not fit well to the fLL equation, which suggests additional processes. Forced dissociation of spectrin from actin seems possible because the spectrin-actin association in the absence of 4.1R is known to be very weak at $K_d \sim 10$ μM (Ohanian 1984, Morris 1995). If band 4.1R normally helps to keep spectrin bound to actin when the membrane is stressed, then spectrin can be stretched and unfolded, but if band 4.1R is missing, then spectrin will detach when the membrane is stressed and spectrin stretching and unfolding will be less likely.

Stress-enhanced labeling of actin and ankyrin exhibits a threshold

Simultaneous exposure of all proteins to thiol-reactive dye allows a comparison of any stress-dependent changes of other cytoskeletal proteins to spectrin. While stress-dependent labeling of spectrin is essentially linear in stress, the stress-enhanced labeling

of spectrin-associated proteins actin and ankyrin (Fig. 3.3A) occurs only beyond a threshold in stress > 0.8 Pa. This high stress exposure of Cys is suggestive of protein dissociation with high force. In general, reaction rates are exponentially accelerated by stress σ :

$$\text{rate} = k_o \, exp(\sigma / \sigma_o)$$

with both the unstressed rate k_o and the stress scale σ_o being characteristic of each reaction (unfolding or dissociation). To relate to the present situation: if reaction-(1) has a high ko and small σ_o while a second reaction-(2) has a low k_o and large σ_o, then there is an understandable transition from reaction-(1) dominated to reaction-(2) dominated at high stress (Fig. 3.3A, inset).

In contrast to the large labeling changes in spectrin, actin, and ankyrin, band 3 shows only slight shear-enhanced labeling at low and high stress (+15%) while band 4.1R shows no significant force-dependent labeling. Band 3's large cytoplasmic tail interacts with the spectrin network through ankyrin and possesses Cys that might be stress-exposed (Zhang 2000), whereas band 4.1R is a more globular stabilizer of spectrin-actin and a connector of the F-actin protofilaments to the membrane. The working model that emerges from the results thus far is that spectrin is stretched and unfolded at low stress while the rest of the network remains intact, whereas high stress dissociates a fraction of spectrin-actin and also extends ankyrin and perhaps dissociates a fraction of ankyrin from spectrin and/or band 3. Further evidence of such a mechanism is provided below.

Loss of band 4.1R limits force-enhanced labeling of ankyrin to $(m_{shear} / m_{static}) = 1.0$ at the highest shear stress of 2 Pa (Fig. 3.3B). Without 4.1R, spectrin dissociation from actin at low stress would certainly reduce the tension on spectrin and not only minimize force-

enhanced unfolding and labeling of spectrin as observed (Fig. 3.2C) but would also seem to minimize stress on ankyrin. Remarkably, a somewhat lower shear stress of 1.6 Pa leads to less labeling of ankyrin than in unstressed (static) 4.1R-null cells (i.e. (m_{shear} / m_{static}) < 1.0). Cys labeling in static cells is dominated by sites on the protein surface and also perhaps involves buried sites that are exposed at a basal rate dictated by a basal cytoskeletal stress in the RBC membrane (Waugh 1997; Discher 1998). With 4.1R-null RBCs, the shear-enhanced spectrin dissociation from actin – which is reduced in levels (Salomao 2008) – could therefore reduce the net tension on ankyrin to levels below static levels. At the same time, band 3 in the 4.1R-null cells at the highest shear exhibits significantly more stress-enhanced labeling than wild-type cells, and previous work with 4.1R-null cells had indeed suggested that Band 3 undergoes a structural change in the absence of 4.1R (Salomao 2008). The exact nature of this change and how it is shear-sensitive is in need of further study, but all of the molecular responses here are very different from normal cells.

Cys Shotgun Mass Spectrometry kinetic maps: half the sites exhibit force-dependent labeling

Cys adducts of IAEDANS and mBBr have both been shown to survive the ionization and fragmentation processes of tandem mass spectrometry (Johnson 2007a), and so we used both dyes to identify and quantify tryptic peptides of spectrin that are labeled in sheared mouse cell membranes. The dyes are roughly the same size as a tryptophan side chain, and labeling of buried cys does not greatly perturb the refolding of proteins (Johnson 2007a). Labeling under static conditions was compared to labeling extent at moderately high shear stress of 1.5 Pa for t = 30 and 60 min, and unreacted Cys in all samples (no reaction went to completion) were capped with IAM, which provided a means to normalize dye results. IAEDANS was entrapped in ghosts first in an attempt to

differentially label fast-reacting Cys on the protein surfaces even though the efficiency of labeling and/or MS detection of this dye is low. Lysates were separated by SDS-PAGE and spectrin bands were excised, trypsinized, and run through LC-MS/MS. Sequence coverage ranged from 75-77% for α-spectrin and 66-70% for β-spectrin. A total of 17 cysteines were detected, with 13 located in repeat domains, and 3 of these were predicted to be surface exposed (Table 3.2).

Force-enhanced labeling for individual tryptic peptides was determined from normalized ion fluxes in the first MS as the ratio for IAEDANS

$$\Phi_{time} = [(\text{cys-IAEDANS})/(\text{cys-IAM})]$$

or else as φ_{time} for mBBr, with $(\Phi, \varphi) \geq 1.25$ appearing to be a sound criterion for force-enhanced labeling. Even at moderately high shear stress, only two cys appeared shear sensitive at 30 min, whereas approximately half of the cysteines show force-enhanced labeling at 60 minutes (Fig. 3.4A). The average (Φ, φ)-values for force-enhanced cysteines were fitted to the fLL equation using the same parameters used for spectrin in normal cells (Fig. 3.1C). This indicates that the stress-dependent average labeling measured by densitometry of SDS-PAGE can be quantified by MS at the (more challenging) level of individual domains. Although the ±25% variation seems within present limits of uncertainty, the fLL equation models the transition from a native state (N) to an unfolded or dissociated state (U) before cys labeling can occur (Fig. 3.4B), and there is certain to be variation in the locations and reactivities of Cys between different domains.

Tabulation of all detected labeled peptides with (Φ, φ)-values in Table 3.2 shows that domain locations as well as predicted accessibilities are highly variable. Solvent

accessibility of cysteines located within repeat domains was predicted according heptad position within the helices (Parry 1992) (Fig. 3.S1; Table 3.3), and of the 13 Cys in repeat domains, 9 were predicted to be buried or partially buried within hydrophobic cores, with 5 showing force-enhanced labeling at 60 min. These domains thus seem likely to have unfolded during shear to increase cys exposure to dye. Interesting but minor exceptions to the rule: two Cys that were predicted to be solution-exposed also show force-enhanced labeling at 60 min.

Labeling kinetics at junctional Cys reveals different binding strengths in spectrin associations

Kinetic mapping of labeled peptides (Fig. 3.5) shows that two cys which are force-exposed at 30 min under high shear are located at or near sites of protein-protein interaction (Fig. 3.5A). Cys β1883 is directly adjacent to the spectrin-ankyrin binding site, whereas cys α473 is located across from the spectrin tetramer interface, which is a couple of repeats distal to the spectrin-ankyrin binding site. Force-exposure of both cysteines correlates with the increased labeling of ankyrin at high shear (Fig. 3A).

Cysteines near the spectrin-actin interaction – in either the CH1 domain (β112) or in repeat 21 of α-spectrin (α2156) – show shear-enhanced labeling only at 60 min in these normal cell membranes (Fig. 3.5B). According to densitometry results, both ankyrin and actin show force-enhanced labeling at high stress (60 min), but the spectrin-actin-4.1R association is much stronger in terms of an effective affinity (K_d = 10-15 M) (Ohanian 1984) compared to spectrin-ankyrin binding ($K_d = 10^{-7}$ M) (Podgorski 1988), which makes it likely that ankyrin dissociates first from the spectrin network. Cys α2155 was predicted to be buried within repeat 21, but its labeling seems indicative of high stress at the spectrin-actin junction.

Cysteine homology between mouse and human spectrins is striking, with past studies revealing cys exposure in several sites seen also in mouse, including α222, α1877, and β595 (Fig. 3.5C). Cys in human β15 also shows increased labeling in shear, which implicates dissociation from ankyrin, and shear-enhanced labeling of human ankyrin was indeed significant if small in previous studies of human membranes (Johnson 2007a). The same cited studies did not reveal a significant shear-dependence to actin labeling, consistent with cysteines in human α-spectrin repeat 21 and β-spectrin's CH1 domain showing no shear-enhancement. Therefore, in human RBCs and likely in mouse RBCs, dissociation of spectrin from actin is uncoupled from forced-dissociation of spectrin from ankyrin.

Several additional differences exist in the labeling patterns of human and mouse spectrin, which may argue that the transmission of force is species dependent. Cys α473 and β1544 show shear-enhanced labeling while the human homologues do not. Cys α1248 in repeat α12 is not homologous to the human cysteine in that repeat, but while both are predicted to be buried, shear-enhanced labeling is seen only in human, which suggests that repeat α12 unfolds in human RBCs and perhaps not in mouse. Cys β1159 is located in the linker between repeats β8-9, based on a crystal structure (Kusunoki 2004), and labeling of this site appears independent of stress in mouse but strongly labeled with stress in humans (Johnson 2007a). Sequence differences in the linker region could have distinct effects on linker flexibility and cys exposure (Fig. 3.S2A).

Cys labeling in relation to atomic models of interaction domains

Homology models of mouse domains were made based on existing crystal structures, suggesting that Cys β112, β1883, and α473 are all partially exposed to solution (Fig 3.6) so that some labeling is expected even in static samples. Cys β112 is within helix E of the

CH1 domain and is very close to the spectrin-actin interface (Fig 6A, 3.S2B). Dissociation from actin is expected to greatly increase the labeling efficiency at least because of decreased steric hindrance. While it is not yet known whether band 4.1R possesses any cryptic Cys that are sequestered within folds or binding interfaces, this protein shows no stress-enhanced labeling but is certainly labeled under all conditions.

The thiol in cys β1883 is directed towards the hydrophobic core of this spectrin repeat, but it is located at the end of domain involved in spectrin-ankyrin binding (Ipsaro 2010) (Fig 3.6B, 3.S2A). Increased exposure and labeling might again reflect enhanced accessibility after dissociation. Alternatively, small structural changes in the complex during shear could allow thiol probes greater access to this cysteine without the dissociation or outright domain unfolding.

Cys α473 is located on a helix that is part of the tetramerization interface between α and β-spectrin (Fig 3.6B, 3.S2C). It is on the opposite side of the helix involved in the interaction (Li 2010), and so labeling of this residue does not necessarily imply dissociation of the spectrin tetramer. However, this could be indicative of extra stress exerted at this junction when cells are sheared.

Ankyrin labeling is shear-enhanced in ankyrin repeats and near the spectrin binding site

Sequence coverage of ankyrin ranged from 38-52%, with five detected cysteines spread along the protein (Fig. 3.7A). Three detected cys are in ankyrin repeats, and all are predicted to be buried according to homology alignment into crystal structures (Fig. 3.7B). Cys 274 in ankyrin repeat 8 shows force-enhanced labeling only at 60 min and contributes to the stress-enhanced labeling measured in densitometry of SDS-PAGE gels

(Fig. 3A). (Φ, φ)-values could not be calculated for cys 316 and 472 in ankyrin repeats 9 and 14, respectively, or Cys 1212 because only peptides with fluorescently modified cysteines were detected (Table 3.5), suggesting that these are highly reactive surface sites that would be well-labeled under static conditions. Such sites would not contribute to stress-enhanced labeling.

Cys 1022 shows force-enhanced labeling at 30 and 60 min and is within only a dozen residues of the β-spectrin-ankyrin interface. The extent and kinetics of stress-enhanced labeling of this site $\varphi_{30,60min}$ = (1.61, 1.76) are similar to that of β-spectrin cys 1883 $\varphi_{30,60min}$ = (1.52, 1.68) (Table 3.5). The comparison suggests a similar mechanism of perturbation, which is detected only at high stress (Fig. 3.3A) and therefore suggests forced dissociation of spectrin-ankyrin.

Conclusions

Both spectrin unfolding and spectrin dissociation from the network appear to contribute to the RBC's response to mechanical stress. At low stress, repeat unfolding resulted in enhanced spectrin labeling while other cytoskeletal proteins were labeled independent of stress. Simultaneous enhanced labeling of spectin, actin, and ankyrin at high stress points to coordinated events, confirmed after examination of individual domain labeling with mass spectrometry. Fast labeling of cysteines at high stress proximal to the spectrin-ankyrin junction verified the weaker ankyrin-spectrin affinity, as compared to the spectrin-actin-4.1R interaction. Stress-enhanced labeling of solution-exposed cysteines in the region of spectrin-actin interaction signaled quaternary structure changes in the cytoskeletal network. Loss of coordinated, stress-enhanced labeling in the absence of band 4.1R illustrates this protein's crucial role in maintaining network integrity in the event of spectrin-actin dissociation at high shear stress.

Mutant RBCs have potentially different molecular responses, and mouse mutants in a given genetic background have advantages over humans in the availability of proper control samples. Labeling studies on 4.1R-null mouse RBCs indeed demonstrate that network disruption is a likely response to mechanical stress when protein complexes are weakly bound together. Preliminary results on human-RBCs with spectrin mutations that lead to an elliptocyte morphology, which – like 4.1R-deficiency – is associated with mechanical fragility (Gallagher 2004), also indicate stress-accelerated spectrin labeling (Fig. S4), and although more study is needed to understand differences from normal cells the shear-enhanced labeling at 60 min (1 Pa) appears similar to that of 4.1R-null cells here and below that of normal RBC (Fig. 2C).

CS-MS was used here to reveal several types of structural changes in addition to domain unfolding. Labeling kinetics provide valuable insight into molecular processes within the network, with some tentative distinctions between weak and strong interactions in protein complexes. All of the spectrin Cys that were concluded here to be significantly stress-enhanced in labeling are in domains with melting temperatures Tm > 37 °C based on studies of individual domains (Fig. 3.S4) (An 2006) or purified intact protein (Brandts 1977). In other words, these domains should be mostly folded at the temperature used in these studies, but force is seen to unfold the domains in intact membranes. The studies here exploited Cys that are in the native sequence, and so further tests of any correlation between thermal unfolding of domains and force-enhanced labeling would benefit from structure-directed insertional mutagenesis of Cys into buried sites. The present studies nonetheless suggest protein interactions and domain folding correlate spatially and temporally with labeling events. It is thus clear that the cytoskeleton of RBCs – and probably other cells – respond in a graded fashion to

force, with the nature of structural change depending on the magnitude and duration of the stress.

References

An X, Guo X, Zhang X, Baines AJ, Debnath G, Moyo D, Salomao M, Bhasin N, Johnson C, Discher D, Gratzer WB, Mohandas N. Conformational stabilities of the structural repeats of erythroid spectrin and their functional implications. J Biol Chem. 2006;281(15):10527-32.

An X, Lecomte MC, Chasis JA, Mohandas N, Gratzer W. Shear-response of the spectrin dimer-tetramer equilibrium in the red blood cell membrane. J Biol Chem. 2002;277(35):31796-800.

Bennett V, Healy J. Membrane Domains Based on Ankyrin and Spectrin Associated with Cell-Cell Interactions. COLD SPRING HARBOR PERSPECTIVES IN BIOLOGY 2009.

Brandts, J. F., Erickson, L., Lysko, K., Schwartz, A. T. & Taverna, R. D. (1977) Biochemistry 16, 3450–3454

Chiancone E, Currell DL, Vecchini P, Antonini E, Wyman J. Kinetics of the reaction of the "masked" and "free" sulfhydryl groups of human hemoglobin with p-mercuribenzoate. J Biol Chem. 1970;245(16):4105-11.

Discher DE, Boal DH, Boey SK. Simulations of the erythrocyte cytoskeleton at large deformation. II. Micropipette aspiration. Biophys J. 1998;75(3):1584-97.

Gallagher PG. Hereditary elliptocytosis: spectrin and protein 4.1R. Semin Hematol. 2004;41(2):142-64.

Giorgi M, Cianci CD, Gallagher PG, Morrow JS. Spectrin oligomerization is cooperatively coupled to membrane assembly: a linkage targeted by many hereditary hemolytic anemias? Exp Mol Pathol. 2001;70:215-230.

Ipsaro JJ, Mondragón A. Structural basis for spectrin recognition by ankyrin. Blood. 2010;115(20):4093-101.

Johnson CP, Gaetani M, Ortiz V, Bhasin N, Harper S, Gallagher PG, Speicher DW, Discher DE. Pathogenic proline mutation in the linker between spectrin repeats: disease caused by spectrin unfolding. Blood. 2007;109(8):3538-43.

Johnson CP, Tang HY, Carag C, Speicher DW, Discher DE. Forced unfolding of proteins within cells. Science. 2007;317(5838):663-6.

Kusunoki H, MacDonald RI, Mondragón A. Structural insights into the stability and flexibility of unusual erythroid spectrin repeats. Structure. 2004;12(4):645-56.

Law R, Carl P, Harper S, Dalhaimer P, Speicher DW, Discher DE. Cooperativity in forced unfolding of tandem spectrin repeats. Biophys J. 2003;84(1):533-44.

Li D, Harper SL, Tang HY, Maksimova Y, Gallagher PG, Speicher DW. A comprehensive model of the spectrin divalent tetramer binding region deduced using homology modeling and chemical cross-linking of a mini-spectrin. J Biol Chem. 2010;285(38):29535-45.

Maillet P, Alloisio N, Morlé L, Delaunay J. Spectrin mutations in hereditary elliptocytosis and hereditary spherocytosis. Hum Mutat. 1996;8(2):97-107.

Mohandas N, Gallagher PG. Red cell membrane: past, present, and future. Blood. 2008;112(10):3939-48.

Morris MB, Lux SE. Characterization of the binary interaction between human erythrocyte protein 4.1R and actin. Eur J Biochem. 1995;231(3):644-50.

Ohanian V, Wolfe LC, John KM, Pinder JC, Lux SE, Gratzer WB. Analysis of the ternary interaction of the red cell membrane skeletal proteins spectrin, actin, and 4.1R. Biochemistry. 1984;23(19):4416-20.

Ortiz V, Nielsen SO, Klein ML, Discher DE. Unfolding a linker between helical repeats. J Mol Biol. 2005;349(4):638-647.

Parry DA, Dixon TW, Cohen C. Analysis of the three-alpha-helix motif in the spectrin superfamily of proteins. Biophys J. 1992;61(4):858-67.

Podgorski A, Alster P, Elbaum D. Interactions among red cell membrane proteins. Biochemistry. 1988;27(2):609-14.

Rief M, Pascual J, Saraste M, Gaub HE. Single molecule force spectroscopy of spectrin repeats: low unfolding forces in helix bundles. J Mol Biol. 1999;286(2):553-61.

Sali A, Blundell TL. Comparative protein modelling by satisfaction of spatial restraints. J Mol Biol. 1993;234(3):779-815.

Salomao M, Zhang X, Yang Y, Lee S, Hartwig JH, Chasis JA, Mohandas N, An X. Protein 4.1R-dependent multiprotein complex: new insights into the structural organization of the red blood cell membrane. Proc Natl Acad Sci U S A. 2008;105(23):8026-31.

Takakuwa Y, Tchernia G, Rossi M, Benabadji M, Mohandas N. Restoration of normal membrane stability to unstable protein 4.1R-deficient erythrocyte membranes by incorporation of purified protein 4.1R. J Clin Invest. 1986;78(1):80-5.

Tang HY, Ali-Khan N, Echan LA, Levenkova N, Rux JJ, Speicher DW. A novel four-dimensional strategy combining protein and peptide separation methods enables detection of low-abundance proteins in human plasma and serum proteomes. Proteomics 2005;5(13):3329-42.

Tchernia G, Mohandas N, Shohet SB. Deficiency of skeletal membrane protein band 4.1R in homozygous hereditary elliptocytosis. Implications for erythrocyte membrane stability. J Clin Invest. 1981;68(2):454-60

Thompson JD, Higgins DG, Gibson TJ. CLUSTAL W: improving the sensitivity of progressive multiple sequence alignment through sequence weighting, position-specific gap penalties and weight matrix choice. Nucleic Acids Res. 1994;22(22):4673-80.

Waugh RE, McKenney JB, Bauserman RG, Brooks DM, Valeri CR, Snyder LM. Surface area and volume changes during maturation of reticulocytes in the circulation of the baboon. J Lab Clin Med. 1997;129(5):527-35.

Zhang D, Kiyatkin A, Bolin JT, Low PS. Crystallographic structure and functional interpretation of the cytoplasmic domain of erythrocyte membrane band 3. Blood. 2000;96(9):2925-33.

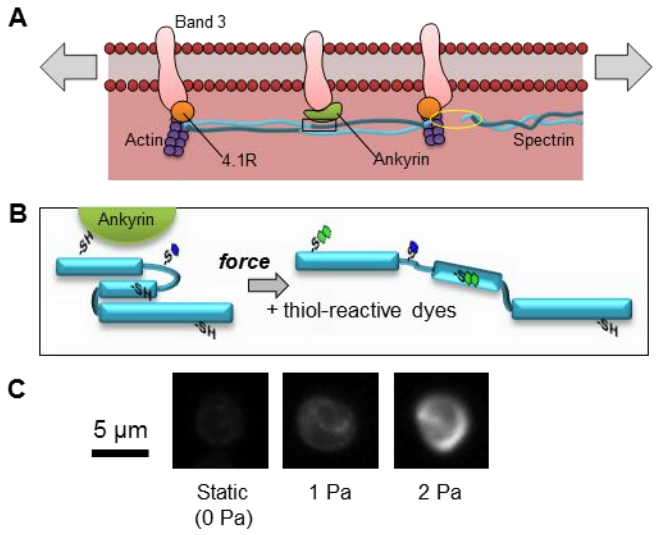

Figure 3.1: Shear stress response of red cell membrane proteins as detected by cys-shotgun labeling.

(A) Schematic shows that shearing of the membrane tends to extend the spectrin-actin network with possible stressing of integral membrane proteins such as Band 3 and and attachment proteins ankyrin and Protein 4.1R. (B) Forces might unfold spectrin repeats or dissociate spectrin from ankyrin (black box) and/or actin (yellow circle). Fluorescent thiol probes loaded into cells react with solvent exposed (blue dye) and newly exposed cysteines (green dye), revealing changes in tertiary and quaternary structure. (C) Stress-dependent labeling of the membrane can be visualized and measured in intact RBC ghosts that were labeled for the same duration at 37 °C but exposed to various physiological levels of shear stress (units of Pascal: Pa).

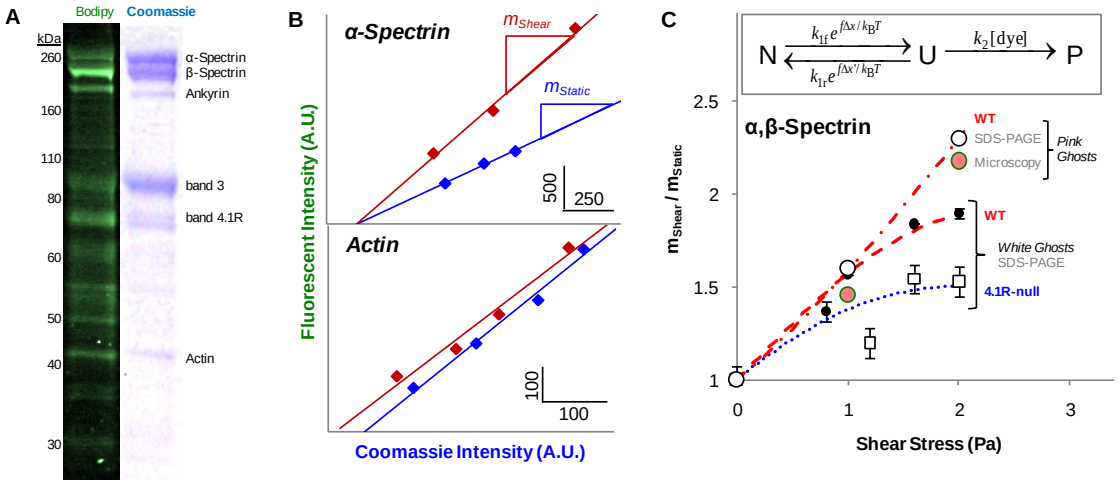

Figure 3.2: Spectin labeling depends on stress and on band 4.1R.

(A) Fluorescence and coomassie-stained images of SDS-PAGE-separated RBC ghost membrane lysate, showing considerable labeling of many cytoskeletal proteins. (B) Fluorescence and coomassie intensity of individual bands was quantified by densitometry for different amounts of the same lysate and then fit to a line ($R^2 > 0.95$). The ratio of slopes, (m_{shear} / m_{static}), for a given shear stress and time (60 min), show that α-spectrin labeling is shear-enhanced while actin labeling is shear-independent. (C) The labeling ratio for α, β-spectrin increases with shear stress, and the results fit to fLL reaction kinetics for a force-accelerated transition from native to unfolded (inset; see Supplement) shown as dotted lines. Densitometry of spectrin from normal pink ghosts (open circles: wildtype, WT), shows the same stress-enhanced fluorescence labeling as that measured by microscopy of intact pink ghosts (pink circles). With white ghosts, labeling of spectrin from normal cells, black dots, exceeds the labeling of Spectrin from 4.1R-null cells.

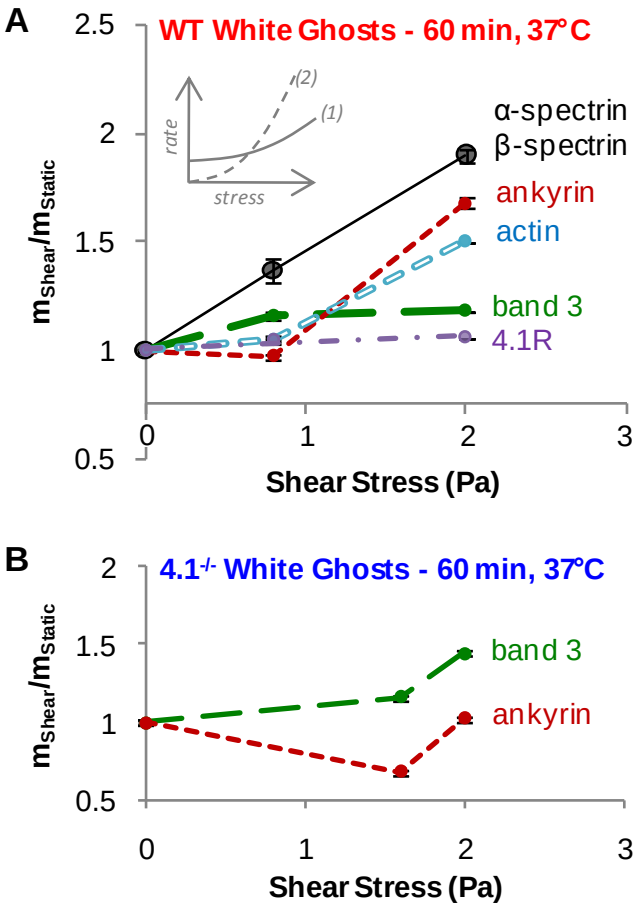

Figure 3.3 Ankyrin and actin labeling exhibit a shear-threshold that depends on band 4.1R.

(A) With normal ghosts, a low shear stress of 0.8 Pa primarily causes force-enhanced labeling of spectrin, but at a higher shear stress of 2.0 Pa, ankyrin and actin also show considerable stress-enhanced labeling while Band 3 and 4.1R show little to no stress-enhanced labeling. (B) With 4.1R-null ghosts, band 3 labeling is stress-enhanced while ankyrin labeling is not. Actin was not be analyzed because actin levels in 4.1R-null cells are lower than in wild-type (Salomi).

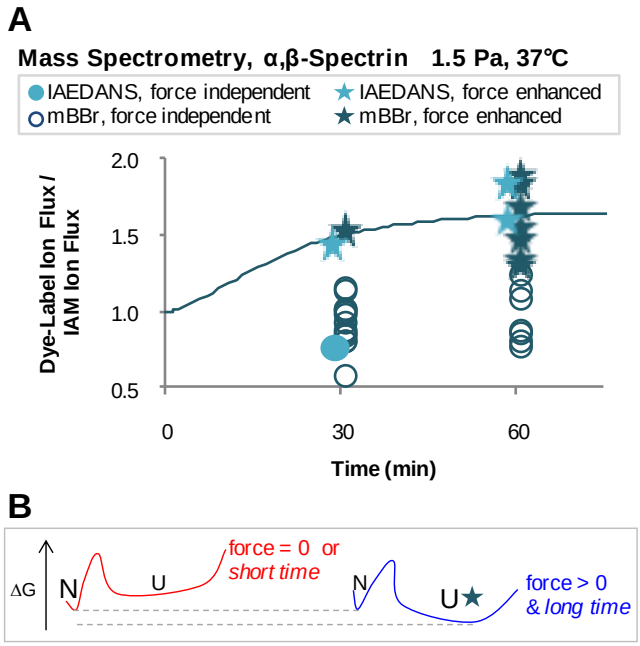

Figure 3.4: Cys Shotgun Mass Spectrometry Labeling kinetics identify force-enhanced and force-independent sites.

(A) Ion fluxes in MS of dye-labeled spectrin peptides were normalized to IAM-modified peptides in the same sample. After 30 min of moderate shear, only two of the detected cysteines showed significant force-enhanced labeling, while at 60 min, about half of the cysteines showed force-enhanced labeling. The fLL fit used the same parameters as in the WT-white ghost analysis (Fig. 2C). (B) The fLL-based free energy landscape for force-sensitive domains. At zero stress or short times, unfolding and labeling of such domains is unlikely, whereas force and time both enhance labeling.

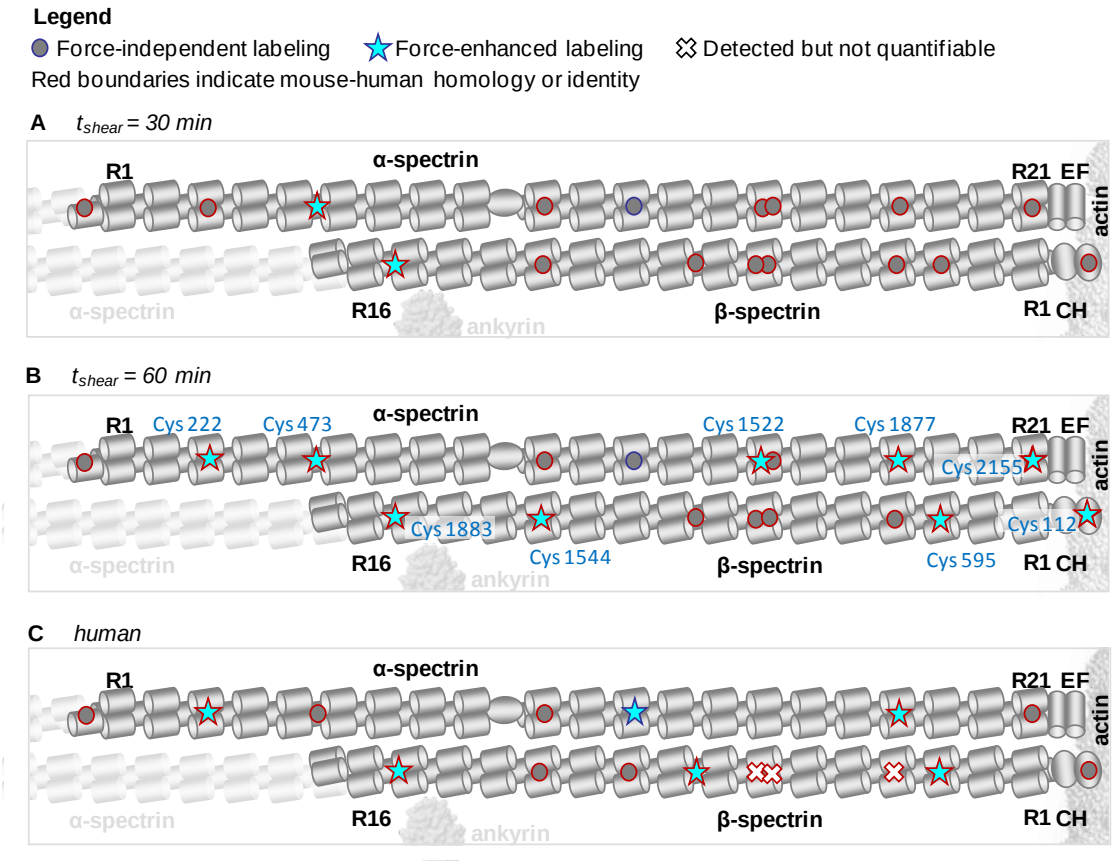

Figure 3.5: Kinetic maps of labeled cys within mouse and human spectrin.

(A) After 30 min of moderately high shear stress (1.5 Pa), only Cys located near the spectrin-ankyrin junction show force-enhanced labeling (stars). (B) After 60 min, Cys near the spectrin-actin junction as well as Cys buried within repeat domains show force-enhanced labeling. At both time points, there are also many Cys for which measurements show labeling is force-independent. (C) Many of the cysteines detected here in mouse spectrins are homologous with the Cys detected in previous studies of human RBCs (6), with some disparities likely due to sequence and/or structure differences. Amino acids and repeat assignments were made according to Uniprot files P08032 (mouse α-spectrin), P15508 (mouse β-spectrin), P02539 (human α-spectrin), and P11277 (human β-spectrin).

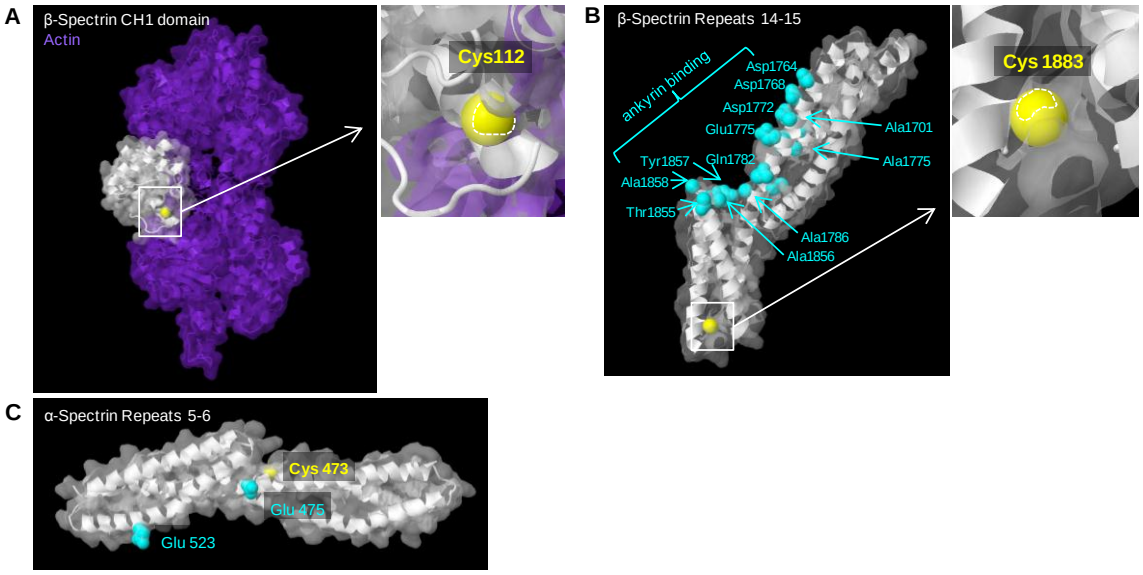

Figure 3.6: Proximity to protein binding sites of some Cys with force-enhanced labeling.

Homology models of mouse spectrin domains were made based on existing crystal structures (see Methods) and permit locations of force-enhanced cysteines to be estimated. Thiol groups are shown yellow in spacefill with the solvent-exposed area encircled with dashed lines. (A) The CH1 domain in β-spectrin (white) is bound to actin (purple) with Cys 112 located near the spectrin-actin interface. (B) β-spectrin repeats 14-15 constitute the ankyrin binding site (cyan-colored side chains), and Cys 1883 is located on the same repeat but not within the ankryin binding site. (C) α-spectrin repeat 5 might associate laterally with β-spectrin near the tetramerization site with key sites colored cyan. Cys 473 is on the opposite face of an interacting helix.

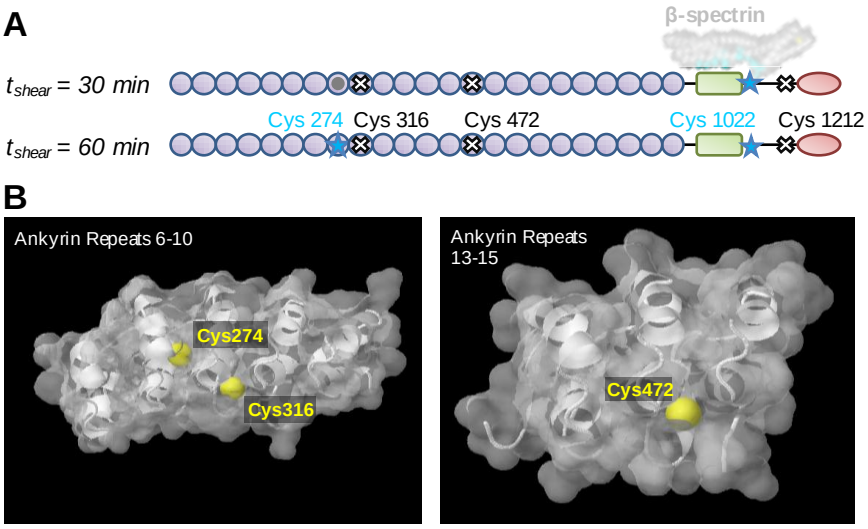

Figure 3.7: Kinetic maps and structural context of labeled cysteines within ankyrin.

(A) Multi-domain structure of ankyrin shows evidence of force-enhanced labeling (stars) at both 30 and 60 min of moderately high shear (1.5 Pa). Detected peptides from ankyrin, are tabulated. (B) Homology models of ankyrin repeats predict Cys 274 and Cys 316 are buried, which seems consistent with Φ, φ values for the former and mBBr labeling for the latter. Cys 472 appears exposed, consistent with extensive labeling by the first dye added IAEDANS.

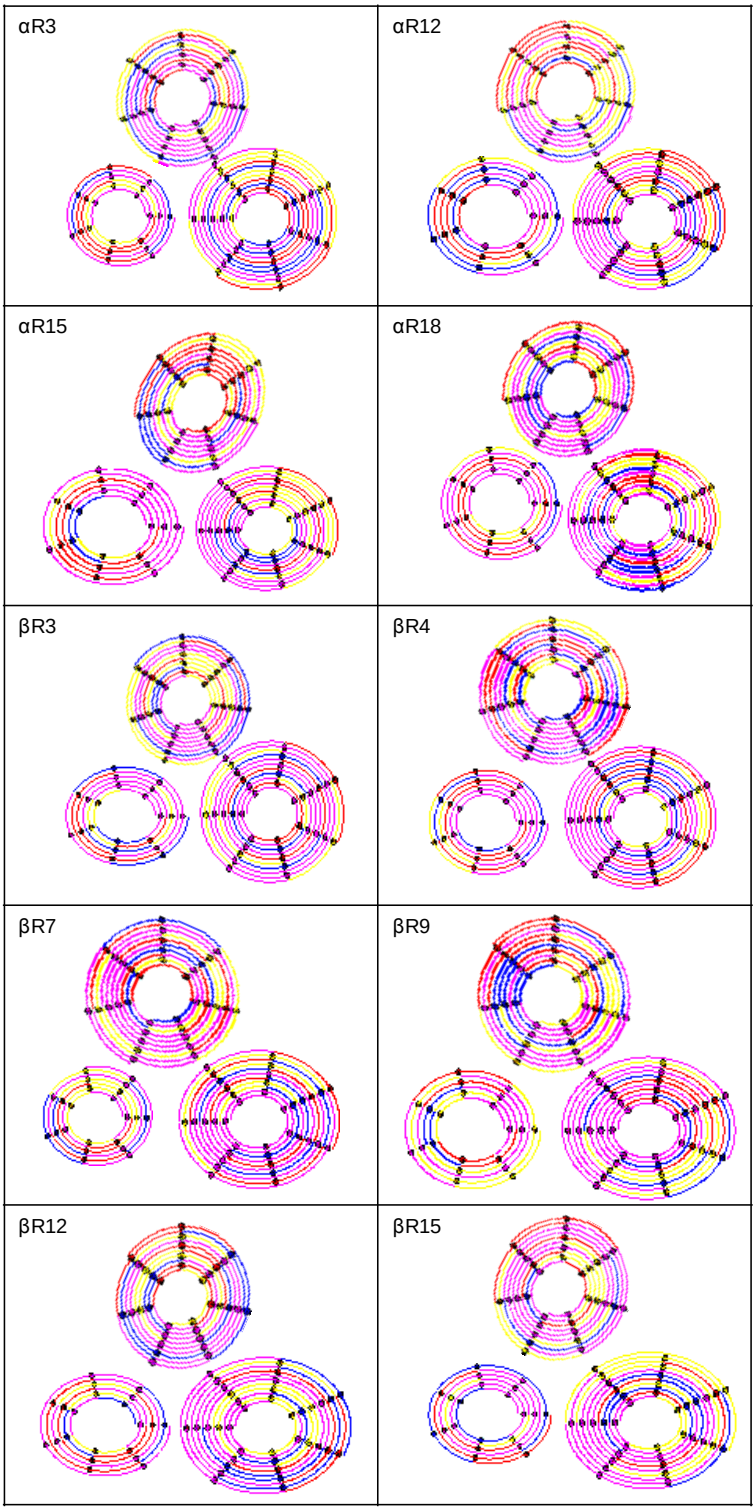

Figure 3.S1: Helical wheel depictions of repeat domains indicating hydrophobically shielded cysteines

Repeat domains containing detected cysteines were represented as helical wheels and arranged according to the schematic described in Parry et. al. Amino acids in linkers connected helices are not shown.

A β-spectrin repeats 8-9

```
                          a  d  a  d  a  d  a        a  d  a  d  a  d
SPTB1_MOUSE 1055-1226     LQAFLQDLDDFKAWLSMAQKAVASEDMPESLPEAEQLLQQHAAIKEEIDAHRDD
SPTB1_HUMAN 1063-1276     LQAFLQDLDDFQAWLSITQKAVASEDMPESLPEAEQLLQQHAGIKDEIDGHQDS
                          ***********:****::************************.**:***.*:*.
                          a  d  a  d        a  d  a  d  a  d  a  d  a
SPTB1_MOUSE 1055-1226     YHRVKASGEKVIEGQTDPDYQLLGQRLEGLDTDWDALRRMWESRGNTLTQCLG
SPTB1_HUMAN 1063-1276     YQRVKESGEKVIQGQTDPEYLLLGQRLEGLDTGWNALGRMWESRSHTLAGCLG
                          *:*** ******:*****:* **********.*:** ******.:**:****
                          a  d  a  d  a  d  a        a  d  a  d  a  d
SPTB1_MOUSE 1055-1226     FQEFQKDAKQAEAILSNQEYTLAHLEPPDSLAAAEAGIRKFEDFLVSMENNRDK
SPTB1_HUMAN 1063-1276     FQEFQKDAKQAEAILSNQEYTLAHLEPPDSLEAAEAGIRKFEDFLGSMENNRDK
                          ******************************* ************* ********
                          a  d  a  d     a  d  a  d  a  d  a  d  a
SPTB1_MOUSE 1055-1226     ILSPVDSGNKLVAEGNLYSNKIMEKVQLIEDRHKKNNEKAQEATVLLKDNLE
SPTB1_HUMAN 1063-1276     VLSPVDSGNKLVAEGNLYSDKIKEKVQLIEDRHRKNNEKAQEASVLLRDNLE
                          :******************:** **********:*********:***:****
```

Legend

Repeat 8 Repeat 9 Helical Linker

B β-spectrin actin binding domain

```
                          aaaaaaaaaaaaaaaaaa          bbbb ccccccccccccc
SPTB1_MOUSE 52-282        EVVQKKTFTKWVNSHLAFVSCRISDLYKDLRDGRMLIKLLEVLSGEMLP
ACTN1_HUMAN 30-255        EKQQRKTFTAWCNSHLRKAGTQIENIEEDFRDGLKLMLLLEVISGERLA
                          *  *:**** * **** :.. :*.:: :*:***  *: ****:***  *
                                eeeeeeeeeeeeeeeee         fffff   gggggggg
SPTB1_MOUSE 52-282        RPTKGKMRIHCLENVDKALQFLKEQRVHLENMGSHDIVDGNHRLVLGLI
ACTN1_HUMAN 30-255        KPERGKMRVHKISNVNKALDFIASKGVKLVSIGAEEIVDGNVKMTLGMI
                          :* :****:* :.**:***:*: .: *:* .:*:.:***** ::.**:*

                          ggggggggg                 aaaaaaaaaaaaaaa
SPTB1_MOUSE 52-282        WTIILRFQIQDIVVQTQEGREQRSAKDALLLWCQMKTAGYPHVNVTNF
ACTN1_HUMAN 30-255        WTIILRFAIQDISVEET------SAKEGLLLWCQRKTAPYKNVNIQNF
                          ******* **** *:        ***:.****** *** * :**: **

                          bbbb   ccccccccccc              eeeeeeeeeeeeeee
SPTB1_MOUSE 52-282        TSSWKDGLAFNALIHKHRPDLIDFDKLKDSNARHNLEHAFDVAERQLGI
ACTN1_HUMAN 30-255        HISWKDGLGFCALIHRHRPELIDYGKLRKDDPLTNLNTAFDVAEKYLDI
                            ******.* ****:***:***:.**:..:.  **: ******: *.

                               fffffff    ggggggggggggggg
SPTB1_MOUSE 52-282        IPLLDPEDVF-TENPDEKSIITYVVAFYHYFSKMKV-
ACTN1_HUMAN 30-255        PKMLDAEDIVGTARPDEKAIMTYVSSFYHAFSGAQKA
                          *:**.**:. * .****:*:*** :*** **  :
```

Legend

CH1 CH2 Surface exposed

C Ankyrin Binding Site

```
SPTB1_HUMAN 1583-1906     ANEAQQYYLDADEAEAWIGEQELYVISDEIPKDEEGAIVMLKRHLRQQRAVEDYGRNIKQ
SPTB1_MOUSE 1575-1900     AHEAQQYYLDAGEAEAWISEQELYVFSDEPPKDEEGAIVMLKRHLRQQRTVEEYGRNIKQ
                          *:*********.******.******:*** ******************:**:*******

SPTB1_HUMAN 1583-1906     LASRAQGLLSAGHPEGEQIIRLQGQVDKHYAGLKDVAEERKRKLENMYHLFQLKRETDDL
SPTB1_MOUSE 1575-1900     LAGRAQSLLSAGHPEGEQIIRLQGQVDKQYAGLKDMAEERRRRLENMYHLFQLKREADDL
                          **.***.*********************:******:****:*:**************:***

SPTB1_HUMAN 1583-1906     EQWISEKELVASSPEMGQDFDHVTLLRDKFRDFARETGAIGQERVDNVNAFIERLIDAGH
SPTB1_MOUSE 1575-1900     EQWITEKEMVASSQEMGQDFDHVTMLRDKFRDFARETGAIGQERVDNV-TIIERLIDAGH
                          ****:***:**** **********:********************** ::*********

SPTB1_HUMAN 1583-1906     SEAATIAEWKDGLNEMWADLLELIDTRMQLLAASYDLHRYFYTGAEILGLIDEKHRELPE
SPTB1_MOUSE 1575-1900     SEAATIAEWKDGLNDMWADLLELIDTRMQLLAASYDLHRYFYTGTEILGLIDEKHRELPE
                          **************:*******************************:***************

SPTB1_HUMAN 1583-1906     DVGLDASTAESFHRVHTAFERELHLLGVQVQQFQDVATRLQTAYAGEKAEAIQNKEQEVS
SPTB1_MOUSE 1575-1900     DVGLDASTAESFHRVHTAFERELHLLGVQVQQFQDVATRLQTAYAGEKADAIQSKEQEVS
                          ************************************************:***.******

SPTB1_HUMAN 1583-1906     AAWQALLDACAGRRTQLVDTADKF--- 324
SPTB1_MOUSE 1575-1900     AAWQALLDACAGRRAQLVDTADKFRFF 326
                          **************:*********
```

Legend

Ankyrin-binding **Clinical/experimental thermally destabilizing mutation sites** Labeled Cys

Figure 3.S2: Spectrin mouse and human sequence alignments

Domain sequences in mouse spectrin were aligned to sequences of existing crystal structures (see Methods). Detected cysteines are highlighted in yellow.

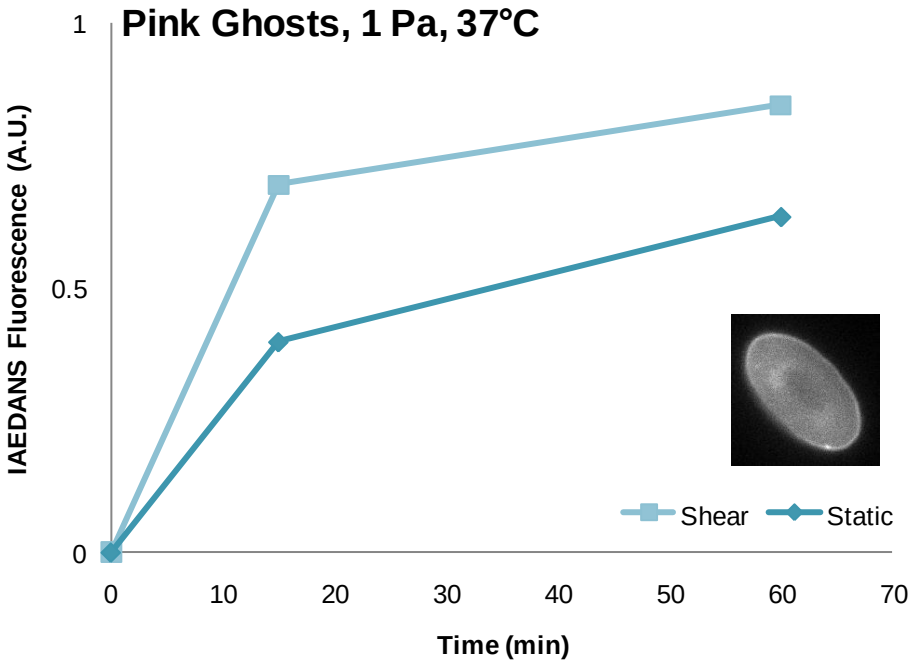

Figure 3.S3: Accelerated cys-labeling of spectrin in Wagner erythrocytes

Human Wagner erythrocytes containing spectrin with a currently uncharacterized mutation were generously provided by the Saad group (State University of Campinas, Brazil). IAEDANS labeled Wagner ghost reveals elliptocyte morphology characteristic of spectrin mutations. After normalizing IAEDANS fluorescence by Coomassie intensity, $\Phi_{15'} \approx 1.7$ and $\Phi_{60'} \approx 1.3$. The latter is closer to the result determined for 4.1R null cells in Fig. 3.2C.

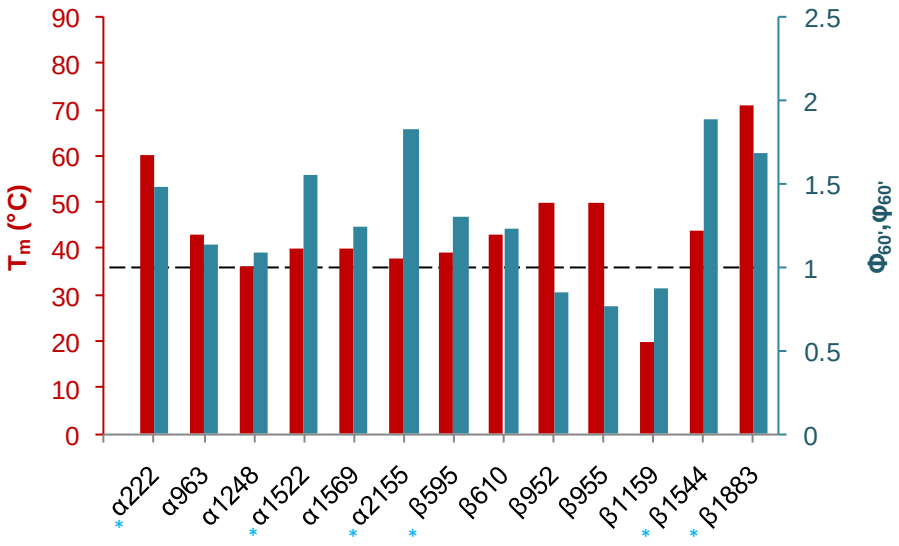

Figure 3.S4: T_M of human spectrin repeat domains compared with mouse spectrin $\Phi_{60'}$, $\varphi_{60'}$

Melting temperatures of individual repeat domains (An 2002) were compared to $\Phi_{60'}$,$\varphi_{60'}$ values shown in Table S1. Blue asterisks correspond to blue stars in Fig. 3.5.

Sample	k_{1f} (min^{-1})	k_{1r} (min^{-1})	k_2[dye] (min^{-1})
WT, Pink Ghosts	0.007	0.014	0.13
WT, White Ghosts	0.04	0.27	0.13
4.1-null, White Ghosts	0.02	0	0.13

Table 3.1: Rate constants from fLL fits of wild-type and 4.1R-null ghosts

The deviation from wild-type behavior provides insight to what is occurring at a molecular level in 4.1R-null erythrocytes. The mechanical fragility was hypothesized to be due to a weakened spectrin-actin interaction, which is also reflected in the fLL fit for 4.1R null spectrin. Effective sheared area was the same for both mutant and wild-type ghosts (data not shown), indicating that spectrin was bound to its partners, such as actin or ankyrin, at the time shear was applied. The lower unfolding rate and the non-existant refolding rate suggest that spectrin dissociation occurs after force is applied. Cysteines in 4.1R null spectrin are not exposed due to force-induced unfolding but rather thermal fluctuations.

Peptide	Cys	Domain	Predicted Accessibility	$\Phi_{30'}$	$\Phi_{60'}$	$\varphi_{30'}$	$\varphi_{60'}$
FYQYSQECEDILEWVK	α165	ABD	---			**0.93**	**0.80**
VNQYANECAQEK	α222	R3	Partially Buried	1.04	1.50	**0.86**	**1.48**
QCLDFHLFYR	α473	linker	---	**1.43**	**1.60**		
DQAEVCQQQQAAPVDEAGR	α963	R10	---			**0.88**	**1.14**
LCESHPDATEDLQK	α1248	R12	Buried			**0.88**	**1.09**
DLEDLEEWINEMLPIACDESYK (4-5%)	α1522	R15	Buried			1.32	2.43
DLEDLEEWINEMLPIACDESYKDPTNIQR						**1.16**	**1.55**
VCDGDEENMQEQLDK	α1569	R15	Exposed	1.26	1.26	**1.02**	**1.24**
RVCDGDEENMQEQLDK (5-37%)				1.04	1.69	0.96	1.88
VQDVCAQGEDILNK	α1877	R18	Buried			**0.98**	**1.34**
VQDVCAQGEDILNKEETQNK (30-41%)						1.17	1.45
NFEMCQEFEQNASAFLQWIQETR	α2155	R21	Exposed	2.12	3.88	**1.13**	**1.83**
IHCLENVDK	β112	CH 1	---	**0.76**	**1.83**		
GYQPCDPQVIQDR	β595	R3	Exposed	0.90	1.56	**0.80**	**1.30**
VSHLEQCFSELSNMAAGR	β610	R4	Partially Buried	1.22	1.67	**1.02**	**1.23**
VNNY**C**VDCEETSK	β952	R7	Buried	0.76	1.23	**0.84**	**0.85**
$VNNYC_{mbbr}VD\mathbf{C}_{mbbr}EETSK$	β955	R7	Partially Buried			**0.57**	0.77
$VNNYC_{IAEDANS}VD\mathbf{C}_{mbbr}EETSK$						**0.57**	**0.87**
GNTLTQCLGFQEFQK	β1159	linker	---			**0.99**	**0.87**
AAEIDCQDIEER	β1544	R12	Buried	0.90	1.46	**0.81**	**1.89**
EQEVSAAWQALLDACAGR	β1883	R15	Buried	1.86	2.13	**1.52**	**1.68**

Table 3.2: Cys labeling ratios for spectrin peptides quantified by Mass Spectrometry.

WT ghosts were pre-labeled with IAEDANS under static conditions at room temperature for 30 min and then labeled with both IAEDANS and mBBr under shear conditions for 30 or 60 min. The cys peptides detected by MS are listed together with amino acid number, spectrin domain, and predicted accessibility within the domain. The various Φ_{time} and φ_{time} are defined in the text, and bold numbers ≥ 1.25 indicate force-enhanced values in Fig. 4, 5. In cases of multiple peptides or labeling states, peptides with the greater ion flux were given preference (see Table 3.3).

Peptide	Cys	$ST_{30'}$	$SH_{30'}$	$ST_{60'}$	$SH_{60'}$
FYQYSQEC$_{[IAM]}$EDILEWVK	α165	1.07E+09	8.42E+08	1.28E+09	8.17E+08
FYQYSQEC$_{[IAEDANS]}$EDILEWVK		2.81E+07	2.06E+07	4.05E+07	2.06E+07
VNQYANEC$_{[IAM]}$AQEK	α222	5.24E+08	5.47E+08	7.83E+08	4.84E+08
VNQYANEC$_{[IAEDANS]}$AQEK		1.14E+07	1.24E+07	1.60E+07	1.48E+07
VNQYANEC$_{[mBBr]}$AQEK		**6.71E+08**	**6.02E+08**	**6.86E+08**	**6.27E+08**
QC$_{[IAM]}$LDFHLFYR	α473	9.62E+06	8.32E+06	1.83E+07	1.10E+07
QC$_{[IAEDANS]}$LDFHLFYR		2.71E+07	3.35E+07	3.44E+07	3.30E+07
DQAEVC$_{[IAM]}$QQQQAAPVDEAGR	α963	3.69E+08	3.63E+08	5.15E+08	3.53E+08
DQAEVC$_{[mBBr]}$QQQQAAPVDEAGR		1.87E+09	1.61E+09	2.26E+09	1.77E+09
LC$_{[IAM]}$ESHPDATEDLQK	α1248	2.72E+08	2.70E+08	3.51E+08	2.71E+08
LC$_{[IAEDANS]}$ESHPDATEDLQK		**9.71E+08**	**8.75E+08**	**1.33E+09**	**1.05E+09**
LC$_{[mBBr]}$ESHPDATEDLQK		6.19E+08	5.42E+08	7.52E+08	6.30E+08
DLEDLEEWINEMLPIAC$_{[IAM]}$DESYK (4%)	α1522	1.78E+07	1.58E+07	1.99E+07	1.82E+07
DLEDLEEWINEMLPIAC$_{[mBBr]}$DESYK (3-5%)		1.86E+07	2.38E+07	1.14E+07	2.34E+07
DLEDLEEWINEMLPIAC$_{[IAM]}$DESYKDPTNIQR		**3.81E+08**	**3.69E+08**	**5.00E+08**	**4.22E+08**
DLEDLEEWINEMLPIAC$_{[mBBr]}$DESYKDPTNIQR		**3.99E+08**	**4.48E+08**	**3.20E+08**	**4.21E+08**
VC$_{[IAM]}$DGDEENMQEQLDK	α1569	**8.74E+07**	**6.74E+07**	**1.12E+08**	**7.62E+07**
VC$_{[IAEDANS]}$DGDEENMQEQLDK		**1.04E+08**	**1.01E+08**	**1.62E+08**	**1.39E+08**
VC$_{[mBBr]}$DGDEENMQEQLDK		**1.29E+09**	**1.02E+09**	**1.54E+09**	**1.30E+09**
RVC$_{[IAM]}$DGDEENMQEQLDK (20-27%)		2.14E+07	2.26E+07	4.04E+07	1.92E+07
RVC$_{[IAEDANS]}$DGDEENMQEQLDK (32-37%)		5.42E+07	5.93E+07	8.23E+07	6.56E+07
RVC$_{[mBBr]}$DGDEENMQEQLDK (5-6%)		6.45E+07	6.53E+07	8.00E+07	7.14E+07
VQDVC$_{[IAM]}$AQGEDILNK	α1877	**1.83E+09**	**1.45E+09**	**2.58E+09**	**1.50E+09**
VQDVC$_{[mBBr]}$AQGEDILNK		**1.62E+08**	**1.26E+08**	**1.59E+08**	**1.24E+08**
VQDVC$_{[IAM]}$AQGEDILNKEETQNK (30-34%)		7.81E+08	7.38E+08	1.13E+09	6.70E+08
VQDVC$_{[mBBr]}$AQGEDILNKEETQNK (38-41%)		1.01E+08	1.11E+08	1.00E+08	8.60E+07
NFEMC$_{[IAM]}$QEFEQNASAFLQWIQETR	α2155	2.53E+07	2.33E+07	3.72E+07	3.07E+07
NFEMC$_{[IAEDANS]}$QEFEQNASAFLQWIQETR		2.05E+06	3.99E+06	9.85E+05	3.16E+06
NFEMC$_{[mBBr]}$QEFEQNASAFLQWIQETR		**3.80E+08**	**3.94E+08**	**2.92E+08**	**4.41E+08**
IHC$_{[IAM]}$LENVDK	β112	1.19E+08	9.31E+07	2.64E+08	1.77E+08
IHC$_{[IAEDANS]}$LENVDK		3.58E+08	2.13E+08	3.27E+08	4.00E+08

GYQPC$_{[IAM]}$DPQVIQDR		8.09E+07	5.56E+07	1.47E+08	1.05E+08
GYQPC$_{[IAEDANS]}$DPQVIQDR	β595	2.20E+08	1.36E+08	2.00E+08	2.28E+08
GYQPC$_{[mbbr]}$DPQVIQDR		**1.98E+09**	**1.09E+09**	**2.37E+09**	**2.14E+09**
VSHLEQC$_{[IAM]}$FSELSNMAAGR		3.68E+08	2.32E+08	6.38E+08	4.84E+08
VSHLEQC$_{[IAEDANS]}$FSELSNMAAGR	β610	2.84E+07	2.19E+07	2.52E+07	3.19E+07
VSHLEQC$_{[mbbr]}$FSELSNMAAGR		**1.11E+09**	**7.16E+08**	**1.30E+09**	**1.25E+09**
VNNYC$_{[IAM]}$VDC$_{[IAM]}$EETSK (5-6%)		1.79E+07	1.32E+07	3.79E+07	2.96E+07
VNNYC$_{[IAEDANS]}$VDC$_{[IAM]}$EETSK (11-15%)	β952	5.58E+07	3.13E+07	7.15E+07	6.86E+07
VNNYC$_{[mbbr]}$VDC$_{[IAM]}$EETSK		**2.93E+08**	**1.81E+08**	**5.42E+08**	**3.58E+08**
VNNYC$_{[mbbr]}$VDC$_{[mbbr]}$EETSK	β955	**5.52E+07**	**2.32E+07**	**6.98E+07**	**4.19E+07**
VNNYC$_{[IAEDANS]}$VDC$_{[mbbr]}$EETSK (22-28%)		2.14E+07	8.96E+06	1.93E+07	1.31E+07
GNTLTQC$_{[IAM]}$LGFQEFQK	β1159	3.72E+08	2.33E+08	4.99E+08	4.90E+08
GNTLTQC$_{[mbbr]}$LGFQEFQK		1.61E+09	9.98E+08	1.98E+09	1.69E+09
AAEIDC$_{[IAM]}$QDIEER		8.59E+07	5.75E+07	1.59E+08	1.26E+08
AAEIDC$_{[IAEDANS]}$QDIEER	β1544	5.77E+08	3.47E+08	5.14E+08	5.96E+08
AAEIDC$_{[mbbr]}$QDIEER		**2.01E+09**	**1.09E+09**	**2.22E+09**	**2.09E+09**
EQEVSAAWQALLDAC$_{[IAM]}$AGR		1.62E+07	8.13E+06	4.62E+07	2.86E+07
EQEVSAAWQALLDAC$_{[IAEDANS]}$AGR	β1883	3.39E+08	3.17E+08	2.83E+08	3.72E+08
EQEVSAAWQALLDAC$_{[mbbr]}$AGR		**9.50E+08**	**7.26E+08**	**9.75E+08**	**1.01E+09**

Table 3.3: Ion flux data of mass-spectometry detected peptides, α, β-Spectrin

Φ_{time} and φ_{time} were calculated from the ratio of IAM and mBBr/IAEDANS peptides in (A) α-spectrin and (B) β-spectrin. When multiple peptides for the same cysteine were detected, peptides with the greater ion-flux values (bold) were used for analysis. In a majority of cases, less abundant peptides make up less than a third of the total pool.

Peptide	Cys	Domain	Helix	Heptad Position	Prediced Accesibility
FYQYSQECEDILEWVK	α165	---	---	---	---
VNQYANECAQEK	α222	R3	A	g	Partially Buried
QCLDFHLFYR	α473	linker	---	---	---
DQAEVCQQQQAAPVDEAGR	α963	R10	---	---	---
LCESHPDATEDLQK	α1248	R12	B	a	Buried
DLEDLEEWINEMLPIACDESYKDPTNIQR	α1522	R15	A	d	Buried
VCDGDEENMQEQLDK	α1569	R15	B,C	linker	---
VQDVCAQGEDILNK	α1877	R18	B	a	Buried
NFEMCQEFEQNASAFLQWIQETR	α2155	R21	A	c	Exposed
IHCLENVDK	β112	CH 1	---	---	---
GYQPCDPQVIQDR	β595	R3	B,C	linker	Exposed
VSHLEQCFSELSNMAAGR	β610	R4	C	g	Partially Buried
VNNY**C**VDCEETSK	β952	R7	A	d	Buried
VNNYCVD**C**EETSK	β955	R7	A	g	Partially Buried
GNTLTQCLGFQEFQK	β1159	R9	A	e	Partially Buried
AAEIDCQDIEER	β1544	R12	C	a	Buried
EQEVSAAWQALLDACAGR	β1883	R15	C	a	Buried

Table 3.4: Predicted accessibility of cysteines within repeat domains

Heptad positions and helix assingment were based on mouse spectrin repeat sequence alignments with chick brain α-spectrin repeats 16 and 17. Amino acids in positions 'a' and 'd' are in the hydrophobic core, and electrostatic interactions often occur between 'c' and 'g' positions of different helices. For the purposes of this study, positions 'a' and 'd' were defined as buried, 'c' and 'g' defined as partially buried, and all other positions defined as solvent exposed. Accessibility is defined solely within the repeat, effects of quaternary structure are not considered.

Peptide	Cys	Domain	$\Phi_{30'}$	$\Phi_{60'}$	$\varphi_{30'}$	$\varphi_{60'}$
TKDELTPLHCAAR	274	ANK8	0.88	1.56	**0.67**	**1.26**
NGLSPIHMAAQGDHLDC$_{mBBr}$VR (100%)	316	ANK9	---	---	---	---
AKDDQTPLHC$_{IAEDANS}$AR (100%)	472	ANK14	---	---	---	---
LCQDYDTIGPEGGSLR	1022	---	---	---	**1.61**	**1.76**
FWLSDCPR (100% IAM)	1212	---	---	---	---	---

Table 3.5: Cys labeling ratios for ankyrin peptides quantified by Mass Spectrometry.

The detected Cys peptides for ankyrin are listed together with amino acid number, domain, Φ_{time} and φ_{time}. Φ_{time} and φ_{time} were not calculated if the Cys-IAM peptide was not detected.

Chapter Four

Early cardiomyocytes need work for continued differentiation

Dr. Rong provided murine embryonic stem cells with cardiac specific puromycin resistance. Erin Chang helped with experiments.

Abstract

Formation of a functional, beating heart is one of the first crucial steps in embryogenesis. Cardiac myocytes begin contracting long before the organ has completely developed. As such, embryonic cardiac myocytes are constantly "doing work" during differentiation. While it is known how the expression of contractile proteins affects the cell's ability to contract, whether the mechanical act of contraction may feed back to the cell's continued cardiac development is not known or understood. We hypothesize that cardiomyocytes contracting in the embryo do work at the optimal efficiency, and lowering this efficiency would perturb the process of myofibrillogenesis. To test this, mouse stem cell derived cardiomyocytes (SCD-CM) were cultured on polyacrylamide substrates of stiffness ranging from soft, intermediate, and hard. When cultured on polyacrylamide gels as single cells, cardiomyocytes spontaneously contract with an efficiency directly related to the elasticity, or stiffness, of the substrate. The contraction velocity of spontaneously beating cells was measured in E5 to E7 avian embryonic and SCD-CM at 9 and13 days of differentiation. Whether contraction velocity followed the expected force-velocity relationship depended on the cardiomyocyte's stage in development. Overall, myofibril

organization was greatest on substrates of stiffness similar to terminally differentiated muscle. Cardiac myocytes on soft substrates showed signs of atrophy, despite having the greatest contraction velocity. Alpha-actinin and f-actin organization in myofibrils on stiff substrates began to resemble stress fibers found in non-muscle cells rather than myofibrils. Live imaging of calcium fluctuations in spontaneously beating cells revealed that calcium channel activity was also stiffness dependent. These results demonstrate that, at initial stages of cardiogenesis, physical work is sufficient for continued development even in the absence of other regulatory factors.

Introduction

Healthy heart muscle is both contractile and compliant, but a myocardial infarct kills beating cardiomyocytes and leads to focal changes in tissue mechanics. Treatment of infarcts either with embryonic stem cells (ESC) or with equivalently re-programmed cells is viewed as promising, but is currently not feasible in a clinical setting. First, incorporation of undifferentiated ESCs into the host tissue after implantation is unreliable (Murry 2003). The inefficiency of these cells to graft onto the infarct region means that a large percentage of the injected cells are wasted. Second, even if the ESCs do form stable grafts they do not differentiate adequately into cardiomyocytes, indicating that the cells are not being properly programmed by the host tissue microenvironment. Third, ESCs that differentiate into inappropriate, non-cardiac tissues have a high risk of becoming cancerous (Loer 2007, Nussbaum 2007, Swijnenburg 2005, Hodgeson 2004).

Implantation of undifferentiated cells into healthy hearts shows limited success in terms of engraftment and evidence of cardiac phenotypic expression (Hodgeson 2004, Dai 2007, Behfar 2002, Laflamme 2005). However, tissue regeneration following stem cell

injection into infarcted heart tissue has proven less successful. Implantation of human ESCs into myocardial infarcts in animal models has been particularly enlightening. Species specific markers have allowed tracking of the incorporation and maturation of implanted cells, showing that graft formation was severely reduced after implantation even in immune-suppressed hearts. Furthermore, in vivo differentiation led to the formation of teratoma growths, which contain all three germ layers found in the embryo and are potentially cancerous (Loer 2007, Swijneburg 2005, Laflamme 2007).

One point that has not been considered in previous studies is that these stem cells are being grafted onto a region of the heart that is mechanically different from healthy muscle (Berry 2006). This seems likely to be important because recent studies from the Discher lab have shown, in particular, that that matrix stiffness is sufficient to induce differentiation of mesenchymal stem cells (Engler 2006). Scar tissue that displaces normal, compliant myocardium in the area of infarct is stiffer than heart muscle, and past results with stem cell therapy might be partially explained by the inappropriate signals that undifferentiated cells receive from this distinct microenvironment. Mesenchymal stem cells injected into infarcted mouse myocardium do not differentiate into cardiomyocytes and instead become osteogenic (Berry 2006). Similarly, undifferentiated stem cells used in tissue repair would receive distinct mechanical cues from a stiff scar than from healthy, compliant muscle, perhaps mis-directing cell differentiation. Cardiomyocytes derived from embryonic stem cells in vitro improve the function of infarcted hearts in animal models and might possess the ability to regenerate damaged tissue (Tomescot 2007, Caspi 2007, Kehat 2004). Differentiation, therefore, offers some protection from incompatible substrate stiffness. Previous work with stem cells raises a number of questions. How does the increased stiffness of fibrotic scar

tissue affect the final phenotype of differentiating cells? At what stage of differentiation are the effects of mechanical microenvironment important – or are they always contributing? Is matrix elasticity an important design rule for cell therapy in vitro? Understanding the role physical forces play in cardiac differentiation is fundamental to a clinically viable stem-cell therapy.

The physical environment within in the embryo changes throughout development. Early in development, embryonic heart tissue is soft, around 1-5 kPa, and stiffens during development (Engler 2008) In comparison, adult muscle tissue is an order of magnitude stiffer than at its embryonic stage (Engler 2004) and can stiffen as much as 400% after a heart attack (Berry 2006) Stiffening of embryonic cardiac tissue coincides with increased levels of sarcomeric proteins. However, the expression of cardiac proteins is only one aspect of cardiogenesis. Higher order organization of cytoskeletal proteins into sarcomeric structures must follow expression in order to form fully functional contractile machinery (Gregorio 2000, Sparrow 2009). In addition, myofibril assembly occurs simultaneously with ion channel expression (Kirby 2007) whether these processes affect each other is not known or understood. What is known is that spontaneous contractions are seen in the earliest stages of cardiogenesis (Kirby 2007, Gregorio 2000). Myofibril assembly and remodeling occurs during cycles of physical stress. *In vitro,* contractility has been shown to encourage myofibril maturation and cytoskeletal remodeling in cardiomyocytes (Engler 2008, Skwarek-Maruszewska 2009), and the ability to remodel the cytoskeleton is important to the transport of ion channels proteins to their proper location (Leach 2005). It would therefore not be surprising that the ability to do work is important to differentiation *in vivo* as well.

Early in culture, protein expression is independent of substrate stiffness in cardiomyocytes (Engler 2008). Rather, adhering these cells to substrates of varying stiffness changes work efficiency, altering the cell's ability to assemble myofibrils (Engler 2008). Yet, for these changes to affect overall beating behavior, organization of the sarcomeric cytoskeleton must somehow regulate the non-sarcomeric cytoskeleton, which is responsible for organizing the excitation machinery. In this study the role work plays in cardiac development is tested in stem cell derived cardiomyocytes (SCD-CM) at very early stages of development. The contraction velocity of spontaneously contracting cells was used to determine the relative force felt by the cytoskeleton under increasing loads. The effects of force on myofibril content and maturation was assessed by the localization of sarcomeric proteins. Live cell imaging of calcium fluctuations in contracting cells after long-term culture examined the effects of myofibril organization on the development of excitation machinery.

Materials and Methods

Reagents

Mouse embryonic stem cell line R1 with cardiac-specific puromycin resistance were provided by Dr. Rong (University of Pennsylvania, Philadelphia). Monoclonal anti-sarcomeric-alpha-actinin (clone EA-53) was purchased from Sigma. Antibodies reactive for both non-muscle myosin IIb and cardiac myosin (CMII 23) and sarcomeric myosin (MF20) were obtained from the Hybridoma Bank. AlexaFluor secondary antibodies, cell-permeable calcium indicator Fluo4-AM, high glucose DMEM, and L-glutamine free MEM were purchased from Invitrogen. Fetal bovine serum (FBS) used in ESC growth and differentiation media was purchased from Hyclone. FBS used in avian embryonic

cardiomyocyte culture was purchased from Sigma. Sulfo-SANPAH was purchased from Thermo Scientific.

Cardiomyocyte culture on elastic substrates

Polyacrylamide substrates

Polyacrylamide (PA) gel substrates were synthesized and covalently attached to glass coverslips as previously described (Engler 2008). Substrate stiffness was controlled by manipulation of the acrylamide/bis-acrylamide ratio. Collagen I was covalently attached to the surface with sulfo-SANPAH.

Stem cell derived cardiomyocyte differentiation

Early cardiomyocytes (CM) were derived from mouse embryonic stem cells, line R1, transfected with a cardiac-specific puromycin-resistant gene. Stem cells were cultured on feeder layers in growth media (DMEM, 4.5 g/L glucose, 100 mM sodium pyruvate, 100 mM non-essential amino acids; LIF 1000 u/L; 0.1 betamercaptoethanol; 15% Hyclone FBS) Stem cells were spontaneously differentiated in embryoid bodies (EB) made from the hanging drops of 600 cells/20 μL in differentiation media (DMEM, 4.5 g/L glucose, 100 mM sodium pyruvate, 100 mM non-essential amino acids; 0.1 mM betamercaptoethanol). After two days in hanging drops, EBs were transferred to rotating cultures for five days, then plated on gelatin coated dishes for 2 days (7+2 EB) or 4 days (7+4 EB). EBs and EB outgrowths were enzymatically dissociated at 7+2 and 7+4 days. SCD-CMs were purified through the addition of 2.5 μg/mL puromycin in the differentiation media throughout the experiment.

Embryonic cardiomyocyte isolation

Primary embryonic heart tissue was isolated from E5 and E7 White Leghorn Chick embryos (Charles River Farms). The tissue was enzymatically dissociated with 0.25% trypsin with EDTA (Invitrogen) for 30 minutes at 37°C, and the resulting cell suspension enriched for cardiomyocytes via 2 hour pre-plating of cardiac fibroblasts on 10 cm tissue culture dish. Embryonic cardiomyocytes were plated on PA substrates and cultured in L-glutamine free MEM with 10% FBS.

Live cell beating studies

PA gels containing spontaneously beating cardiomyocytes were imaged at 63x magnification using a DIC objective on a 37°C heated stage within 5% CO_2 humidified chamber. Contractions were recorded using a photometric Cascade CCD camera capturing 20 frames/second. Δμm/frame of cardiomyocyte end-to-end length was determined with the Manual Tracking plugin in ImageJ. To visualize cellular calcium, cells were loaded with Fluo-4 AM for one hour at room temperature prior to imaging. Roughness measurements of ΔFluo-4 AM intensity micrographs were determined using the Roughness plugin in ImageJ.

Indirect Immunofluorescence Microscopy

Myofibril organization was assessed after 1-5 days in culture. Immediately before fixation, cells were rinsed with PBS and permeabilized with 0.2 mg/mL saponin in relaxing buffer (0.12 M KCI, 4 mM MgCI2, 20 mM Tris-HCl, pH 6.8, 4 mM EGTA, 4 mM ATP) for 5 min at room temperature. Cells were then fixed with 3.7% formaldehyde in PBS for 10 minutes at room temperature. For staining of z-discs, cells were incubated with anti-sarcomeric-alpha-actinin (1:500) followed by AlexaFluor-488 conjugated goat anti-mouse IgG (1:2000). For staining thick filaments, cells were incubated with anti-sarcomeric-myosin (1:500). To visualize premyofibrils, cells were stained for thick

filaments then lightly fixed immediately prior to incubation with CMII 23 (1:250) followed by AlexaFluor-623 goat anti mouse IgG (1:2000). F-actin was labeled with TRITC conjugated phalloidin. Sarcomeric spacing was measured from micrographs using ImageJ (NIH; Bethesda, MD). As previously described (Carroll 2004) myofibril content was determined by the summation of striated areas visualized by s-α-actinin divided by the total area of the cell (Fig. 4.4A). Premyofibril areas, visualized by the presence of NMM IIB in striated areas, were excluded (Fig. 4.4B).

Latrunculin Recovery Assay

Latrunculin-A (lat-A) inhibits actin filament formation by sequestering actin monomers. In muscle cells, actin filaments in premyofibrils are disassembled while thin filaments in mature myofibrils are protected (Sanger 2005). Here, embryonic chick CMs (E7) were cultured on PA gels for 16 hrs. Cells were treated with 20 μM lat-A. After 30 minutes, lat-A was removed. Cells were fixed after 0.5, 1.5, and 3 hrs of recovery time. In latrunculin-blebbistatin experiments, CMs were treated with lat-A as described above and allowed to recover for 24 hours. In experimental samples, 25 μM blebbistatin was added to the media during the full recovery time. In control samples, CMs recovered in the presence of plain media. Premyofibril formation was measured by immunofluorescence of s-α-actinin and NMMIIb, where s-α-actinin spacing less than 1.7 ± 0.02 μm or the presence of NMMIIb within striated patterns indicated premyofibril areas.

Results and Discussion

Increased load reduces cellular deformation during contraction

Changes in end-to-end length occur during contraction in muscle tissue in vivo. In the contracted state, pressure from the cytosol pushing against the membrane (Fig. 4.1a) stresses the cytoskeleton and the sarcolemma (Ozawa 2001). Unlike cell cultured on dishes or coverslips, cardiomyocytes on PA gels can move their edges in during contraction, recapturing this behavior *in vitro*. On soft substrates, end-to-end length decreases during contraction, resulting in wrinkling or deformation of the cell (Fig 4.1B). Changes in end-to-end length are minimal when cardiomyocytes are adhered to stiff substrates (Fig. 4.2C), likely due to their increased load. Not only are deformations minimal, but stresses felt in the cytoskeleton are of a completely different nature, possibly leading to remodeling (Fig 4.1A).

Force-velocity relationship depends on developmental stage

Early cardiomyocytes from 7+2 EB, do not possess the all the components of a mature contractile machinery. Several, but not all, myofibrillar proteins are present, and much of the excitation machinery (sarcoplasmic reticulum, dyads, etc.) still needs to be expressed. After 4 days cultured on PA substrates, contraction velocity of 7+2 CM is inversely related to substrate stiffness. The inverse relationship between velocity and substrate stiffness indicates that after exerting a given amount of energy to contract, the CM cytoskeleton "feels" a force or load inversely related to elasticity. Conversely, 7+4 CMs cultured on PA substrates for 2-4 days had low contraction velocities independent of stiffness. In 7+4 day EB, it is known that CMs are beginning to undergo a stage of development, and signals from non-cardiomyocytes may be necessary at this stage of

development. In comparison to terminally differentiated chick CMs, the shape of the force-velocity curves are the same, but the magnitudes of E7 CM velocities are much higher than 7+2 CM velocities. Velocities of E5 CM are more comparable to those found in 7+2 CM. It is likely that as the excitation-contraction machinery matures, the force-velocity curve shifts upwards.

In the absence of other regulatory factors, work is sufficient to continue myofibril assembly

SCD-CM were cultured on PA substrates for 2-4 days then fixed and stained for s-α-actinin to determine myofibril area. Myofibril content, measured as shown in Fig. 4.4, is greatest at intermediate stiffness (Fig 4.5A), though CMs on stiff substrates have the largest total cell area (Fig 4.5B). This applies even to 7+4 CMs, which were shown to have low contraction velocities compared to 7+2 CMs. Previous work has shown that embryonic CMs do the most efficient work on intermediate stiffness (Engler 2008), and these data show that not only can early CMs handle the same load as terminally differentiated CMs, but that work partially compensates for the loss of external, non-cardiac regulation. It is also interesting to note that differences in myofibril content between CMs on intermediate and stiff substrates is not significantly different.

Loads resembling adult, not embryonic, muscle promotes myofibril maturation

Myofibril content only partially describes the cytoskeletal differences in CMs across stiffness. Myofibril maturation, i.e. the higher organization of myofibrils into aligned bundles, depends on the work CMs do during myofibril assembly. Representative images of s-α-actinin staining show that even though 7+2 CMs on soft substrates had the least myofibril content, after 4 days in culture their myofibrils are highly aligned with

each other (Fig 4.6A), similar to 7+2 CMs on intermediate stiffness (Fig 4.6D). However, after 6 days in culture, myofibril content is drastically decreased and higher organization is lost (Fig. 4.6B). Maturation is greatest in 7+2 CMs on intermediate stiffness and is maintained after two additional days in culture (Fig 4.6E). While 7+2 CMs on stiff substrates had similar myofibril content, myofibrils are not aligned (Fig 4.6G). Defects in higher organization are still seen after 6 days in culture (Fig. 4.6H). Lower contraction velocities in CMs from 7+4 EB coincides with decreased myofibril content (Fig. 4.6C,F,I) compared to their younger counterparts.

Myofibril to stress fiber transition seen in cardiomyocytes on stiff substrates

Impedance of myofibril maturation is accompanied by cytoskeletal remodeling in CMs on stiff substrates. In healthy cardiac muscle cells, actin fibers compose thin filaments, which are in register with s-α-actinin in the z-discs. This is seen in the corresponding actin and s-α-actinin striation within CMs on soft and intermediate substrates (Fig. 4.7). Only on stiff substrates do CMs not have matching actin and actinin striations (Fig. 4.7). Interestingly, though punctuate actinin staining is present, the lack of polarization within the cell makes it difficult to determine whether some s-α-actinin bands are z-discs perpendicular to a myofibril or diffuse staining along an actin stress fiber (SF) (Fig 4.7E, arrow). Thin filament disassembly may indicate a similar confusion on the cell's part. Diffuse s-α-actinin along myofibrils is clearly seen even in polarized CMs on stiff substrates (Fig 4.8) and is reflected in the greater standard deviation of sarcomere spacing along a myofibril (Fig 4.8) as compared to CM on intermediate substrates..

Beating is necessary for the formation of new myofibrils

Though the results above indicate that work is necessary for the maturation of myofibrils, latrunculin recovery studies were done to assess the necessity of work to the formation of new myofibrils. CMs continue to spontaneously contract even in the presence of latrunculin (Sanger 2005) and therefore feel different load based on substrate stiffness. Conversely, CMs treated with blebbistatin do not contract, though myofibrils and premyofibrils remain intact and calcium transients are unaffected (Farman 2008). The effects of blebbistatin are reversible, and CMs begin contracting seconds after blebbistatin washout (Farman 2008). Titin-based passive tension, however, is not affected by blebbistatin. Here, premyofibrils in E7 chick CMs on PA substrates were completely disassembled and allowed to reassemble while the cells contracted under different loading conditions. CMs on 11 kPa substrates had the greatest myofibril content at all time points as well as the fastest premyofibril formation rate (Fig. 4.9A). This was followed by CMs on 34 kPa, then 1 kPa substrates (Fig. 4.9A). Next, long-term myofibril formation was measured in CMs on 11 kPa substrates under normal, and contraction-inhibited conditions. CMs treated with lat-A as above were allowed to recover for 24 hours in the presence or absence of blebbistatin. CMs exposed to blebbistatin during lat-A recovery were unable to form myofibrils (Fig. 4.9B). Lack of beating also resulted in myofibril disassembly (Fig 4.9C). Interestingly, these cells do not resemble CMs on soft substrates, which also have decreased myofibril content. Possibly a different mechanism of myofibril down-regulation may be in play, though which pathway most closely resembles the physiological mechanism of muscular atrophy is not clear.

Spontaneous calcium fluctuations are greatest in cardiomyocytes on intermediate stiffness

In vivo, formation of the contractile apparatus is a platform to build and refine the excitation machinery (Kirby 2007). In early cardiomyocytes, such as 7+2 CMs, excitation is predominantly caused by influx of extracellular calcium through SERCA2 channels (Kirby 2007, Wei 2005). Spontaneous contractions are caused by simultaneous opening of several channels. Here, 7+2 CMs were cultured on PA substrates for two weeks, long after cytoskeletal remodeling took place. Intracellular calcium in CMs was visualized with Fluo-4 AM, and flux of calcium into the cell seen as increases in Fluo-4AM intensity. Calcium flux during contraction was statistically similar in CMs on all substrates. However, during the time between contractions, the quiescent phase, some CMs exhibited more cell-wide calcium fluctuations over time and were defined as "fluctuating cells" (Fig. 4.10). In addition, fluctuating cells had a higher frequency of calcium sparks throughout the cell at a given moment of time (Fig 4.11). This behavior was chiefly seen in 7+2 CM on intermediate substrates (Fig. 4.12), and correlated with beating frequency. Because the amplitude of calcium flux during contraction was not stiffness dependent, 1) either the number of calcium channels at the membrane are similar across substrates, or 2) calcium channels have different functionalities based on substrate and their numbers at the membrane were regulated to achieve flux at a pre-programmed magnitude. If the levels of functioning SERCA 2 channels are similar across substrates, differences in SERCA activity must result from changes in cytoskeletal organization that occurred in response to load. Otherwise, long-term cytoskeletal remodeling indirectly affects channel function by changing the cell's intrinsic mechanical properties. Ion channel organization during early stages of development is a little explored area of cardiogenesis. Often, their presence at the membrane or averaged effects on cell-wide electrophysical function has been the focus of previous developmental studies (Wei 2005, Sachinidis 2003, Maltsev 1993). The

mechanism behind the regulation of ion channel gating by diseased-based cytoskeletal changes in adult muscle has been carefully studied (Kohl 2006, Franco-Obregón 2002, Vandecaetsbeek 2009), however, these findings cannot be applied to early-stage cardiomyocytes, which have a much simpler contractile machinery. Putative mechanical-based regulation of calcium channel cycling to the sarcolemma during differentiation is an interesting route for future investigation.

Conclusion

Physical force drives cytoskeletal organization in cardiomyocytes once proteins are expressed, allowing the cells to continue differentiation. This work describes an inside-out process of cytoskeletal remodeling, where deformations in the cell during contraction stress the cytoskeleton. The type of load on the cell changes the deformation and therefore the stress on the cytoskeleton. Cells decipher the pattern of cytoskeletal stresses to gain information on the physical properties of their surroundings. The principles outlined in this work can be applied to other cells as well. Non-muscle cells also exert force on their substrate in a similar manner as muscle cells, but on a smaller scale. Previous work has focused on integrin-based mechanotransduction, an outside-in process in which differences in cellular attachment to extracellular matrix lead to cytoskeletal remodeling in the form of stress fibers. While this process is intricately described *in vitro*, its relevance *in vivo* is questionable since stress fibers is an *in vitro* phenomena. Furthermore this model does not describe cadherin based mechanotransduction, which is dominated by differences in cortical tension (Manning 2010). The inside-out process illustrated in this work fits into both cell-ECM and cell-cell modes of mechanotransduction. Future studies utilizing techniques to study protein

deformations in stressed cells is a key step in understanding the physics behind cellular processes.

References

Behfar A, Zingman LV, Hodgson DM, Rauzier JM, Kane GC, Terzic A, Pucéat M. (2002) Stem cell differentiation requires a paracrine pathway in the heart. FASEB J. 16(12):1558-66.

Berry MF, Engler AJ, Woo YJ, Pirolli TJ, Bish LT, Jayasankar V, Morine KJ, Gardner TJ, Discher DE, Sweeney HL. (2006) Mesenchymal stem cell injection after myocardial infarction improves myocardial compliance. Am J Physiol Heart Circ Physiol. 290(6):H2196-203.

Carroll S, Lu S, Herrera AH, Horowits R. (2004) N-RAP scaffolds I-Z-I assembly during myofibrillogenesis in cultured chick cardiomyocytes. J Cell Sci. 117(Pt 1):105-14.

Caspi O, et al. (2007) Transplantation of human embryonic stem cell-derived cardiomyocytes improves myocardial performance in infarcted rat hearts. J Am Coll Cardiol. 50(19):1884-93.

Dai W, Field LJ, Rubart M, Reuter S, Hale SL, Zweigerdt R, Graichen RE, Kay GL, Jyrala AJ, Colman A, Davidson BP, Pera M, Kloner RA. (2007) Survival and maturation of human embryonic stem cell-derived cardiomyocytes in rat hearts. J Mol Cell Cardiol.43(4):504-16.

Engler AJ, Griffin MA, Sen S, Bönnemann CG, Sweeney HL, Discher DE. (2004) Myotubes differentiate optimally on substrates with tissue-like stiffness: pathological implications for soft or stiff microenvironments. J Cell Biol. 166(6):877-87.

Engler AJ, Sweeney HL, Discher DE, Schwarzbauer JE. (2006) Matrix Elasticity Directs Stem Cell Lineage Specification. Cell 126: 677-689.

Engler AJ, Carag-Krieger C, Johnson CP, Raab M, Tang HY, Speicher DW, Sanger JW, Sanger JM, Discher DE. (2008) Embryonic cardiomyocytes beat best on a matrix with heart-like elasticity: scar-like rigidity inhibits beating. J Cell Sci. 121:3794-802.

Farman GP, Tachampa K, Mateja R, Cazorla O, Lacampagne A, de Tombe PP. (2008) Blebbistatin: use as inhibitor of muscle contraction. Eur J Physiol. 455:995–1005.

Franco-Obregón A, Lansman JB. (2002) Changes in mechanosensitive channel gating following mechanical stimulation in skeletal muscle myotubes from the mdx mouse. J Physiol. 539(Pt 2):391-407.

Hodgson DM, Behfar A, Zingman LV, Kane GC, Perez-Terzic C, Alekseev AE, Pucéat M, Terzic A. (2004) Stable benefit of embryonic stem cell therapy in myocardial infarction. Am J Physiol Heart Circ Physiol. 287(2):H471-9.

Kehat, I, et al. (2004) Electromechanical integration of cardiomyocytes derived from human embryonic stem cells. Nature Biotechnology. 22(10):1282-9.

Kirby ML, ed. Cardiac Development. New York:Oxford University Press, 2007.

Kohl P, Bollensdorff C, Garny A. (2006) Effects of mechanosensitive ion channels on ventricular electrophysiology: experimental and theoretical models. Exp Physiol 91(2):307–321.

Laflamme MA, Gold J, Xu C, Hassanipour M, Rosler E, Police S, Muskheli V, Murry CE. (2005) Formation of human myocardium in the rat heart from human embryonic stem cells. Am. J. Pathol. 167:663-71.

Laflamme MA, Chen KY, Naumova AV, Muskheli V, Fugate JA, Dupras SK, Reinecke H, Xu C, Hassanipour M, Police S, O'Sullivan C, Collins L, Chen Y, Minami E, Gill EA, Ueno S, Yuan C, Gold J, Murry CE. (2007) Cardiomyocytes derived from human embryonic stem cells in pro-survival factors enhance function of infarcted rat hearts. Nat Biotechnol. 25(9):1015-24.

Leach RN, Desai JC, Orchard CH. (2005) Effect of cytoskeleton disruptors on L-type Ca channel distribution in rat ventricular myocytes. Cell Calcium. 38(5):515-26.

Loer, J et al. (2007) Human embryonic stem cell transplantation to repair the infarcted myocardium. Heart 93;1278-1284.

Maltsev VA, Rohwedel J, Hescheler J, Wobus AM. (1993) Embryonic stem cells differentiate in vitro into cardiomyocytes representing sinusnodal, atrial and ventricular cell types. Mech Dev. 44(1):41-50.

Manning ML, Foty RA, Steinberg MS, Schoetz EM. (2010) Coaction of intercellular adhesion and cortical tension specifies tissue surface tension. Proc Natl Acad Sci U S A. 107(28):12517-22.

Murry CE, Field LJ, Menasché P. (2005) Cell-based cardiac repair: reflections at the 10-year point. Circulation 112:3174-83.

Nussbaum J, et al. (2007) Transplantation of undifferentiated murine embryonic stem cells in the heart: teratoma formation and immune response. FASEB. 21:1345-1357.

Ozawa E, Nishino I, Nonaka I.(2001) Sarcolemmopathy: muscular dystrophies with cell membrane defects. Brain Pathol. 11(2):218-30.

Sachinidis A, Fleischmann BK, Kolossov E, Wartenberg M, Sauer H, Hescheler J. (2003) Cardiac specific differentiation of mouse embryonic stem cells. Cardiovasc Res. 58(2):278-91.

Skwarek-Maruszewska A, Hotulainen P, Mattila PK, Lappalainen P. (2009) Contractility-dependent actin dynamics in cardiomyocyte sarcomeres. J Cell Sci. 122(Pt 12):2119-26.

Sparrow JC, Schöck F. (2009) The initial steps of myofibril assembly: integrins pave the way. Nat Rev Mol Cell Biol. 10(4):293-8.

Swijnenburg RJ, Tanaka M, Vogel H, Baker J, Kofidis T, Gunawan F, Lebl DR, Caffarelli AD, de Bruin JL, Fedoseyeva EV, Robbins RC. (2005) Embryonic stem cell immunogenicity increases upon differentiation after transplantation into ischemic myocardium. Circulation 112:I166;72.78.

Tomescot A, et al. (2007) Differentiation in vivo of cardiac committed human embryonic stem cells in postmyocardial infarcted rats. Stem Cells. 25(9):2200-5. Epub 2007 May 31.

Vandecaetsbeek I, Raeymaekers L, Wuytack F, Vangheluwe P. (2009) Factors controlling the activity of the SERCA2a pump in the normal and failing heart. Biofactors. 35(6):484-99.

Wang J, Sanger JM, Sanger JW. (2005) Differential effects of Latrunculin-A on myofibrils in cultures of skeletal muscle cells: insights into mechanisms of myofibrillogenesis. Cell Motil Cytoskeleton. 62(1):35-47.

Wei H, Juhasz O, Li J, Tarasova YS, Boheler KR. (2005) Embryonic stem cells and cardiomyocyte differentiation: phenotypic and molecular analyses. J Cell Mol Med. 9(4):804-17.

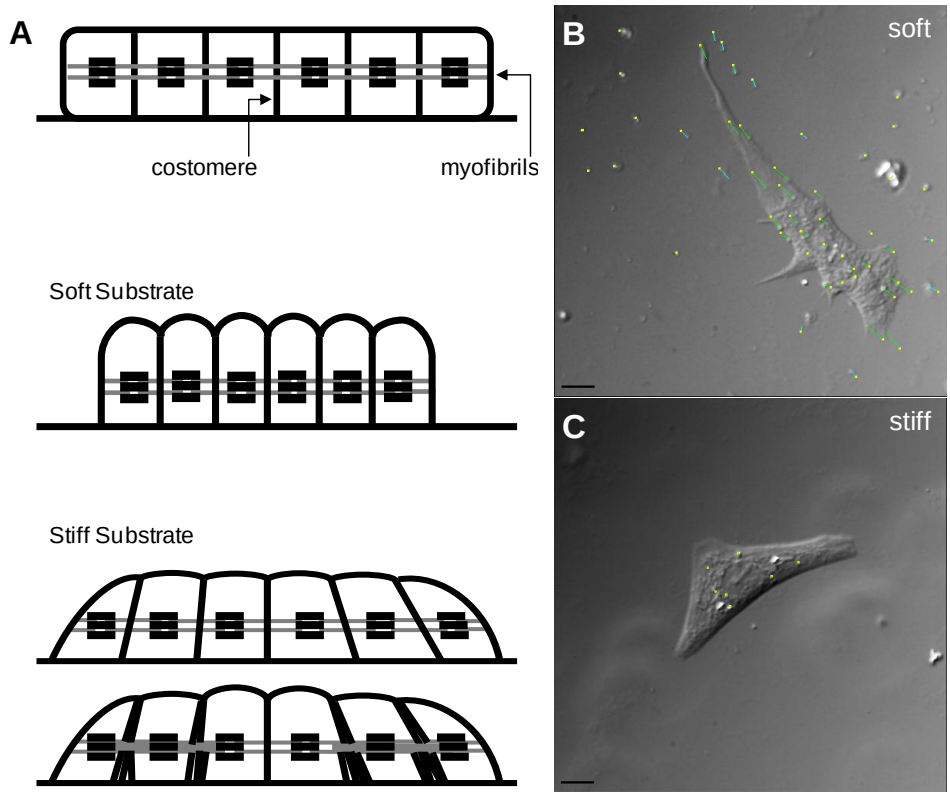

Figure 4.1: Differential stress based on substrate stiffness

(A) Myofibrils are attached to the substrate through costameric proteins. Myofibril shortening deforms the cell, stressing the costameres and the cytoskeleton as a whole. Additional stress is felt on stiff substrates, possibly leading to remodeling. (B-C) In 7+2 EB, distinct objects inside and outside isolated cells were tracked during one contraction cycle to show the qualitative relationship between substrate elasticity, load, and work. Displacements inside the cell are shown in green, displacements outside the cell are shown in blue. Yellow squares indicate the position of the object in the relaxed state. Scale bars are 10 μm. CMs on soft substrates (B) objects inside and outside the cell have large displacements. Wrinkling of the cell can be seen as well. On stiff substrates (C), similar to the elasticity of an infarct scar, objects inside the cell show minimal displacement while objects outside the cell show no movement during contraction.

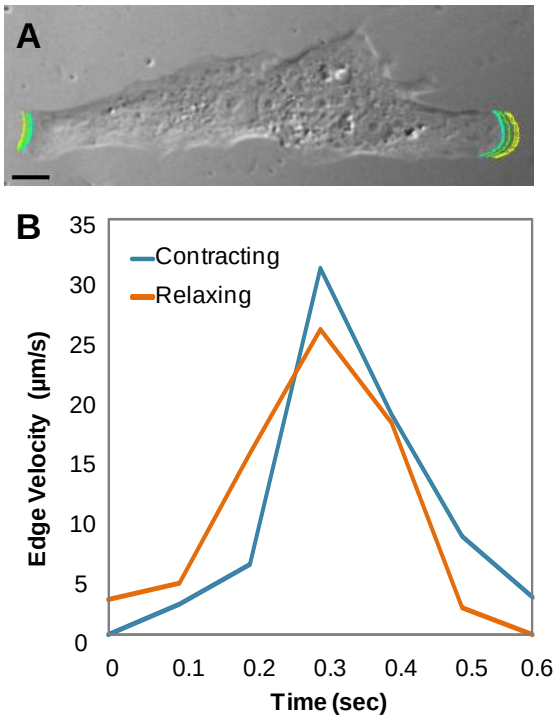

Figure 4.2: Edge velocity of spontaneously contracting cardiomyocytes

Contraction velocity was defined as change in edge position over time. (A) Even in an ideal cell, the velocity of one edge can differ from the other, and the characteristic velocity for the cell is the average of all edge velocities. (B) Load, therefore velocity, was not constant throughout contraction. As a convention the maximum velocity during inward contraction was used in all velocity calculations. Scale bar is 10 µm.

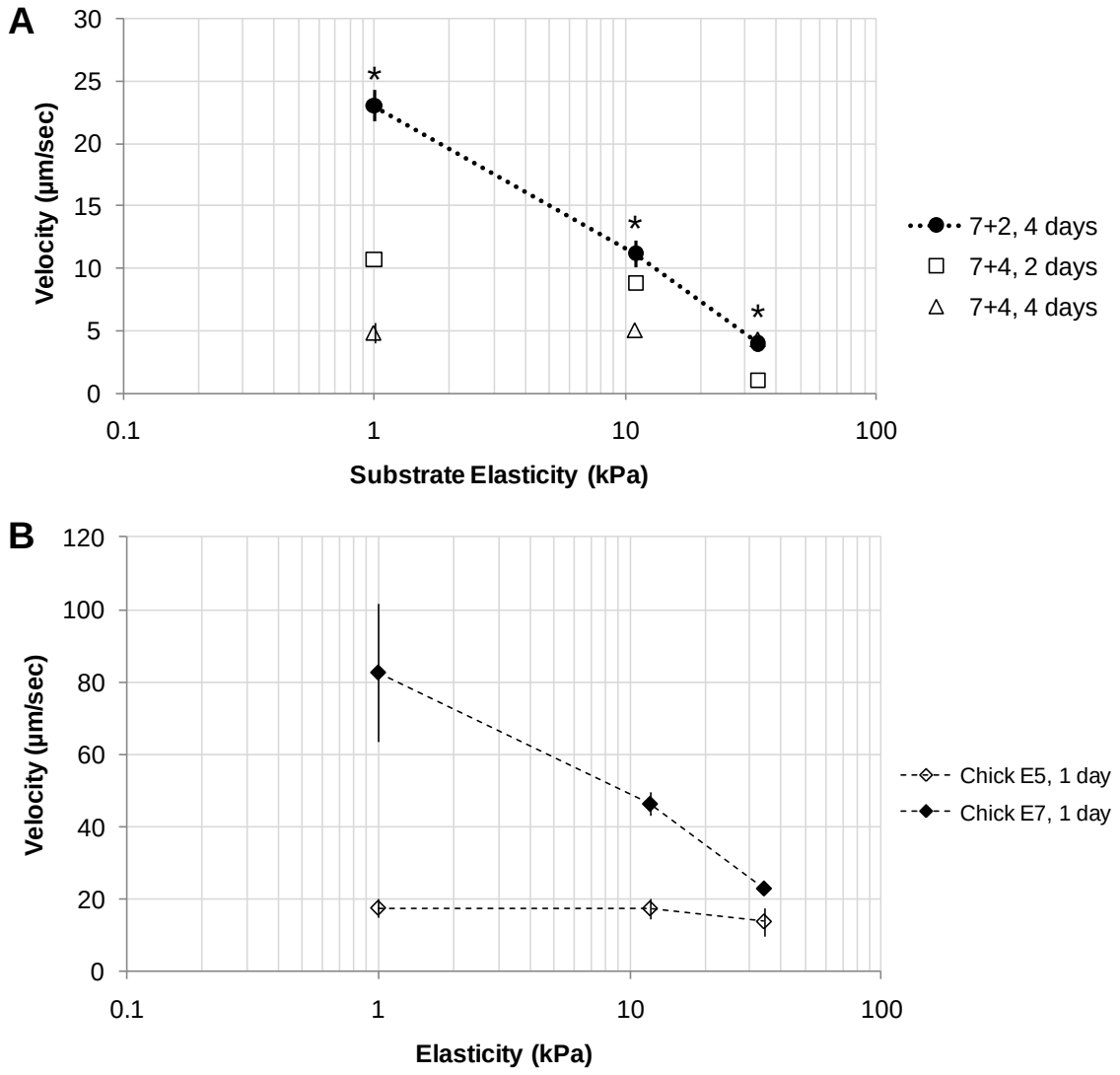

Figure 4.3: Velocity of Spontaneous Contractions in CM on PA substrates

PA substrate stiffness was varied by bis-acrylamide crosslinker concentrations, and final elasticity measured by Atomic Force Microscopy. 7+2, 4 days refers to cardiomyocytes from 7+2 day EB which have been cultured on PA substrates 4 days. (A) Cultures of 7+2 day CM had 40-60% spontaneously beating cells whose contraction velocity was inversely related to stiffness. CM isolated from 7+4 day EB had 10% spontaneously contracting cells and, compared to 7+2 day CM, low contraction velocities after two days

of culture on PA gels. An additional two days of culture on PA gels did not improve cardiomyocyte performance. (B) Terminally differentiated embryonic chick CMs were isolated from chambered embryonic hearts at incubation days 5 and 7. For chick embryonic CMs, E5 refers to egg incubation day 5, etc. CMs were cultured on PA gels 24 hours in L-glutamine free media, and cultures had 30-40% spontaneously contracting cells. E7 CMs show the same inverse relationship between velocity and elasticity, though the velocity magnitudes are much greater compared to embryonic CM. Contraction velocities of E5 CMs are comparable to 7+2 day SCD-CM. Error bars are standard error of the mean.

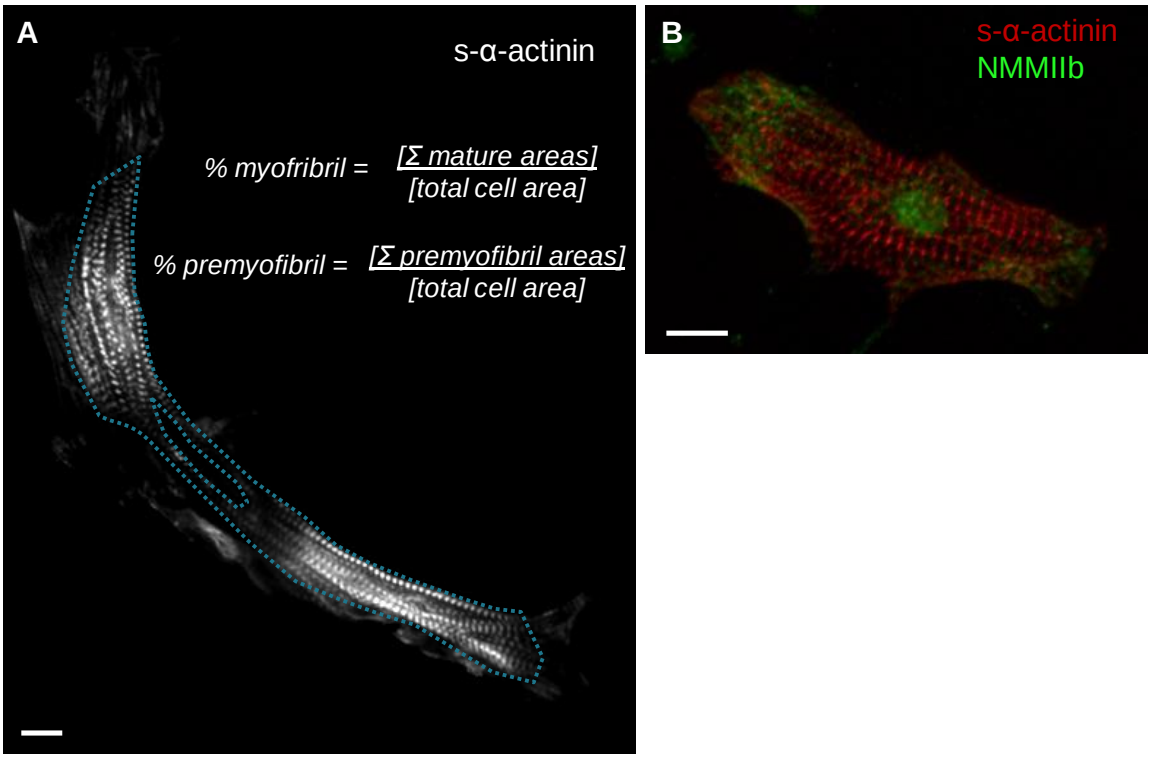

Figure 4.4: Myofibril Analysis of Representive Cells

Myofibril content consisted of areas of the cell containing "mature" myofibrils. (A) Area was classified as "mature" if sarcomere spacing = 1.7 ± 0.02 μm and (B) NMMIIb incorporation was minimal. Scale bars are 10 μm.

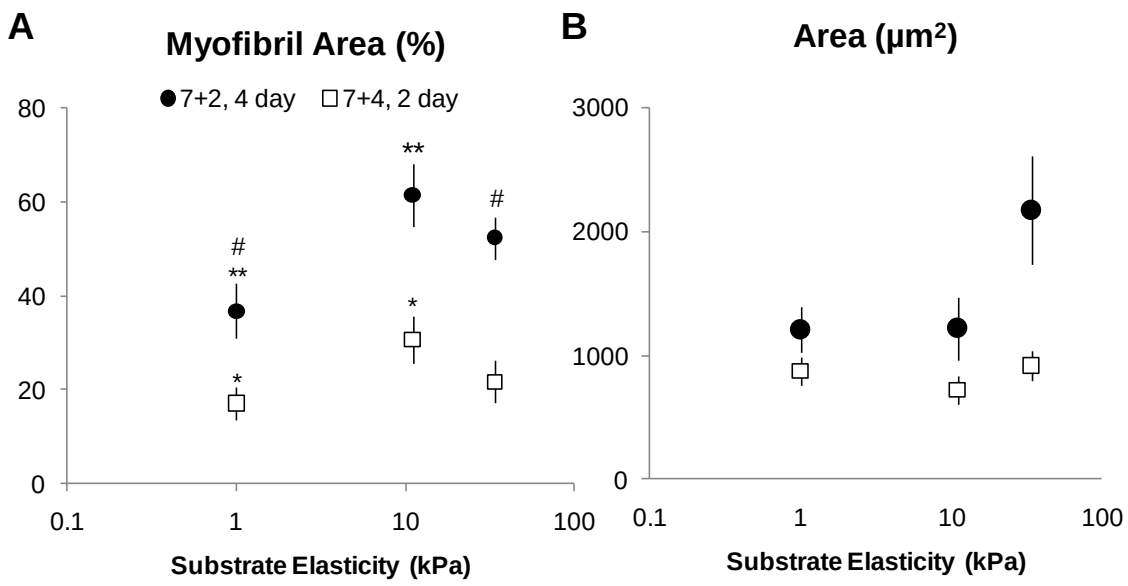

Figure 4.5: Myofibril Content in Contracting CM

The degree of myofibril assembly was based on % area of the cell with organized sarcomeres. (A) Myofibril assembly continues in the absence of other regulatory factors and is greatest on intermediate stiffness. CM on soft substrates have less myofibril content than CMs on intermediate or stiff substrates, which have similar degrees of myofibril assembly. (B) Myofibril content does not correlate with cell area. Error bars are standard error of the mean and n = 20-26.

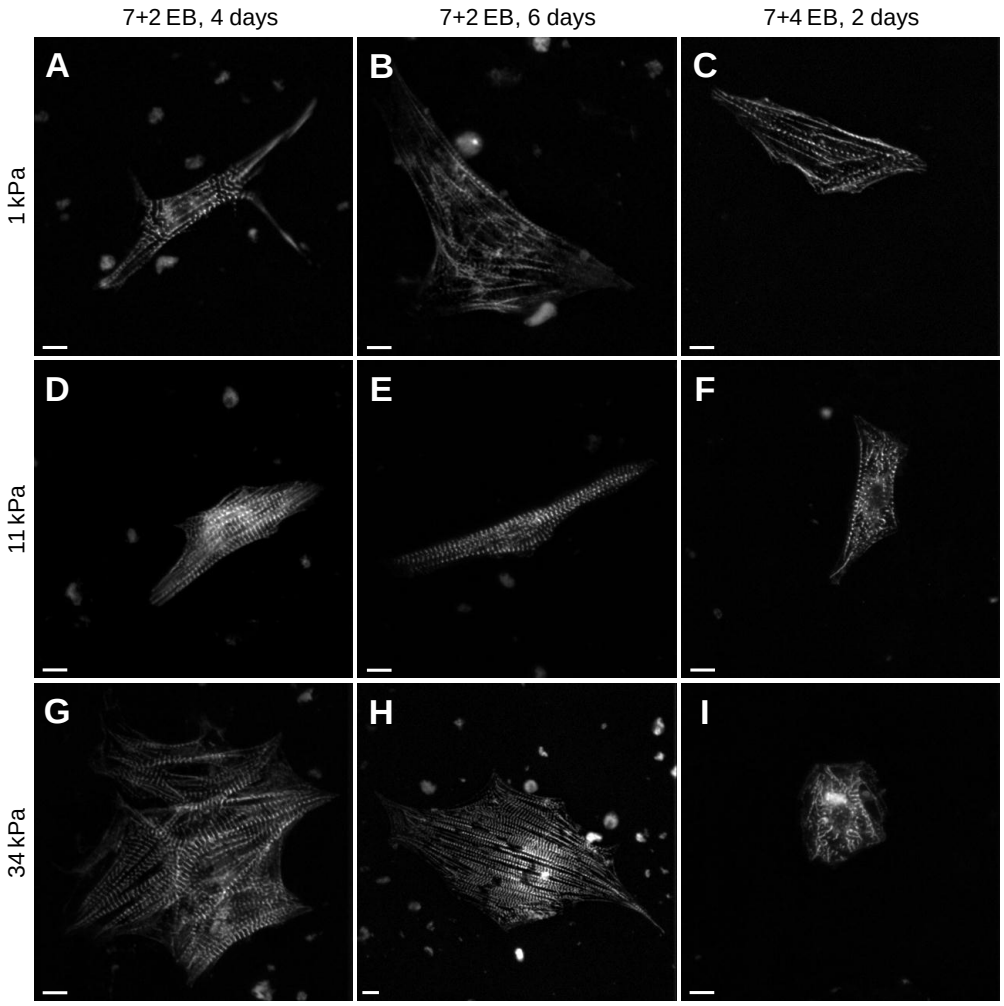

Figure 4.6: Representative CMs

(A, D, G) After short culture times, myofibril in CMs on soft substrates have similar sarcomere spacing, but differ in length. Sarcomere spacing and myofibril content are similar in CMs on intermediate and stiff substrates, though CMs have greater organization on 11 kPa. (B, E, H) After longer culture times, myofibril content and organization break down on soft substrates and are maintained on intermediate and stiff substrates. (C, F, I) Low contraction velocities in CMs from 7+4 EBs correlates with low myofibril content.

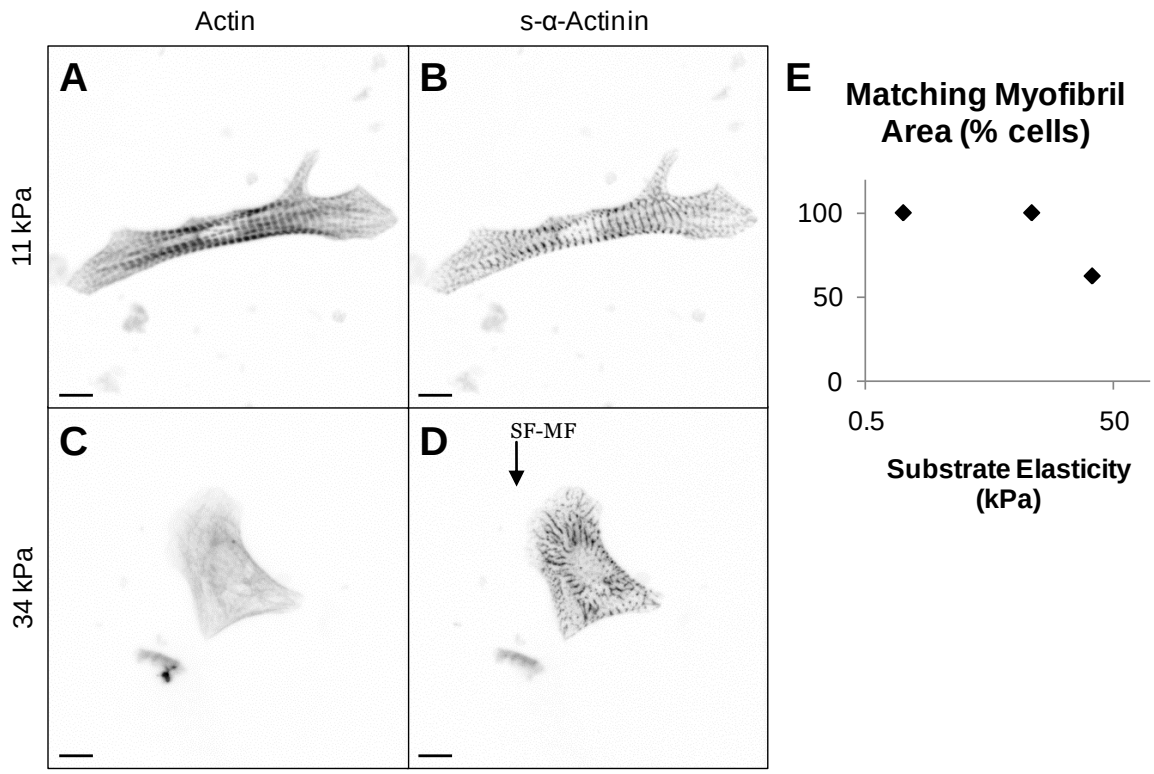

Figure 4.7: Actin vs. Alpha-Actinin striation

(A-D) Representative matching and unmatching cells show that on 11 kPa substrates, actin striation (A) matches s-alpha-actinin striation (B). Only on stiff substrates are actin thin filaments disassembled (C) despite punctuate actinin (D). Pictures were inverted to better visualize striations. Scale bars are 10 μm. (E) Myofibril analysis based on actin staining was compared to s-alpha actinin. Myofibril areas within 5% agreement were considered matching. n = 20-26.

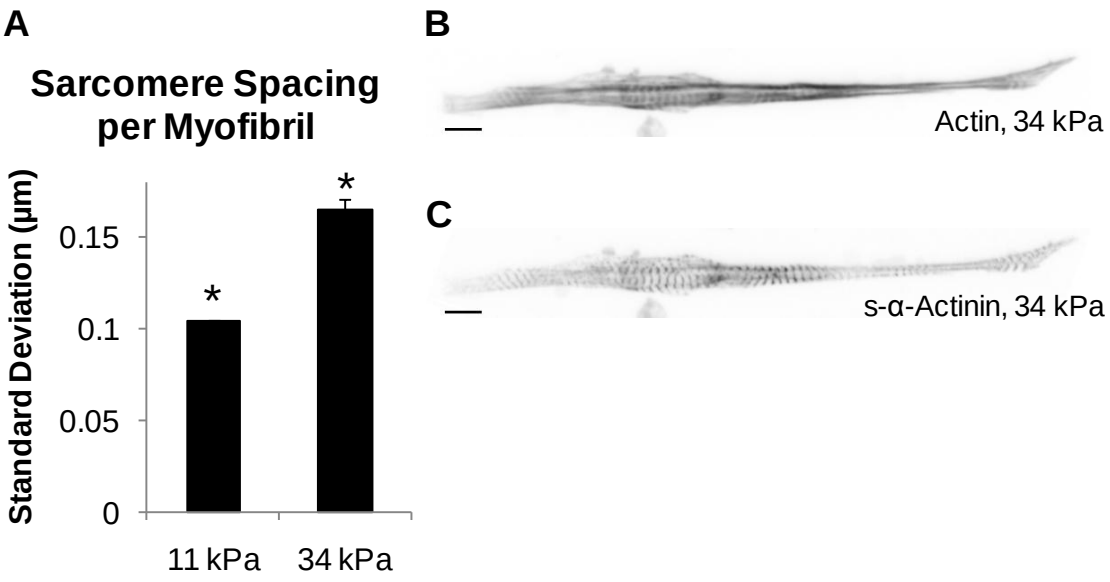

Figure 4.8: Stress-fiber like myofibrils

(A) The variation of sarcomere spacing along a myofibril was greater on stiff substrates compared to intermediate substrates, indicative of an uneven force distribution within the cell. (B-C) Representative CM with varied sarcomere spacing. Myofibrils have more diffuse actin staining (B) and areas of diffuse s-alpha-actinin (C). Picture inverted for better visualization of fibers. Scale bars are 10 μm, and error bars are standard error of the mean.

A

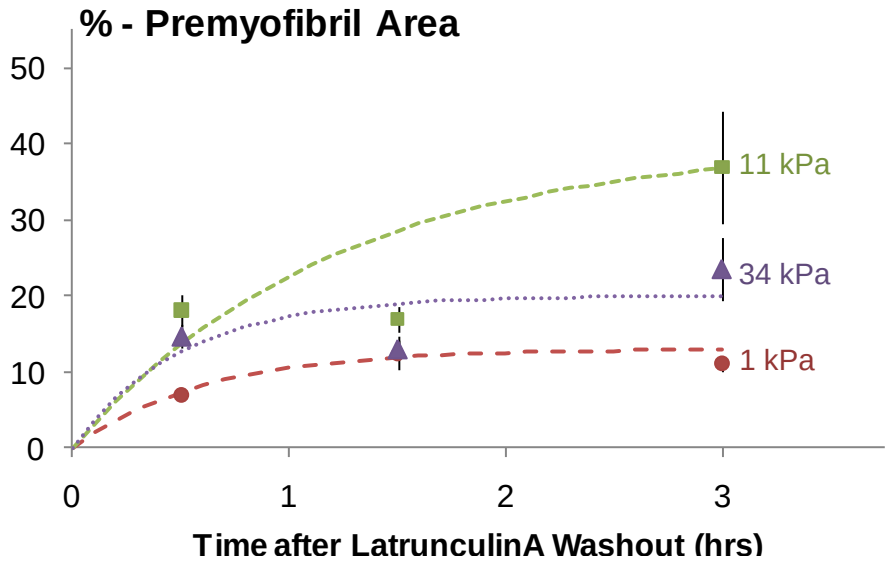
% - Premyofibril Area
50
40
30
20
10
0
0
1
2
3
11 kPa
34 kPa
1 kPa
Time after LatrunculinA Washout (hrs)

B

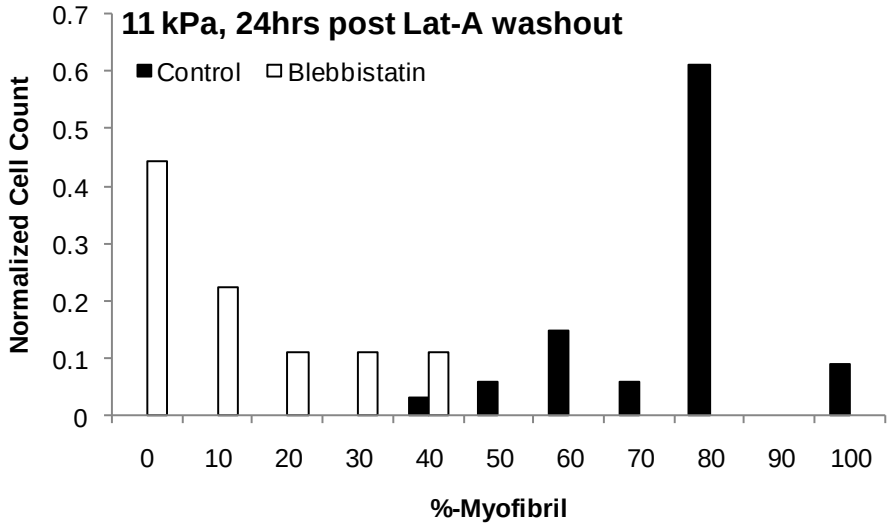
11 kPa, 24hrs post Lat-A washout
Control
Blebbistatin
Normalized Cell Count
0.7
0.6
0.5
0.4
0.3
0.2
0.1
0
0
10
20
30
40
50
60
70
80
90
100
%-Myofibril

C

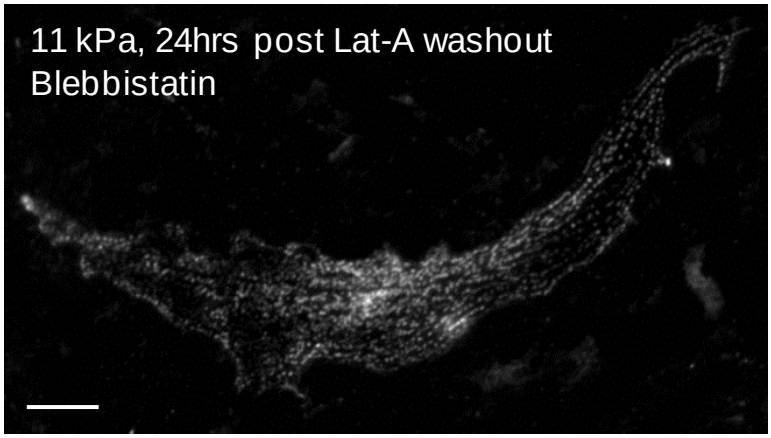
11 kPa, 24hrs post Lat-A washout
Blebbistatin

Figure 4.9: Latrunculin Recovery Assays

Latrunculin treatment disassembles actin filaments in premyofibrils, but thin filaments in mature myofibrils are protected. CMs treated with Latrunculin still beat spontaneously. (A) Under normal conditions, terminally differentiated chick embryonic CMs recover from quickly and form new myofibrils soon after drug washout. On intermediate stiffness, premyofibril content and premyofibril formation rate is optimal. (B) When beating is inhibited, myofibril assembly is down regulated, and a population of cells showed virtually complete myofibril disassembly. (C) A representative cell with 0% myofibril content illustrates the lack of s-α-actinin organization. Scale bar is 10 μm.

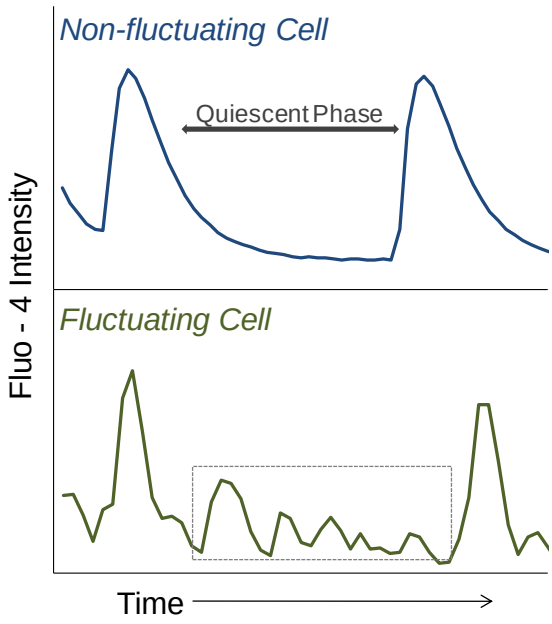

Figure 4.10: Average Fluo-4 Intensity in Representative CM

Spontaneously contracting CM from 7+2 EB, cultured 14 days on PA gels, were loaded with Fluo-4AM for 1 hr at room temperature. The amplitude of calcium influx at the moment of contraction is independent of substrate stiffness. However, in the time between contractions, defined as the quiescent phase, CMs cultured at intermediate stiffness showed greater fluctuations in average Fluo-4 intensity per cell over time.

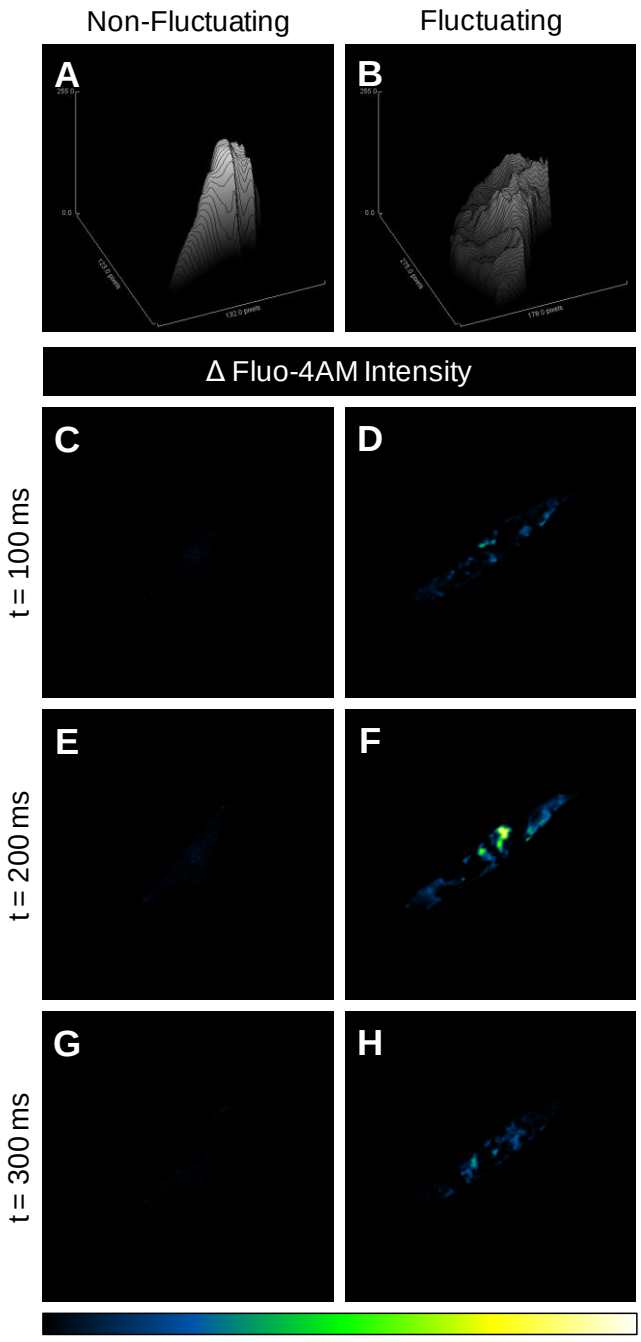

Figure 4.11: Calcium sparks in fluctuating cells

At a given time point, fluctuating cells showed more varied calcium fluctuations across the cell due to the greater number of spontaneous calcium sparks.

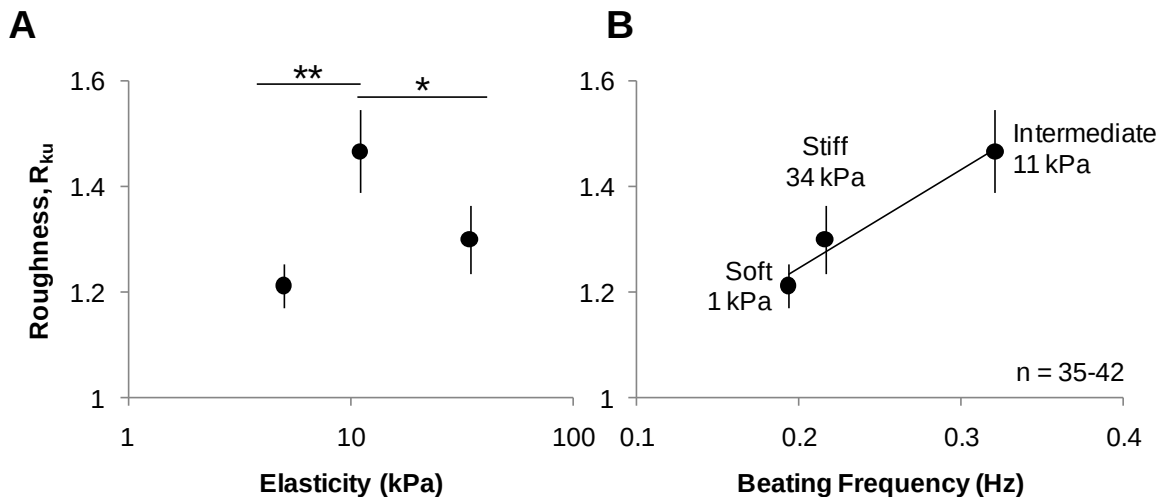

Figure 4.12: Calcium homeostasis

(A) Fluctuations across the cell at a given instant were characterized by the roughness Kurtosis of the ΔFluo-4 intensity profile for each time frame and averaged over the entire movie. These fluctuations were greatest on 11 kPa substrates and (B) correlated with beating frequency. Error bars are standard error of the mean.

CHAPTER FIVE

Conclusions

The importance of physical force in biological processes is a conceptually appealing but still largely controversial idea. Advances have been made understanding the role of mechanical environment to cytoskeletal organization, but demonstrating their effects on other cellular processes and their physiological relevance has yet to be done. Many would argue that mechanical environment has little to no effect on processes such as differentiation or disease pathogenesis. Yet the currently used experimental systems are not suitable for studying mechanosensitive processes. How can you know whether physical force is important to differentiation if you lack the ability to measure forces within a developing embryo in real time? If you cannot stress a protein in a physiological way, can you really predict its *in vivo* behavior? This thesis is a step towards arguing for and developing new techniques and ideas to solve mechanobiology problems. Chapter Two challenged the notion that we can understand a protein's response to stress using traditional biochemical techniques. The concept of separating mechanical stability from thermal stability further illuminated the molecular mechanism of dystrophin function and the possible role truncated dystrophins plays in muscular dystrophy. Chapter Three demonstrated that cytoskeleton response to stress is dynamic and occurs at fast time scales. Such conformational changes would not occur in static cells and would be virtually impossible to detect without use of the Cys-Shotgun technique. Chapter Four purports that processes such as differentiation are regulated by cytoskeletal stress. Spectrin proteins, with their mechanoresponsiveness and interactions with important signaling centers in the cell may be the missing link connecting physics with biology.